A STUDY OF SUMMER MIDDAY LOW-VISIBILITY EVENTS IN THE LOS ANGELES AREA

Thesis by
Susan M. Larson

In Partial Fulfillment of the Requirements

for the Degree of

Doctor of Philosophy

California Institute of Technology

Pasadena, California

June, 1988

(Submitted October 20, 1987)

for Grampa

and for Gramma

"*Die Welt ist so leer,*

wenn man nur Berge, Flüsse und Städte darin denkt,

aber hie und da jemand zu wissen,

der mit uns übereinstimmt,

mit dem wir auch stillschweigend fortleben,

das macht uns dieses Erdenrund erst

zu einem bewohnten Garten."   *Goethe*

so danke ich

eric, madeleine, mark, joe,

jennifer, marlys, sonja, und j. alfred.

ACKNOWLEDGEMENTS

ABSTRACT

The reduction of visibility due to air pollutants in the Los Angeles atmosphere can be severe. During summer midday periods, visibility can be reduced to less than a few kilometers. A five-site air monitoring network operated during the summer of 1984 provided data needed to characterize the summer midday visibility problem in the Los Angeles area. Light scattering and absorption by fine aerosol particles was found to account for more than 80% of the light extinction at the five sites studied. Carbonaceous aerosols and sulfates were responsible for approximately half of that fine aerosol burden. The theories of light scattering and absorption, and the data collected describing the physical and chemical characteristics of the suspended particulate matter and gaseous pollutants were used to calculate the light scattering coefficient and extinction coefficent present on each experiment day. The theoretically computed scattering and extinction coefficients are in reasonable agreement with measurements of those quantities.

One method of presenting the results of a visibility model in a readily understood fashion is to produce synthetic photographs that simulate the appearance of the scene of interest in the presence of a specified level of air pollution. A procedure for creating such synthetic photographs is developed, and methods for testing the accuracy of image processing-based visibility models are explored. The contrast reduction observed when objects are viewed through a polluted atmosphere is reproduced in the synthetic photographs, and with the inclusion of a radiative transfer code to calculate sky intensities, the appearance of the sky can be accurately simulated.

Since carbonaceous aerosol is the largest single contributor to fine particle concentrations in the Los Angeles atmosphere, pollutant abatement programs directed at visibility improvement must consider the reduction of primary carbon

particle concentrations. The effects on visibility of strategies that have been proposed for reducing the emissions of primary carbon particles are examined. It is estimated that the mean light extinction coefficient in the Los Angeles area atmosphere could be reduced by 8% to 15% by means of carbon particle emission controls costing 80.4×10^6 year^{-1}. Controls on other emissions would further improve local visibility.

Table of Contents

List of Figures

List of Tables

CHAPTER 1

INTRODUCTION

1.1 Light Scattering and Absorption in the Atmosphere

Many of the phenomena resulting from the interaction of light with gases and particles in the atmosphere are familar sights. Some, like rainbows, halos, coronas, the colors accompaning sunrises and sunsets, and even the blue of a clear day sky are sources of enjoyment. (For a discussion of the causes of a variety of these occurrences, see Minnaert, 1954.) However, in polluted atmospheres, light scattering and absorption by airborne pollutant particles act to reduce visual range and to degrade the appearance of the surrounding scenery.

This work describes an effort to characterize the causes of visibility degradation observed in a polluted atmosphere, to model the process of visibility reduction, and to consider methods to improve visibility. Methods developed are applied to create an understanding of the causes of the summer midday low-visibility events that commonly are observed in the Los Angeles area. This introductory chapter begins by giving historical background information on the evolution of studies of the attenuation of light in the atmosphere, and provides a discussion of the basic properties and causes of light extinction. Then an outline of the research objectives pursued in Chapters 2 through 5 of this work is presented.

1.2 Historical Background

In 1760, Bouguer formulated a law describing the apparent brightness of an object viewed at a distance. He deduced the law from experiments, but mathematically it can be explained as follows.

Light scattering is a process by which all or a portion of a light beam is redirected, but in which total light intensity is conserved. Assume that the light intensity reduction, dI, in the original direction of propagation due to scattering over a differential distance dx through a medium is proportional to the incident light intensity, I, and to the length of the path element dx. Then the change in light intensity can be written:

$$dI = -b_{scat} I dx \tag{1.1}$$

where b_{scat} is a proportionality constant called the scattering coefficient, having units of inverse length. To determine the light intensity, I, received from an object with inherent intensity I_0 located at a distance x from the observer, Equation (1.1) can be integrated to obtain:

$$I = I_0 e^{-b_{scat} x} \tag{1.2}$$

If light is absorbed by the medium rather than scattered, a similar expression results:

$$I = I_0 e^{-b_{abs} x} \tag{1.3}$$

where b_{abs} is the light absorption coefficient (units are inverse length). If both scattering and absorption occur, then

$$I = I_0 e^{-(b_{scat} + b_{abs}) x}$$

$$I = I_0 e^{-b_{ext} x} \tag{1.4}$$

where b_{ext} is called the light extinction coefficient (again having units of inverse length). Equation 1.4 is known as Bouguer's law (Middleton, 1968).

In 1789 de Saussure constructed a device to attempt to measure the transparency of the air, and in 1868 Wild made photometric measurements of the brightness of screens held at different distances. During the mid 19th century, the

attenuation of beams of light was studied as an important consideration in the performance of lighthouses. But providing an explanation for the blue color of the sky was still a challenge for scientists studying the optics of the atmosphere.

In 1908 Nichols summarized the then current "theories of the color of the sky." Clausius (1849) believed that a blue sky was caused by the presence of water bubbles in air. Hagenbach (1872) maintained that light reflecting off of moving bodies of air caused the color. Lallemand (1872) and Hartley (1889) favored the theory that ozone fluoresced at blue wavelengths in the upper atmosphere, and Rayleigh (1871a,b) theorized that the amount of light that is scattered by small particles in the atmosphere varies inversely with the fourth power of the wavelength of light, and that this would give the sky its blue color. Rayleigh concluded in 1899 that the small particles scattering the sun's light could be the air molecules themselves. Rayleigh scattering became the accepted theory, even though Nichols (in 1908) had thought that the sky color "cannot be altogether accounted for by the assumption of an atmosphere conforming to Rayleigh's formula."

The light scattering process described by Rayleigh is only valid for particles having diameters smaller than about one-tenth the wavelength of the incident light. In 1908 Mie formulated a theory based on solutions to Maxwell's equations as applied to spheres in an electromagnetic wave in order to describe how light interacts with particles in the processes of light scattering and absorption. Mie theory reduces to Rayleigh scattering in the limit of small, light scattering particles, and can be used to calculate the scattering and absorption coefficients due to a suspension of particles in the atmosphere (Equations 1.2, 1.3).

The effects of light scattering and absorption by particles suspended in the atmosphere were further studied and evolved into considerations of the link between light extinction, visibility, and pollutant aerosols. In 1924 Koschmieder

published his "Theorie der horizontalen Sichtweite." Koschmieder used the term "Sichtweite," or visibility, to describe the greatest distance at which a black object could still be distinguished from the background of the horizon sky. Allard in 1876 studied visibility in terms of the degree of attenuation of a beam of light at night. Middleton (1968) traces the English usage of the term "visibility" to Bennett (1930) who used the word, perhaps as a translation of Koschmieder's "Sichtweite", to describe the clearness with which objects can be seen. The word "aerosol" (from the prefix "aero" and the word "solution", according to the American Heritage Dictionary, 1980) to describe a system of particles suspended in gases was used by Winkel and Jander in 1934, and by Schmauss and Wigand in 1929. The term "Luftplankton" (Luft = air) used by Weber in 1916 to refer to the particles that swim in the air, never entered common scientific usage.

Routine measurements of visual range were made after World War I, and much research on visibility was accomplished during World War II. Duntley (1948) presented work that was "begun during the war as part of a study of the visibility of distant targets; it is presented in the belief that the theory may find peacetime uses." Research into the causes of visibility reduction and methods to improve visibility continue today.

1.3 Contributions to Light Extinction

If air molecules were the only scatterers present in the atmosphere, visibility would be restricted to approximately 300 km, but additional visibility reducing particles enter the atmosphere from natural and man-made sources. Natural sources include soil and rock dust, sea spray, natural fires, condensation of natural gaseous emissions, and volcanos. These sources cannot always be viewed as contributing small amounts of material. For example, in 1883, the eruption of Krakatoa "raised clouds of ash to 90,000 feet, and turned day into night at

Batavia 100 miles away. Within a few weeks the smaller particles, remaining high in the stratosphere, had spread across a broad belt of latitudes and completely around the globe. For several years this impalpable dust produced spectacular lighting effects at sunrise and sunset" (McCartney, 1976). (For another account of the Krakatoa eruption see Péne du Bois, 1947.) Anthropogenic sources of atmospheric particles include fuel combustion and industrial processes as well as the exhaust from vehicles and a variety of fugitive sources (e.g., road dust and tire wear debris). Total annual average anthropogenic particulate emissions in the United States are estimated at 125-385 Tg/year (Seinfeld, 1986).

The size of atmospheric particulate matter varies greatly. The size of an air molecule is on the order of 10^{-4} μm, while the size of most airborne particulate matter ranges in diameter from 0.01 μm to 50 μm. The amount of light scattered by these particles (and therefore the scattering coefficient) depends on the ratio of the particle diameter to the wavelength of incident light. The most effective scattering occurs when the particles have a diameter about the same size as the wavelength of incident light. The scattering coefficient also depends on the particle number concentration and on the index of refraction of the particles. Figures 1.1-1.5 illustrate the relationship of these particle properties to the scattering coefficient for an aerosol with a size distribution like that measured on September 27, 1984 at Pasadena, California. Mie theory was used to calculate the scattering coefficient results given in those figures, by methods that are described in detail in Chapters 2 and 3 of this work.

Figure 1.1a shows the volume distribution of the particles measured in an ambient aerosol sample at Pasadena, California. The distribution indicates the contribution that the particles in each of a series of particle diameter intervals make to the total volume of particles measured. Figure 1.1b illustrates the distribution

of light scattering as a function of particle size for the same aerosol.

The graphs show that even though there is a substantial volume of large particles present, these large particles contribute little to the amount of light that is scattered. For the aerosol size distribution observed on September 27, 1984 and an assumed refractive index of 1.5-0.0i, the scattering coefficient declines as the wavelength of light increases (Figure 1.2). Figure 1.3 shows the variation in the scattering coefficient with changes in the real part of the refractive index, and Figure 1.4 describes the variation in scattering resulting from a variation in the imaginary part of the refractive index. The scattering coefficient increases in direct proportion to the total number of particles present (all other factors held constant) as illustrated in Figure 1.5. The scale factors used in Figure 1.5, are multiplicative factors applied to the number of particles in each diameter range of the size distribution in order to examine the effect of particle number on the scattering coefficient.

In addition to light scattering by air molecules and by particles, light can be absorbed by gases (chiefly NO_2) and by particles (chiefly elemental carbon). These factors also contribute to the amount of light extinction in the atmosphere.

1.4 Visibility and Air Pollution

In atmospheres containing large concentrations of particles and absorbing gases, as is possible in polluted areas, visibility can be reduced to less than a few kilometers. While visibility reduction may be the most easily perceived feature of a polluted atmosphere, other effects of air pollution include possible damage to materials and to plants, and health hazards to animals and to humans. In an extreme example, during a severe air pollution episode which lasted from December 5-9 in London in 1952 over 4,000 excess deaths were reported (Seinfeld, 1986).

Because of the varied effects of airborne particulate matter, ways to reduce
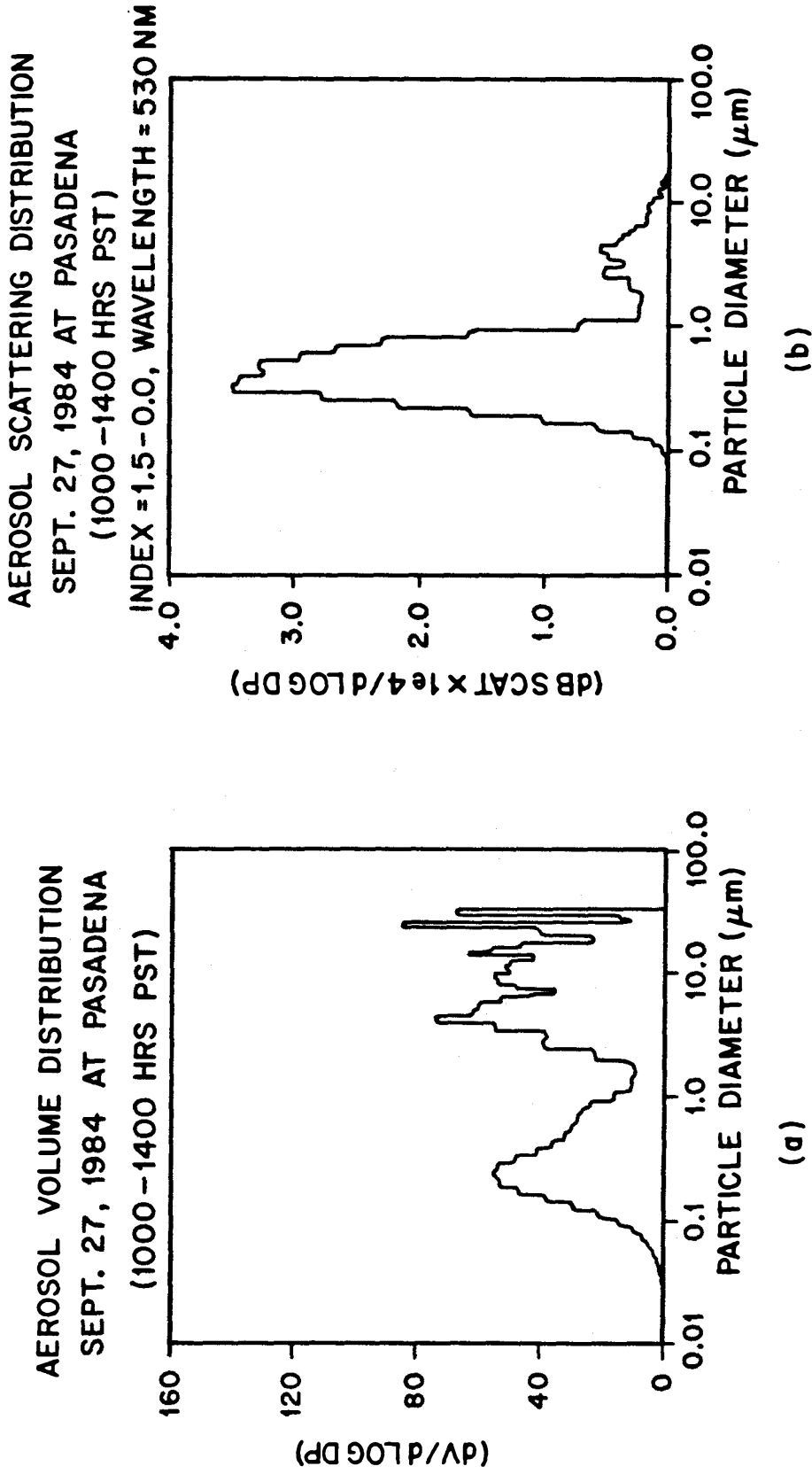
FIGURE 1.1. Volume distribution (a) and scattering distribution (b) for Pasadena aerosol measured on September 27, 1984.
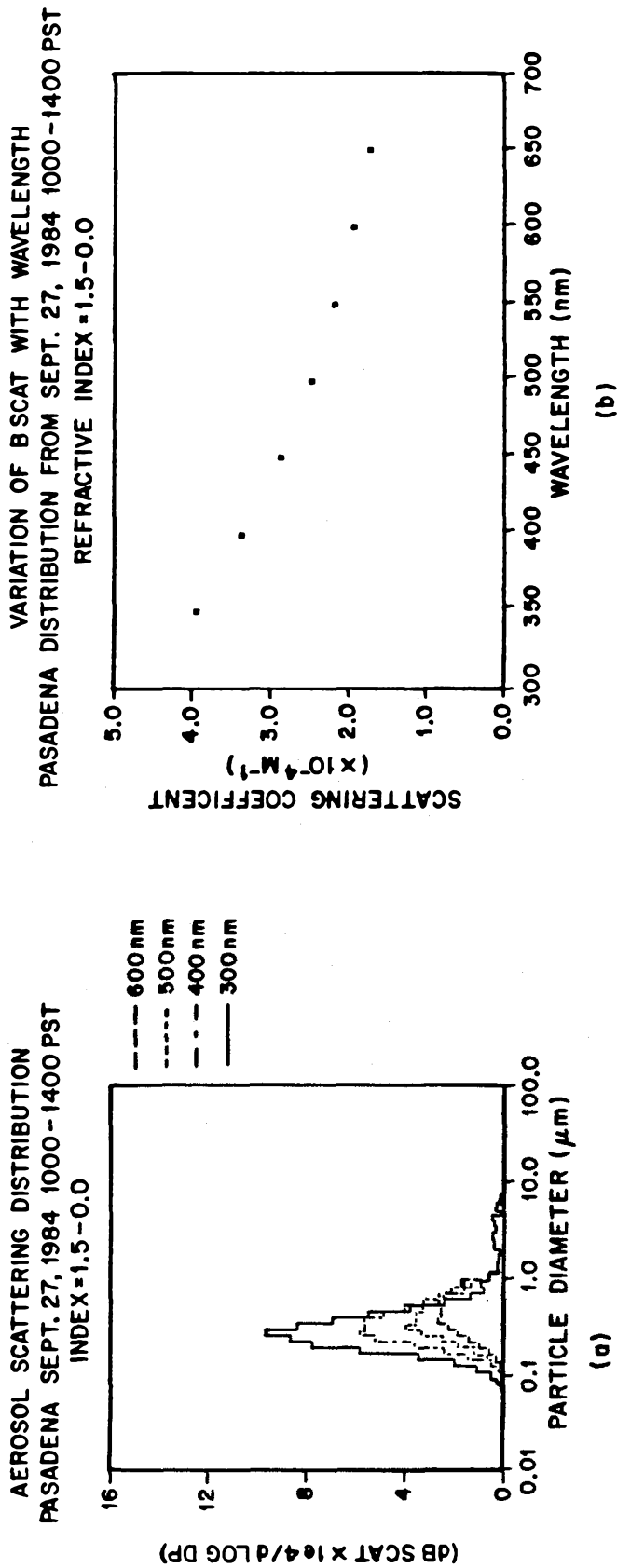
FIGURE 1.2. Dependence of scattering distribution
(a) and scattering coefficient (b) on wavelength.

Size distribution is for Pasadena aerosol measured on September 27, 1984. The assumed refractive
index is 1.5-0.0i.
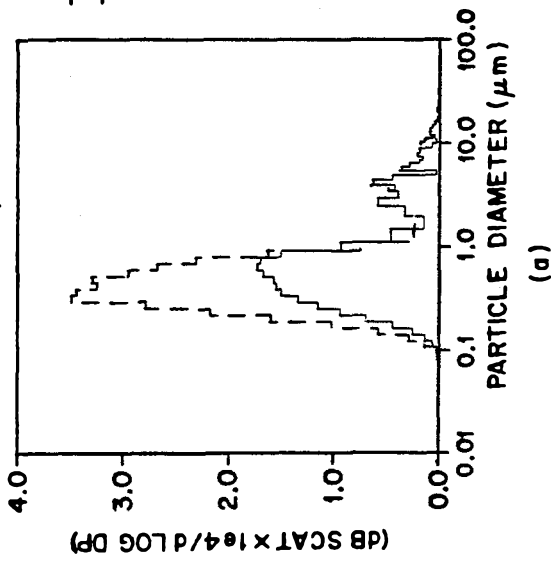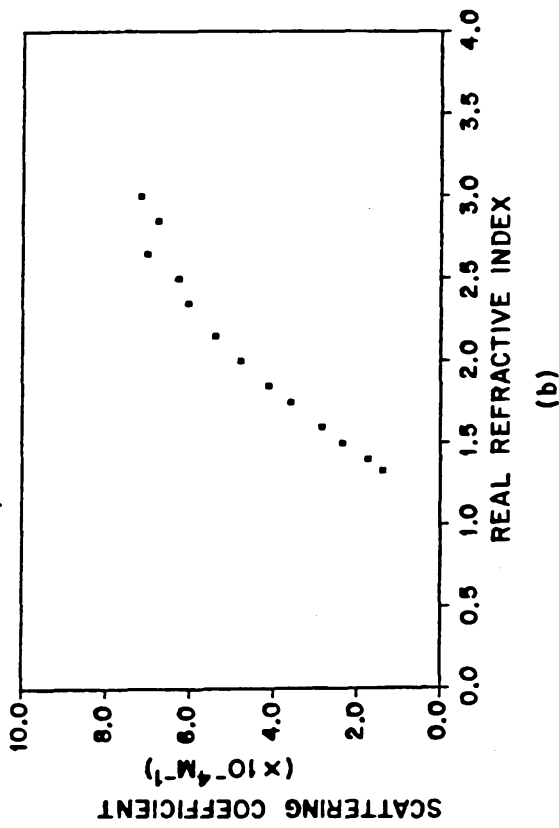
FIGURE 1.3. Dependence of scattering distribution (a) and scattering coefficient (b) on the real part of the refractive index.

Size distribution is for Pasadena aerosol measured on September 27, 1984. The assumed imaginary part of the refractive index is 0.0.
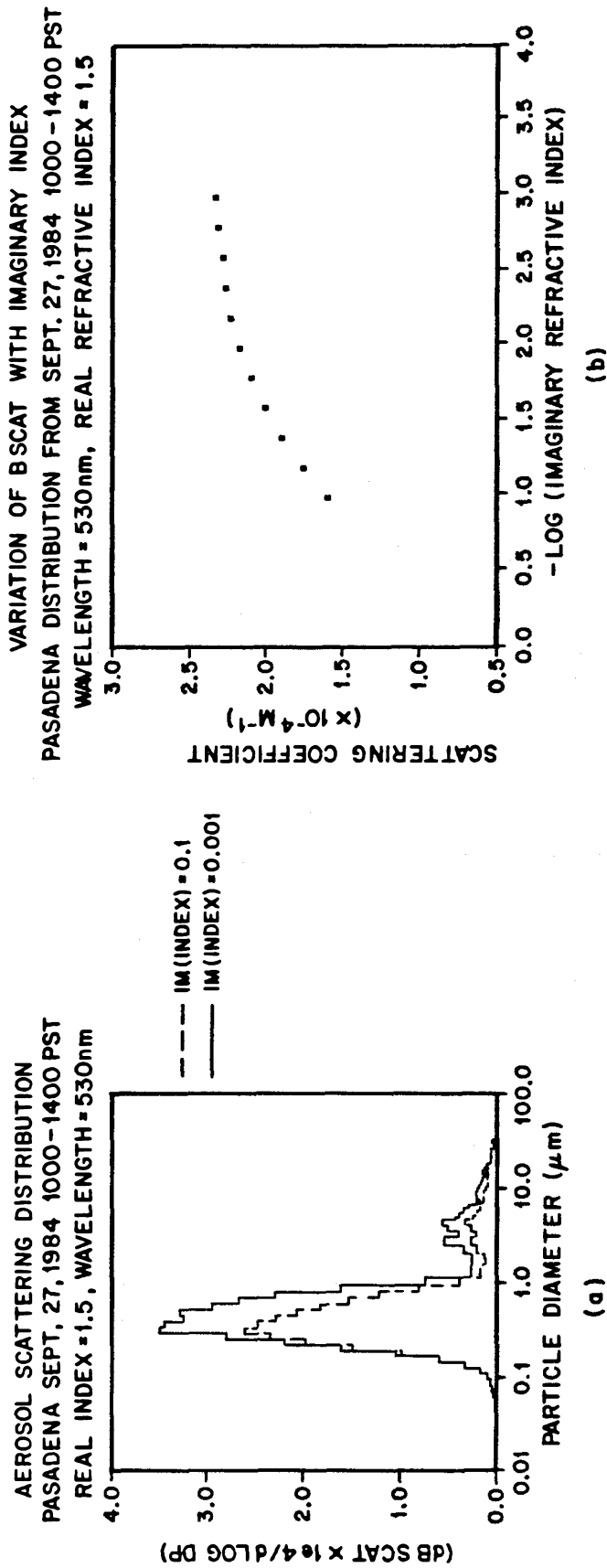
FIGURE 1.4. Dependence of scattering distribution (a) and scattering coefficient (b) on the imaginary part of the refractive index.

Size distribution is for Pasadena aerosol measured on September 27, 1984. The assumed real part of the refractive index is 1.5.
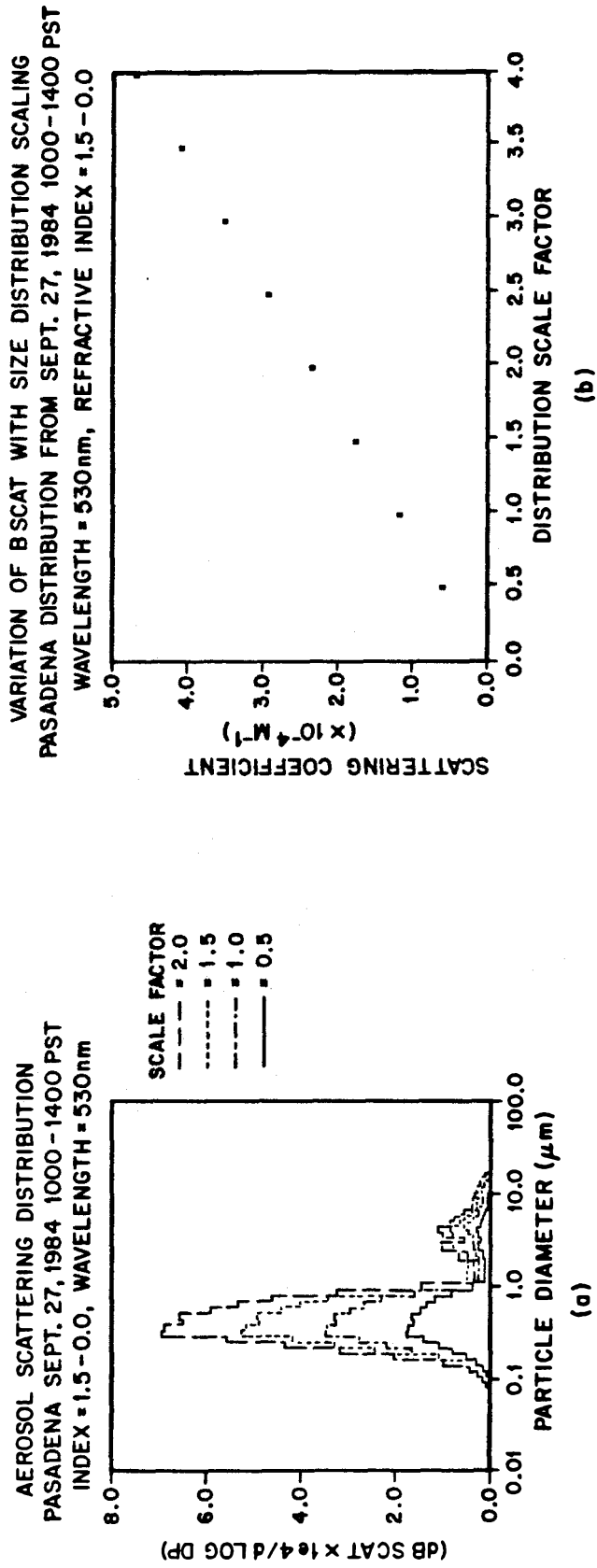
FIGURE 1.5. Dependence of scattering distribution (a) and scattering coefficient (b) on the total number concentration of particles.

Size distribution is for Pasadena aerosol measured on September 27, 1984. The assumed refractive index is 1.5-0.0i.

suspended particulate matter concentrations are sought. In order to deliberately engineer a solution to any air pollution problem, the problem first must be fully characterized. Pollutant concentration and chemical composition must be measured, along with the concomitant effects to be controlled, such as visibility reduction. The emission sources that contribute the pollutants of interest must be identified. Then mathematical models can be developed that describe the cause and effect relationships between pollutant emissions and resulting ambient pollutant concentrations, and between pollutant concentrations and effects such as reduction in visual range. These models must be tested against well defined case studies in order to demonstrate their accuracy. If a model is known to perform well, its predictive capabilities can be used to study the effect of proposed emission control strategies on air quality in advance of the actual construction of the control equipment involved. Controls can then be implemented with confidence that a goal can be met, whether the goal is to protect health, limit material damages, or control visibility. The use of a visibility model to predict the effect of an emission control program is shown schematically in Figure 1.6.

In this research, the sequence of steps from problem characterization, through model development and verification, to control strategy evaluation are applied to study the summer midday visibility problem in the Los Angeles area. Chapter 2 describes an experimental program that was conducted during 1984 to characterize the Los Angeles visibility problem during summer midday periods and to gain an understanding of the factors that contribute to that visibility problem. A calculation scheme is presented by which the atmospheric extinction coefficient is computed from the chemical and physical properties of the suspended particulate matter and from the concentration of light absorbing gases in the atmosphere. The calculated extinction coefficients are compared to measured values in order to assess the accuracy of the calculation procedure.

USE OF A VISIBILITY MODEL TO PREDICT
THE EFFECT OF AN EMISSION CONTROL PROGRAM

```
┌─────────────────────────┐
│   Select air pollutant  │
│   abatement program     │
└─────────────────────────┘
            │
            ▼
┌─────────────────────────┐
│      Reconstruct        │
│ aerosol size distribution│
│ and chemical composition │
└─────────────────────────┘
            │
            ▼
┌─────────────────────────┐
│      extinction         │
│      coefficient        │
└─────────────────────────┘
            │
            ▼
┌─────────────────────────┐        ┌─────────────────────┐
│  IMAGE  PROCESSING      │        │  Actual photograph  │
│                         │        │  of scene taken     │
│   ┌─────────────┐       │◄───────│  under very clean   │
│   │  VISIBILITY │       │        │     conditions      │
│   │   MODEL     │       │        └─────────────────────┘
│   └─────────────┘       │
└─────────────────────────┘
            │
            ▼
┌─────────────────────────┐
│  Simulated photograph   │
│    of scene in the      │
│     presence of         │
│    emission controls    │
└─────────────────────────┘
```
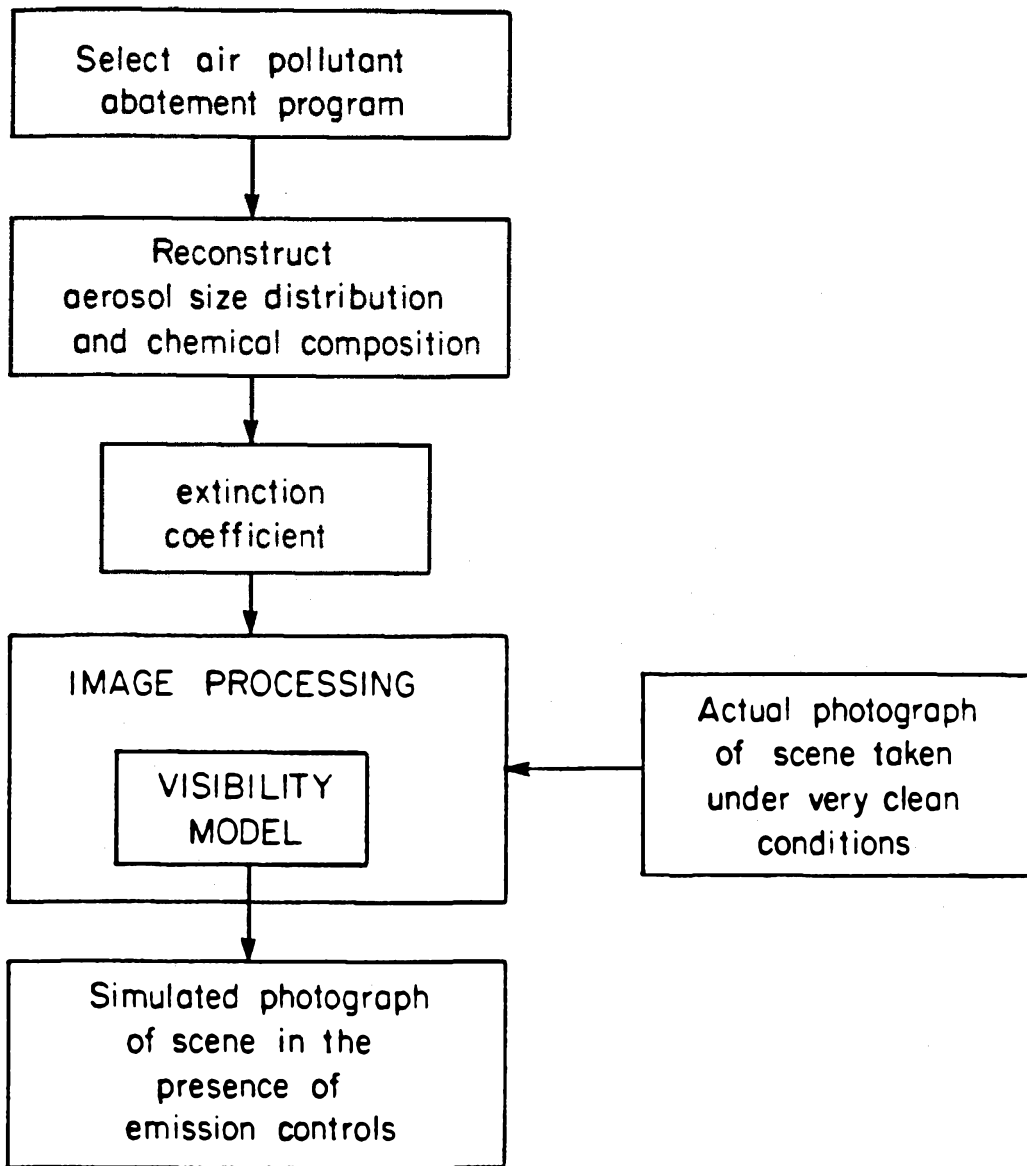
FIGURE 1.6. The use of a visibility model to predict the effect of an emission control program.

In Chapter 3 a simple image processing-based visibility model is presented, in which synthetic photographs are used to illustrate the results of visibility calculations. The simulated photographs illustrate the predicted appearance of a scene under specified air pollution conditions. To verify the model, the synthetic photographs are compared to actual photographs of the scene taken under the conditions modeled. Chapter 4 describes an attempt to improve the performance of the model in representing the color of the sky observed in polluted conditions.

The problem of visibility control is considered in Chapter 5, using the results of the aerosol carbon emission control strategy study by Gray (1986) which sought the most cost-effective controls available to reduce primary aerosol carbon concentrations in the Los Angeles area. The effect on visibility that would occur due to the reduction in carbon particle concentrations that could accompany Gray's proposed emission controls is predicted and discussed. Chapter 6 contains a summary of the findings of each chapter and restates the conclusions drawn from the work.

1.5 References

Allard, E. 1876. Mémoire sur l'intensité et la portée des phares. Dunod, Paris.

The American Heritage Dictionary of the English Language, 1980. Houghton Mifflin Company, Boston, MA.

Bennett, M.G. 1930. The physical conditions controlling visibility through the atmosphere. *Quarterly Journal of the Royal Meteorological Society* 56, 1-29.

Bouguer, P. 1760. Traité d'optique sur la gradation de la lumière. H.L. Guerin et L.F. Delatour, Paris.

Clausius, 1849. Poggendorff's Analen, **76**, 161; **84**, 449.

Duntley, S.Q. 1948. The reduction of apparent contrast by the atmosphere. *Journal of the Optical Society of America* 38, 179-191.

Gray, H.A., 1986. Control of atmospheric fine primary carbon particle concentrations. Ph.D. thesis, California Institute of Technology, Pasadena, California.

Hagenbach, 1872. Poggendorff's Annalen **147**, 77.

Hartley, 1889. *Nature* **39**, 474.

Koschmieder, H. 1924. Theorie der horizontalen Sechtweite. *Beitr. Phys. Freien Atm.* **12**, 33-53, 171-181.

Lallemand, 1872. Comptes Rendus de l'Acadèmie des Sciences **75**, 707.

McCartney, E.J. 1976. *Optics of the atmosphere – Scattering by molecules and particles*. Wiley, Chapters 1 and 3.

Middleton, W.E.K. 1968. *Vision through the atmosphere*. University of Toronto Press, Chapters 1, 2 and 3.

Mie, G. 1908. Beitrage zur Optik trüber Medien, speziell kolloidaler Metallösungen. *Ann. der Phys.* **25**, 377-445.

Minnaert, M. 1954. *The nature of light and color in the open air.* Dover.

Nichols, E.L. 1908. Theories of the color of the sky. Proceedings of the American Physical Society **26**, 297-511.

Pène Du Bois, W. 1947. *The Twenty-one Balloons.* Puffin Books.

Rayleigh, 1871a. On the light from the sky, its polarization and colour. *Phil. Mag.* **41**, 107-120, 274-279.

Rayleigh, 1871b. On the scattering of light by small particles. *Phil. Mag.* **41**, 447-454.

Rayleigh, 1899. On the transmission of light through an atmosphere containing small particles in suspension, etc. *Phil. Mag.* **47**, 375-384.

Saussure, H.B. de, 1789. Description d'un diaphanomètre ou d'un appareil propre à mesurer la transparence de l'air. *Mem. de l'Acad. de Turin* **4**, 425-440.

Schmauss, A., Wigand, A. 1929. Die Atmosphäre als Kolloid. Hamburg, F. Vieweg und Sohn.

Seinfeld, J.H. 1986. *Atmospheric chemistry and physics of air pollution.* Wiley, Chapters 1, 2 and 7.

Weber, L. 1916. Die Albedo des Luftplanktons. *Ann. der Phys.* **51**, 427-449.

Wild, H., 1868. Über die Lichtabsorption der Luft. *Ann. der Phys.* **134**, 568-583; **135**, 99-114.

Winkel, A., Jander, G. 1934. Schwebstoffe in Gasen (Aerosole) Stuttgart, F. Enke.

CHAPTER 2

CHARACTERISTICS OF SUMMER
MIDDAY LOW-VISIBILITY EVENTS
IN THE LOS ANGELES AREA

2.1 Abstract

A five-site air monitoring network provided data during the summer of 1984 on suspended particulate matter and on gaseous pollutants that contribute to the midday visibility problem in the Los Angeles area. Light scattering and absorption by fine aerosols caused more than 80% of the light extinction at the five sites studied. Carbonaceous aerosols and sulfates were responsible for approximately half of that fine aerosol burden.

Data taken at Pasadena were used to test a model for calculating the components of the extinction coefficient present on each experiment day. Computed scattering coefficient values at Pasadena on average are within 26% of the measured values. Comparison of the observed and predicted frequency distributions of the extinction coefficient values at Pasadena show that the median extinction coefficient value is reproduced closely. Agreement is less favorable for the higher extinction events. The model and data can be used to study the effect on visibility of an emission control program.

2.2 Introduction

The suspended particulate matter and gaseous pollutants present in the regional haze that frequently occurs in the Los Angeles air basin can act to decrease visual range to less than a few kilometers (Cass, 1979, Hidy et al., 1974, White and Roberts, 1977). In the Los Angeles area, photochemical smog is heaviest during the summer months of July, August, and September, and the midday periods during these months are often the times when severe visibility reduction is most apparent to the general public.

Light extinction in the atmosphere is caused by the scattering and absorption of light by suspended particulate matter and by gases. Thus the extinction coefficient, a measure of the amount of light scattered and absorbed in the atmosphere, can be expressed as a sum of several components: light scattering by particles (b_{scat_p}), light absorption by particles (b_{abs_p}), light absorption by gases (b_{abs_g}), and light scattering by air molecules $(b_{Rayleigh})$:

$$b_{ext} = b_{scat_p} + b_{abs_p} + b_{abs_g} + b_{Rayleigh} \qquad (2.1)$$

The value of the extinction coefficient can be obtained in several ways. A nephelometer can be used to measure the scattering contribution to the extinction coefficient (Charlson et al., 1967). If scattering is the main cause of light extinction in a region, then the nephelometer measurement provides an approximate value of the extinction coefficient (Harrison, 1979). The extinction coefficient also can be measured using telephotometers or teleradiometers (Dzubay and Clubb, 1981; Harrison and Mathai, 1981; Malm et al., 1981). Alternatively, visual range values obtained by human observers can be inserted into Koschmieder's formula in order

to estimate the extinction coefficient (Johnson, 1981; Hoffmann and Kuehnemann, 1979). Koschmieder's formula is expressed by:

$$V_R = \frac{-lnA}{b_{ext}} \qquad (2.2)$$

where V_R, the visual range, is the distance at which an average observer can just barely distinguish a black object silhouetted against the horizon sky (McCartney, 1976). This meteorological visual range is routinely measured by trained observers at controlled airports and is reported in terms of the visual range which prevails around at least half of the horizon circle, but not necessarily in continuous sectors (Williamson, 1973). Parameter A in Equation 2.2 represents the limiting contrast threshold for visual detection by the average human observer. Proposed values for the parameter A vary considerably, but values from 0.02 to 0.05 are commonly used (Middleton, 1968). The applicability of Koschmieder's formula depends on the accuracy of the value chosen for the threshold contrast, the availability of black target objects, and on the uniformity of illumination and atmospheric properties between the observer and horizon (Middleton, 1968).

In order to deliberately engineer an improvement in visibility, the specific pollutants causing the reduction in visibility must be identified. Several researchers (White and Roberts, 1977; Cass, 1979; Trijonis, 1979; Groblicki et al., 1981) have employed regression analyses between observed extinction coefficients and pollutant concentrations to estimate the level to which certain pollutants affected visibility. There are potentially serious disadvantages to this approach, however. Empirically determined extinction efficiencies that are unrealistically high or low can be obtained for some aerosol species, and estimation of the effect on visibility of liquid water in the aerosol poses problems. An alternative to purely empirical visibility analyses can be constructed in which the physical and chemical nature

of the suspended particulate matter and of the gaseous pollutants are used to calculate on a physical basis the contributions to the extinction coefficient by means of Mie theory. Given the size distribution and chemical composition of the atmospheric aerosol and NO_2 concentration data, the extinction coefficient can be calculated directly (Ouimette, 1980; Larson et al., 1987). Such visibility models have yet to be used as an integral part of the design process for engineering improvements in regional visibility, most probably because the data requirements of such models are difficult to satisfy.

The purpose of the present study is to develop an experimental protocol and a visibility modeling approach which is based directly on theories of light scattering and absorption by which the causes of regional visibility problems can be characterized. Methods developed are tested in the Los Angeles area, and the goal of that investigation is to both measure and model the frequency distribution of the summer midday low visibility events for which Los Angeles is so well known. First, an atmospheric sampling program conducted at five sites in the Los Angeles area is described. Measurements made every sixth day during the summer of 1984 are used to acquire a data base representative of the distribution of visibility events occurring in that summer. From the chemical and physical description of the aerosol resulting from the sampling program, both scattering coefficient and extinction coefficient values are calculated. The calculated results are compared to the extinction coefficient values estimated from airport observations of visual range. Comparisons are also made between the calculated scattering coefficients and the scattering coefficients measured with nephelometers. These results provide a baseline description of the cause and effect relationship between the various air pollutants and visual range that can serve as a basis for the design of an emission control program directed at improving visibility in portions of the Los Angeles air basin during summer midday periods.

2.3 Experimental Program

During the summer months of July, August, and September of 1984, a sampling network consisting of five stations was operated in the Los Angeles air basin. Geographically, the site locations spanned a distance of over 95 kilometers, from Lennox, California (located eight kilometers from the coast) eastward to San Bernardino. The intermediate sites were located at Pasadena, Azusa, and Upland, California (Figure 2.1). Atmospheric aerosol samples were collected at each station from 1000-1400 hours (PST) every sixth day over the summer, for a total of fifteen experiment days. Each of the particulate sampling stations was colocated with a South Coast Air Quality Management District (SCAQMD) air monitoring station. The SCAQMD data on NO_2 concentrations were used to supplement the particulate sampling network data. Airport weather (including temperature and relative humidity information) and visibility reports were available near the Lennox, Pasadena, Upland and San Bernardino sites (Table 2.1). The Pasadena, Upland, and Azusa sites were equipped with integrating nephelometers (Meteorology Research, Inc. model 1550) for measurement of the atmospheric scattering coefficient.

In order to characterize the chemical composition of the aerosol, 4-hour average filter samples were taken for both fine particulate matter ($d_p \leq 2.1 \ \mu$m) and for total particulate matter. Information on the coarse mode aerosol ($d_p \geq 2.1 \ \mu$m) was determined by subtracting fine particulate matter concentrations from total particulate matter concentrations. Fine particle samples were collected downstream of an AIHL-design cyclone separator (John and Reischl, 1980) which removed the coarse particulate matter from the air stream. In each size range, a set of three parallel filter holders was used for sample collection, each filter holder containing a
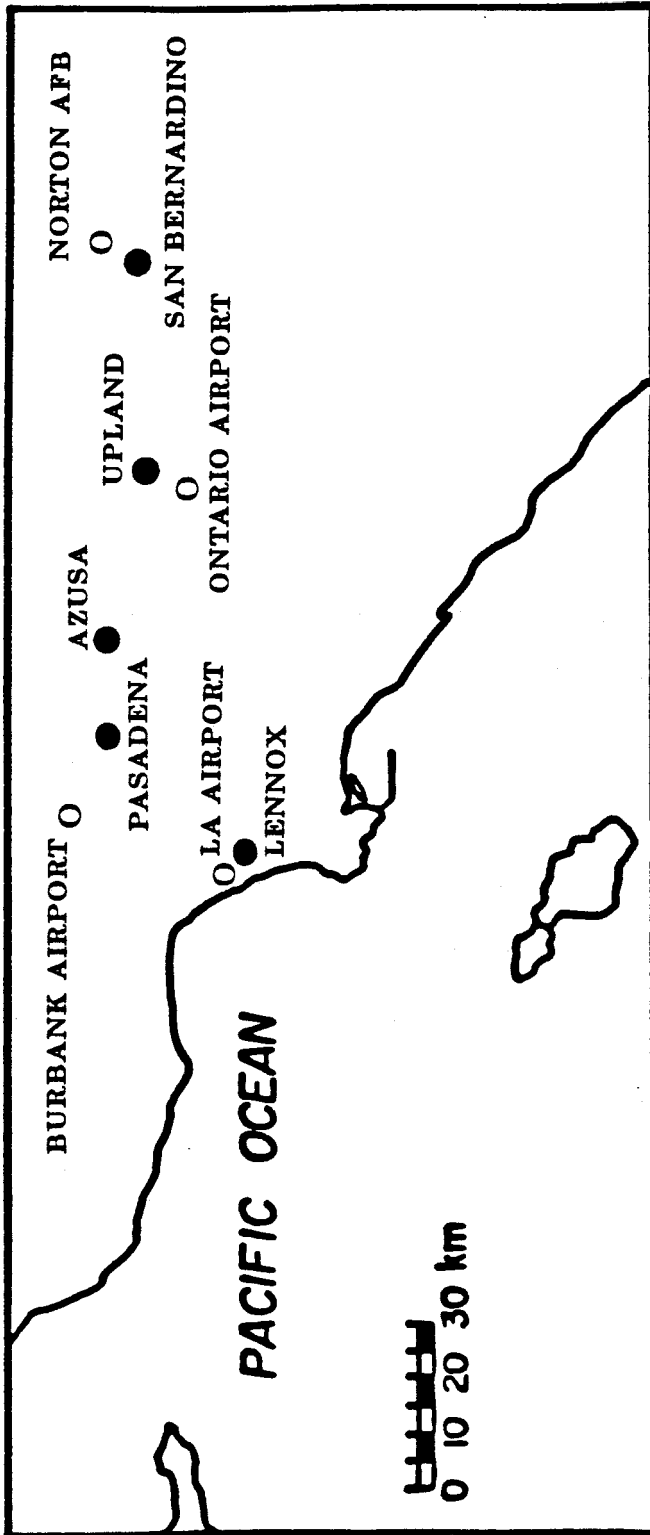
FIGURE 2.1. Air monitoring site locations (•) and airports (O).

TABLE 2.1. Distance between site location and nearest airport.

Airport	Station	Distance
Los Angeles	Lennox	4.8 km
Ontario	Upland	5.6 km
Norton Air Force Base	San Bernardino	1.6 km
Burbank	Pasadena	16.1 km

filter substrate that was compatible with a particular chemical or physical analysis. A 47 mm diameter Teflon (Membrana) filter, through which air was sampled at a rate of 10 lpm, was used to determine the dry mass concentration of suspended particulate matter by repeated weighing at low relative humidity before and after sampling. The samples collected on the Teflon filters also were analyzed by X-ray fluorescence analysis (XRF) to quantify the concentration of 34 trace elements (ranging in atomic weight from aluminum to lead) present in the aerosol.

Aerosol samples for ionic species determination were collected on Nuclepore filters (47 mm diameter, 0.4 μm pore size) at an air flow rate of 5 lpm. The Nuclepore filters then were extracted and information on the concentration of the water soluble ions NO_3^-, and $SO_4^=$ was obtained by ion chromatography. These samples also were analyzed by atomic absorption for the concentrations of Na^+, K^+, Mg^+, and Ca^{+2}. Sulfur, potassium and calcium were measured by more than one method and a choice between data sets must be made. The concentration of these elements obtained by XRF was used for subsequent calculations. Aerosol samples collected on quartz fiber filters (Pallflex QAO, 47 mm diameter, air flow rate 10 lpm) were analyzed by the method of Johnson et al. (1981) to determine the organic and elemental carbon concentrations. These filters were prefired to 600°C for two hours prior to use in order to reduce their carbon blank.

At Pasadena, this filter-based sampling system was accompanied by a photographic record of visual conditions and by measurement of the aerosol size distribution, relative humidity and solar radiation intensity, making the Pasadena site the most extensively equipped site on the network. The aerosol size distribution was measured with a Thermal Systems Incorporated electrical aerosol analyzer (EAA) over the particle diameter range from 0.0075 μm to 1.0 μm and with a Particle Measuring Systems model CSASP-100-HV optical particle counter (OPC) in 31

particle diameter intervals over the range from 0.5 μm to 50 μm. Measurements of total solar radiation intensity were made with an Eppley Laboratory pyranometer (model PSP). To document the visual conditions at Pasadena, photographs were taken of five standard vistas at noon (PST) during each sampling period. The photographs were taken from the roof of the 44-meter-tall Millikan Library on the Caltech campus. This vantage point allowed for unobstructed views of several scenes which varied in direction and character (same scenes as in Larson et al., 1987). Pictures were taken utilizing camera mounts and a tripod to ensure reproducibility of the field of view. A Canon TLb, 35 mm, single-lens-reflex camera equipped with an ultraviolet light cutoff-filter was used to take photographs of each scene over a range of f-stops to ensure proper exposure. A Kodak color chart was incorporated in each series of photographs in order to confirm accurate color reproduction. Kodachrome ASA 25 film was used for all of the field photographs.

2.4 Data Analysis

The data set acquired during the 1984 summer experiments will be evaluated to address two objectives. First, the data set will be used to provide a description of the Los Angeles summer midday low-visibility problem by detailing information on both the visual range and corresponding pollutant concentrations and composition. Then that data set will be used to test the ability of model calculations to link pollutant particle size distribution and composition measurements to visual range in a cause and effect manner.

Midday Extinction Coefficient Values. The frequency distribution of summer extinction coefficient values at Los Angeles area airports averaged over the midday period 1000-1400 hours PST is shown in Figure 2.2. These values were obtained by conversion of human observer visual range data into extinction co-

efficient values using Koschmieder's formula with the contrast threshold (A in Equation 2.2) set to 0.02. The solid curve is formed from data for all days of record during the months July, August and September, while the triangles mark the extinction coefficient values on the 15 days that the aerosol sampling experiments described in this paper were conducted. It is seen that the aerosol sampling events are distributed over the range of high and low visibility events that occurred that year. The 50th percentile extinction coefficient value increases from 2.3×10^{-4} m^{-1} (corresponding to 17.0 km visual range) at the coast near Los Angeles International Airport (LAX) to 3.4×10^{-4} m^{-1} (11.5 km visual range) at the inland site at Ontario. The lowest median visual range (highest median b_{ext} value) among the airport sites examined is at Ontario. These data are consistent with the spatial distribution of the long term average airport visual range data for the Los Angeles area presented by Trijonis (1980) which likewise show that the lowest average airport visibilities in this area occur near Ontario. The Los Angeles International Airport site, which experienced the lowest median extinction coefficient value during the summer of 1984, also experienced the highest single day worst case extinction coefficient value, as seen in Figure 2.2. Clearly, no single statistic adequately conveys the visibility differences between the sites studied, illustrating the merit of describing regional visibility problems in terms of the frequency distribution of high and low visibility events.

Aerosol Characteristics. Day-to-day changes in the light scattering and absorption by aerosols are the principal cause of the variations in extinction coefficient and visual range shown in Figure 2.2. In order to provide a description of aerosol properties to support scattering and absorption calculations, the data from the large number of independent measurements of aerosol properties made during the summer of 1984 were used.

-27-
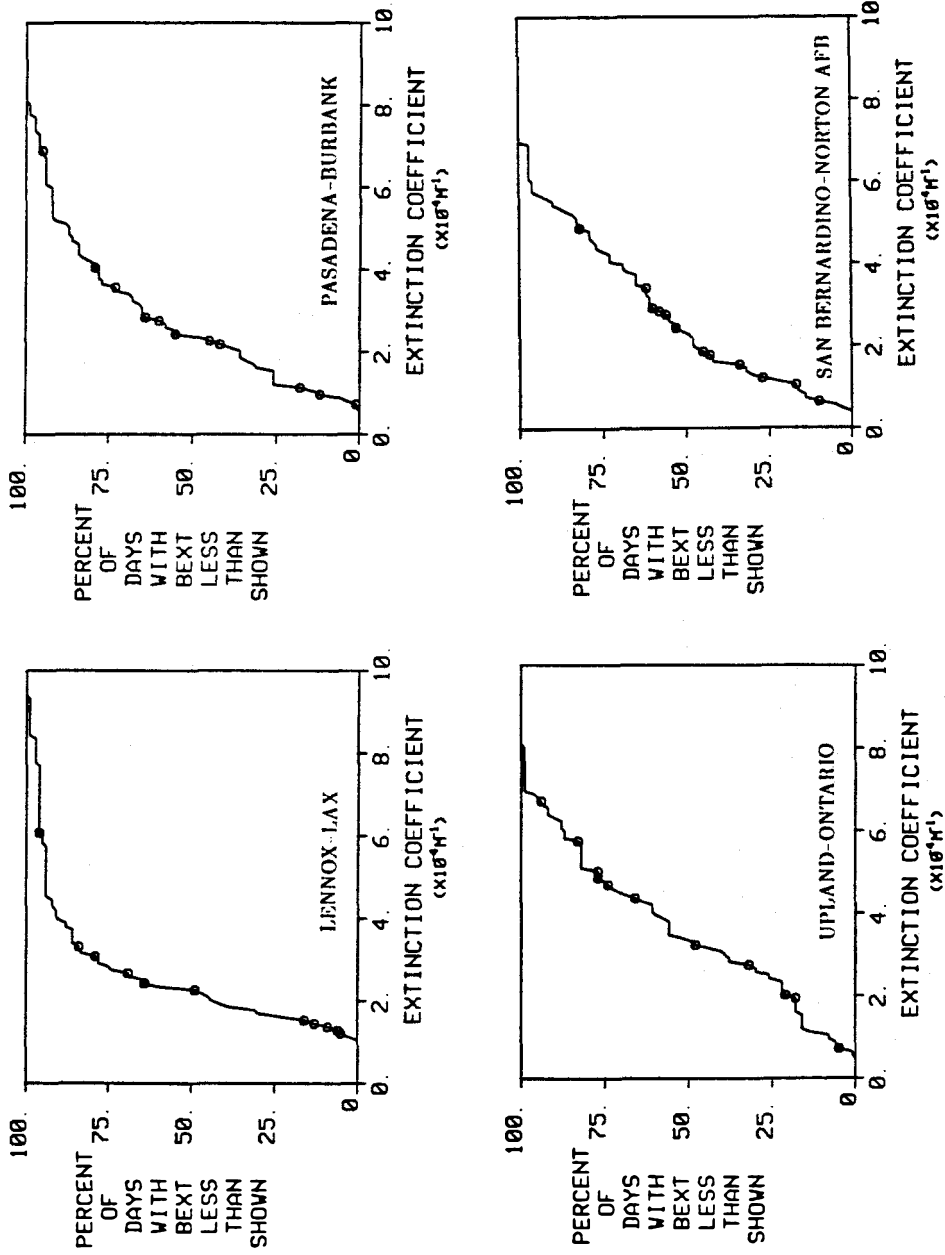
FIGURE 2.2. The frequency distribution of summer extinction coefficient values at Los Angeles area airports averaged over the midday period 1000-1400 hours PST.

To construct a material balance on the chemical composition of the aerosol, the procedure of Larson et al. (1987) was followed. In this procedure, trace metals measured were converted to their common oxides (Stelson and Seinfeld, 1981). The mass of organic carbonaceous material was taken to be 1.4 times the organic carbon mass measured (Gray et al., 1986). An ion balance on the water soluble ionic compounds in the aerosol was constructed, and NH_4^+ ion in the aerosol was estimated to be present in the amount needed to close the ion balance. The speciation of ionic material was assigned according to the scheme in Table 2.2. A portion of the airborne particulate matter may not be identified by the chemical analyses performed. Using the nomenclature of Sloane (1984), this mass of dry material that is measured gravimetrically, but not accounted for in the chemical analysis is refered to as the "residue". Following chemical characterization, the aerosol water content during each sampling event was estimated using the semi-empirical approach formulated by Sloane (1984). In this procedure, data on the ambient relative humidity and the particulate matter solubility are used to estimate the amount of water present in the aerosol.

The results of the chemical analysis of the filter samples are presented in Figures 2.3 and 2.4, where the chemical composition of fine and coarse particulate matter for the 1000-1400 hour (PST) period on experiment days for each site are shown. Data collected on the experiment days indicate the character of the aerosol present during summer midday periods in the Los Angeles area. Table 2.3 lists the average chemical composition for each site over the summer for the fine and coarse particle modes. Results indicate the presence of sulfate in the fine particle mode, with nitrates appearing mostly as coarse suspended particulate matter. Elemental carbon and organic material are important contributors to the fine aerosol component, and are also present in the coarse particulate matter. Crustal material (included in the category of "other identified" material) makes, as would

TABLE 2.2. Speciation of ionic material.

Na^+	was associated with	Cl^-
NH_4^+	was associated with	SO_4^{-2}
NH_4^+	remaining, if any, was associated with	NO_3^-
Na^+	remaining, if any, was associated with	NO_3^- remaining, if any
Na^+	remaining, if any, was associated with	SO_4^{-2} remaining, if any

be expected, a greater contribution to the coarse material. There is noticeably more coarse airborne crustal material at the eastern sites (Azusa, Upland, San Bernardino) than at the more westerly locations (Lennox and Pasadena). Aerosol water is estimated to constitute from 4.4% to 17.0% of the fine aerosol on average at midday during the summer. Waggoner et al. (1981) find a 14% increase in light scattering between a Pasadena aerosol at 30% relative humidity and the same aerosol at 60% relative humidity. This small increase indicates that a small amount of water is present in the aerosol at 60% relative humidity. The relative humidities at midday during the 1984 summer were observed to average only 45.0% (range 14.6% to 67.2%), and the small amount of water estimated to be present in Table 2.3 is consistent with Waggoner et al.'s data.

Scattering Coefficient Calculations. At the Pasadena monitoring site, aerosol size distribution data were taken in conjunction with the measurements of aerosol chemical characteristics. At that site, the atmospheric aerosol scattering coefficient and the total light extinction coefficient were computed from aerosol properties and other available data using the data reduction procedure of Larson et al. (1987). The calculation proceeded as follows.

Using the measured masses of individual chemical constituents, and the densities of these components, the contributions to total aerosol volume were first calculated. From the volume contributions, the volume average refractive indices for the fine and for the coarse modes of the aerosol size distribution were computed based on the refractive indices for each component. These refractive indices were used along with the size distributions in a Mie scattering code to calculate the aerosol scattering coefficient, b_{scat_p} (Wickramasinghe, 1973). A typical example of the translation of the particle size distribution into the distribution of light scattering as a function of particle size is given in Figure 2.5. Although fine par-

CHEMICAL COMPOSITION OF FINE PARTICULATE MATTER

SUMMER 1984 (1000-1400 PST)
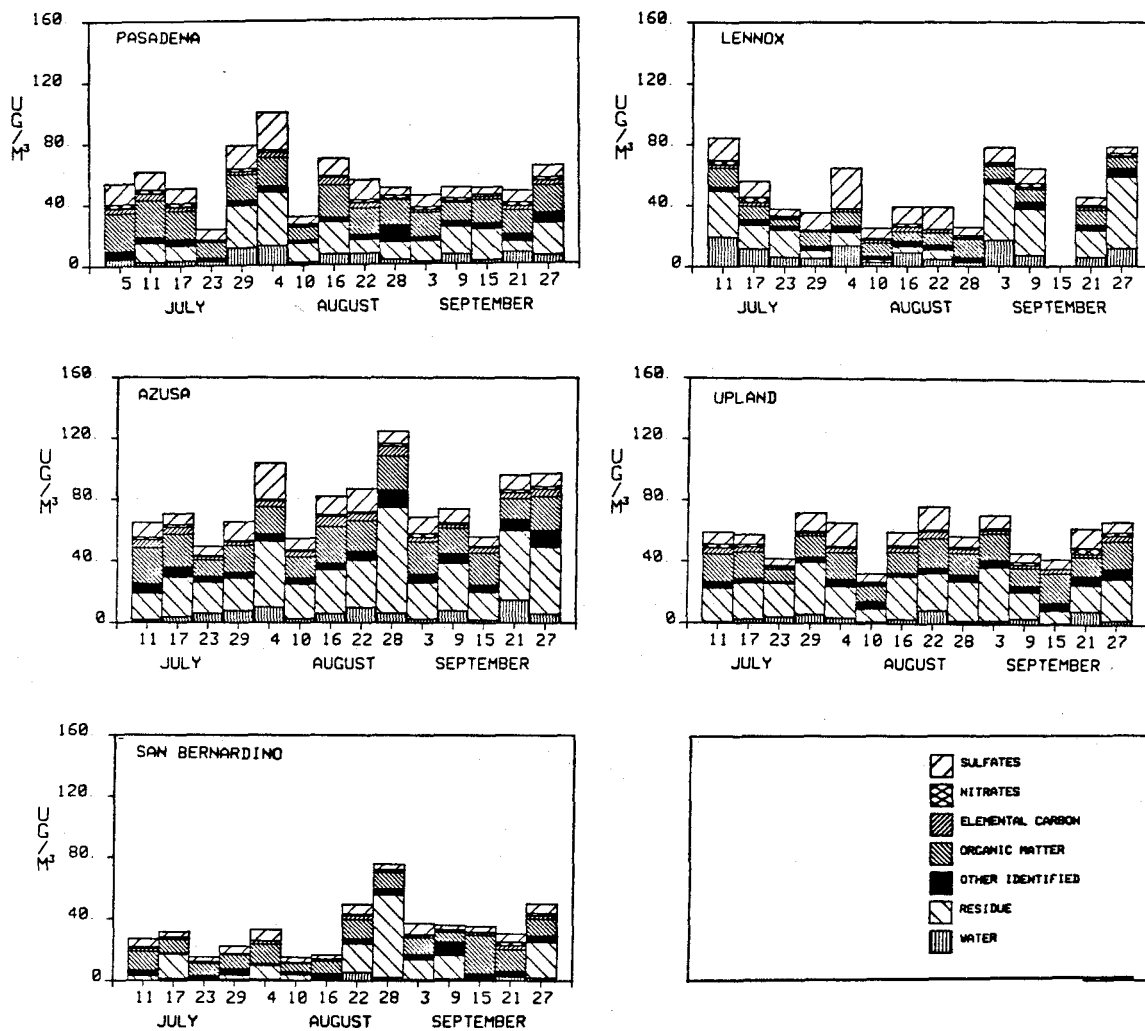
FIGURE 2.3. Chemical composition for the fine suspended particulate matter for each site.

CHEMICAL COMPOSITION OF COARSE PARTICULATE MATTER

SUMMER 1984 (1000-1400 PST)
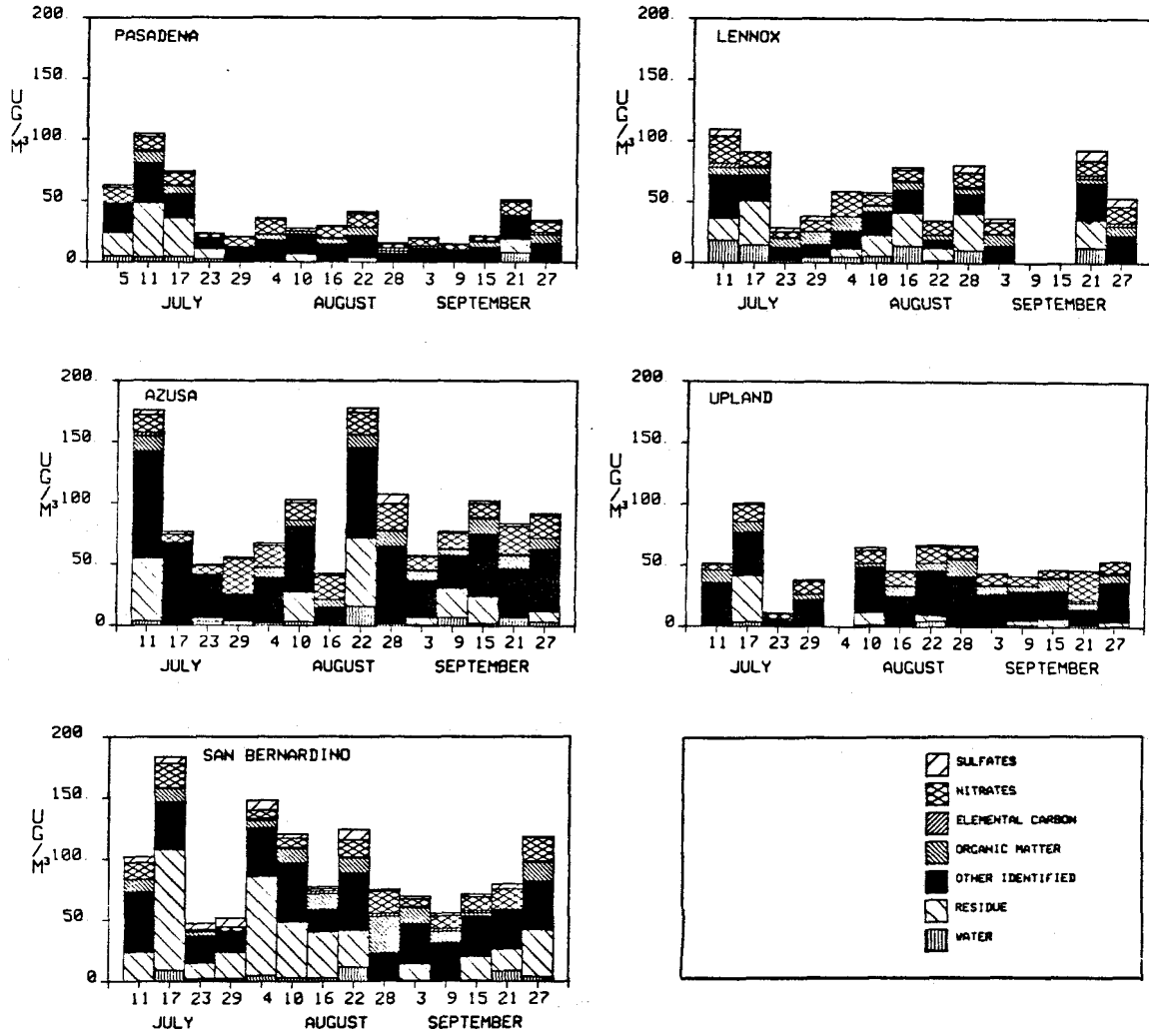
FIGURE 2.4. Chemical composition for the coarse suspended particulate matter for each site.

TABLE 2.3. Average chemical composition of aerosol.

Average per cent by mass of fine suspended particulate matter

	Lennox	Pasadena	Azusa	Upland	San Bernardino
Sulfates	21.3	18.0	13.4	14.8	14.8
Nitrates	3.0	3.4	1.8	2.6	2.9
Elemental Carbon	3.8	4.4	5.3	4.8	4.2
Organics	19.8	32.0	25.3	26.6	36.9
Other Identified	7.4	8.1	7.9	7.5	11.8
Residue	27.7	24.4	38.4	37.6	25.1
Water	17.0	9.7	8.0	6.1	4.4
Fine mass ($\mu g/m^3$)	52.0	55.6	78.3	58.1	34.1

Average per cent by mass of coarse suspended particulate matter

	Lennox	Pasadena	Azusa	Upland	San Bernardino
Sulfates	5.8	3.5	2.8	1.7	4.8
Nitrates	20.1	21.4	20.7	21.5	11.6
Elemental Carbon	1.8	2.5	0.8	1.2	1.3
Organics	13.7	9.1	8.0	13.7	11.2
Other Identified	29.4	45.9	52.0	52.6	38.0
Residue	18.6	12.7	11.4	6.9	29.1
Water	10.7	4.9	4.4	2.4	4.1
Coarse mass ($\mu g/m^3$)	63.6	38.8	90.7	52.5	94.8

ticle and coarse particle modes contribute comparable amounts of material to the Pasadena aerosol volume distribution, light scattering is dominated by scattering by particles smaller than 1 μm in diameter.

By combining these scattering coefficient predictions with data on aerosol light absorption, light absorption by NO_2, and scattering by air molecules, midday values of the total atmospheric extinction coefficient were computed at Pasadena. The particle absorption coefficient, b_{abs_p}, was obtained by multiplying the measured total elemental carbon concentration by the light absorption efficiency of Los Angeles elemental carbon. The light absorption efficiency of Los Angeles elemental carbon was taken to be 11.9 m^{2}g^{-1}, as measured by Conklin and Cass (1981). The chief gaseous pollutant which absorbs light is NO_2. The gaseous absorption coefficient, b_{abs_g}, was determined from the dependence of the absorption of light by NO_2 on NO_2 concentration (Dixon, 1940; Hodkinson,1966; Groblicki et al., 1981). Tabulated values of the Rayleigh scattering coefficient for the atmospheric gases were taken from Penndorf (1957), and were corrected for ambient temperature on each experiment day. Results of the calculated contributions to the atmospheric extinction coefficient at Pasadena are presented in the upper right hand corner of Figure 2.6.

Model Evaluation. In order to test the validity of the calculations, the modeled extinction coefficients values at Pasadena were compared to the extinction coefficients implied by the measured visual ranges acquired at the closest airport. Modeled scattering coefficients were also compared to the scattering coefficients measured by a nephelometer located at that site. Since the calculated components of the extinction coefficient are wavelength dependent, this dependence must be taken into account when making comparisons between measured and modeled values.
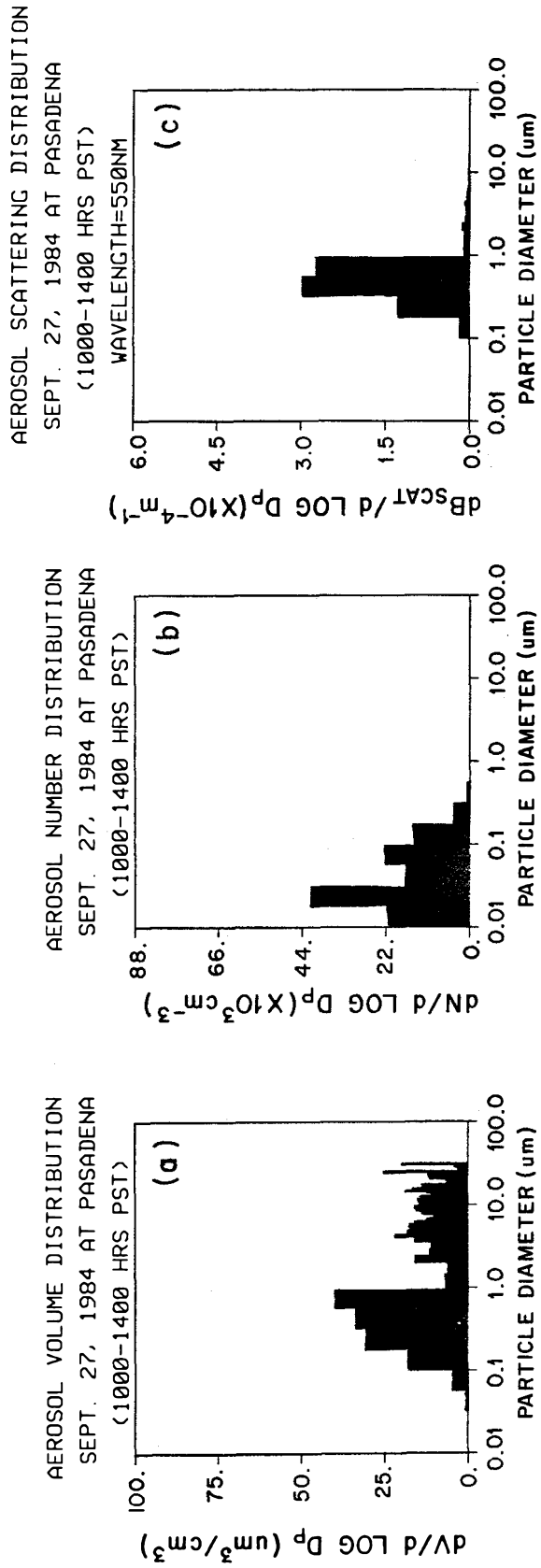
FIGURE 2.5. Aerosol volume, number, and scattering
distributions for the Pasadena site on September 27, 1984.

(a) Aerosol volume distribution, (b) Aerosol number distribution, (c) Aerosol scattering distribution.

CONTRIBUTION TO THE EXTINCTION COEFFICIENT

SUMMER 1984 (1000-1400 PST)
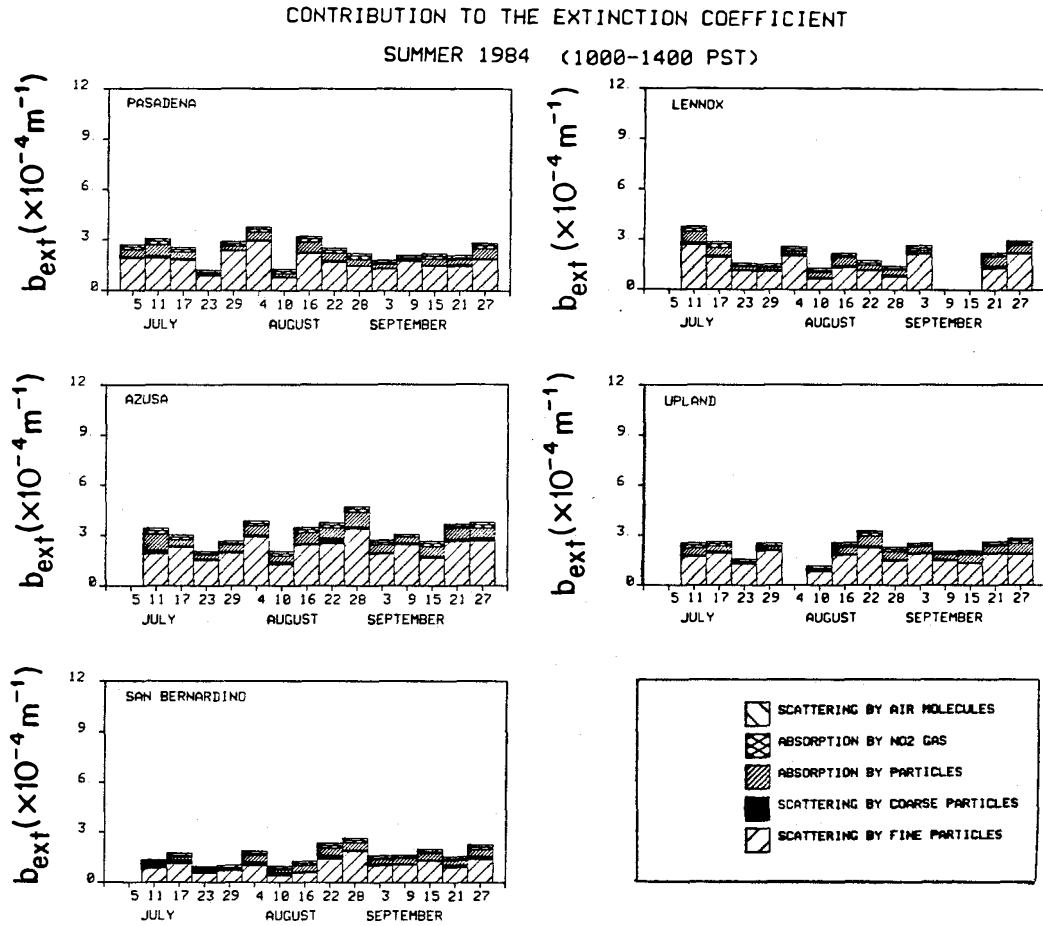
FIGURE 2.6. Average modeled (wavelength=550 nm) contributions to the extinction coefficient $(\times 10^{-4} m^{-1})$ for each site.

The human eye has maximum sensitivity at a wavelength of approximately 550 nm (Middleton, 1968). This wavelength is the chosen value for defining the standard visual range which is obtained by using Koschmieder's formula (Heintzenberg and Quenzel, 1973). When comparing the extinction coefficient values inferred from human observer reports at the airports against modeled extinction values, the calculations were carried out at a wavelength of 550 nm.

However, the light source in the MRI 1550 nephelometer has a broad spectrum centered more about the blue wavelengths. In this model nephelometer, the light source is a xenon flashtube equipped with an ultraviolet cutoff filter. The model 1550 has been estimated to have a "peak wavelength" of 480 nm (Harrison, 1979) and a "peak sensitivity" of between 460 and 490 nm (Charlson et al., 1967). Harrison (1979) reports "effective wavelengths" in the range of 479-488 nm, and early instrument calibrations were based on an assumed effective wavelength of 460 nm (Ahlquist and Charlson, 1967, 1968; Charlson et al., 1967). In this work, a wavelength of 460 nm was used in the calculation of the scattering coefficients that are compared against nephelometer measurements.

Direct comparisons of the measured and modeled scattering coefficient (wavelength = 460 nm) at Pasadena and the frequency distribution of the modeled extinction coefficients at Pasadena (wavelength = 550 nm) versus the measured extinction coefficient at Burbank Airport (threshold contrast of both 0.02 and 0.05) are shown in Figure 2.7. Observed and predicted scattering coefficient values at Pasadena are highly correlated (r = 0.83). On average, the predicted scattering coefficient values are lower than actual observations by 26%. That degree of agreement between Mie theory calculations and field observations is comparable to that obtained by other recent investigations. Ouimette (1981) reported an average ratio of scattering coefficients as calculated by Mie theory to scattering coefficients as measured by a nephelometer of 0.85±0.34 for Zilnez Mesa in Arizona. For a

China Lake, California, site the calculated values overestimated measured values by an average of 52%. Agreement to within 7-11% was found by Dzubay and Clubb (1981) between telephotometer measurements of the extinction coefficient and the sum of nephelometer b_{scat} measurements, opal glass b_{abs_p} determinations, and b_{abs_g} obtained from NO_2 concentrations. Sloane (1983) used Mie theory to calculate scattering coefficients with agreement between predicted and measured values of 5-36%, depending on whether an internal or external aerosol mixture was considered. In that work, the amount of the residue was determined by regression between scattering coefficients and aerosol components. In previous work Larson et al. (1987) obtained agreement to within 20% between measured and modeled scattering coefficient values.

Examination of Figure 2.7b shows that median extinction coefficient values predicted from pollutant data at Pasadena and observed at Burbank Airport are in close agreement. The highest extinction coefficient event at Burbank is underpredicted by data taken at Pasadena. Exact agreement is not expected in this case. Burbank and Pasadena are separated by a distance of 16 km, which is greater than the distance to extinction on a very smoggy day. The pollutant properties at these two sites could easily differ by enough to account for the differences shown in Figure 2.7b.

Light Extinction Estimates at Other Sites. At monitoring sites other than Pasadena, all of the aerosol and other data needed to use the light scattering model are available except for the requisite aerosol size distribution measurements. In previous studies (Gray et al., 1986), it has been noted that the long-term average fine aerosol chemical composition (e.g., percentage of sulfates, elemental and organic carbon) is similar at most sites in the western portion of the Los Angeles basin, while the fine aerosol concentration (fine mass in $\mu g/m^3$) varies
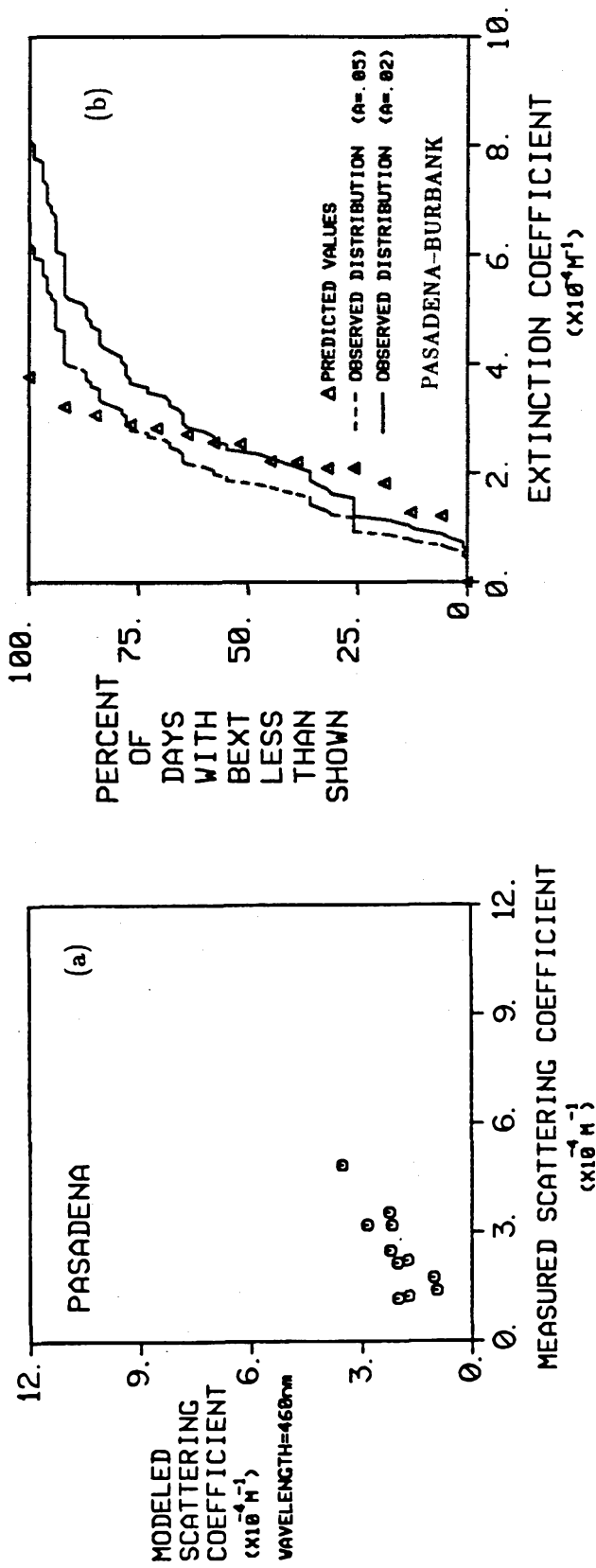
FIGURE 2.7. Measured versus modeled (wavelength=460 nm) scattering coefficient and extinction coefficient frequency distribution for Pasadena.

from site to site. If relative fine aerosol properties were similar from site to site, but the sites differed mainly in the total number concentration of particles present, then the relative aerosol size distribution measured at Pasadena over a particular midday period might be used to approximate the relative aerosol size distribution at other monitoring sites on that day.

To test that hypothesis, the aerosol size distributions for the fine particle mode and the coarse particle mode measured at Pasadena were rescaled separately to match the fine aerosol and coarse aerosol volumes implied by the filter-based measurements made at Lennox, Azusa, Upland and San Bernardino on the same experiment day. The volume-average refractive index for fine and coarse aerosol was computed on a site-by-site basis by the method described previously. Then predicted midday light scattering coefficient and extinction coefficient values were calculated as before for Lennox, Azusa, Upland and San Bernardino for the summer of 1984. Average contributions to the extinction coefficient at all sites are shown in Table 2.4, and the differences between individual days are shown in Figure 2.6. Scattering coefficient predictions were compared to measured values at sites equipped with nephelometers as shown in Figure 2.8, and the distributions of predicted extinction coefficient values were compared to extinction coefficients estimated from airport observer data at those sites near airports, as shown in Figure 2.9.

The observed and predicted extinction coefficient frequency distributions (Figure 2.9) match as well for the Lennox-LAX site as they did for the Pasadena-Burbank site at which all model inputs were obtained by direct measurements at Pasadena. Lennox is located directly upwind of Pasadena on average during summer afternoons (De Marrais, Holzworth, and Hosler, 1967), and the two sites may see aerosol constituents that have some characteristics in common, including a similar fine particle mode size distribution. The agreement is less favorable for the

TABLE 2.4. Contributions to the modeled extinction coefficient.

Average per cent of total extinction coefficient (wavelength=550nm)

	Lennox	Pasadena	Azusa	Upland	San Bernardino
Fine particle scattering	67.0	70.0	70.0	71.1	60.0
Coarse particle scattering	4.7	2.6	4.6	3.5	9.2
Particulate absorption	16.3	15.1	16.6	14.6	16.1
NO_2 absorption	5.6	6.4	4.4	4.7	6.1
Rayleigh scattering	6.4	6.0	4.2	5.8	8.7
b_{ext} $(x10^{-4}m^{-1})$	2.23	2.33	3.21	2.37	1.66
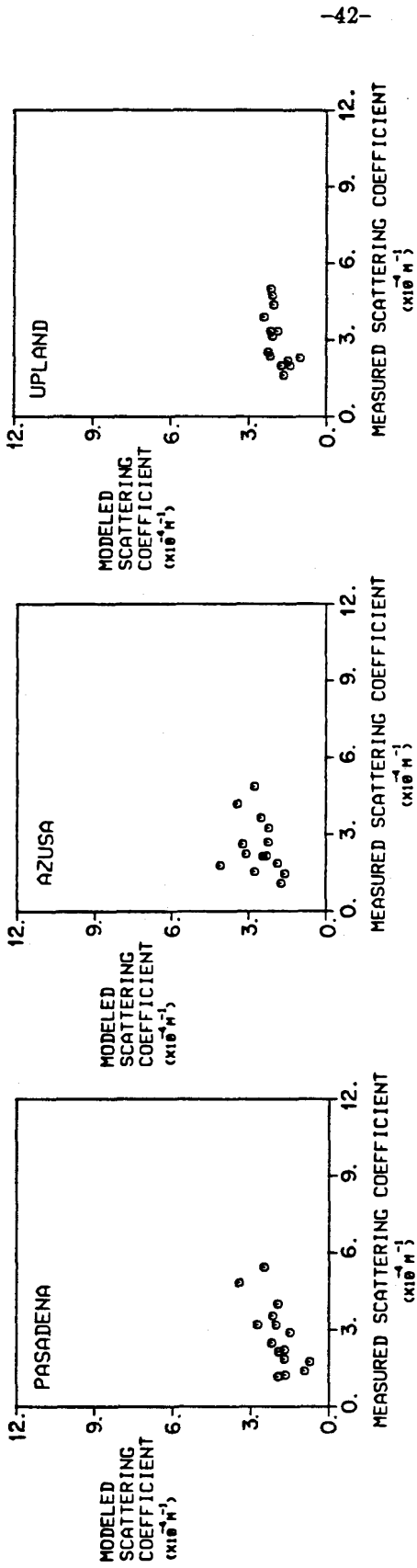
FIGURE 2.8. Measured versus modeled (wavelength=460 nm) scattering coefficient for each nephelometer site.
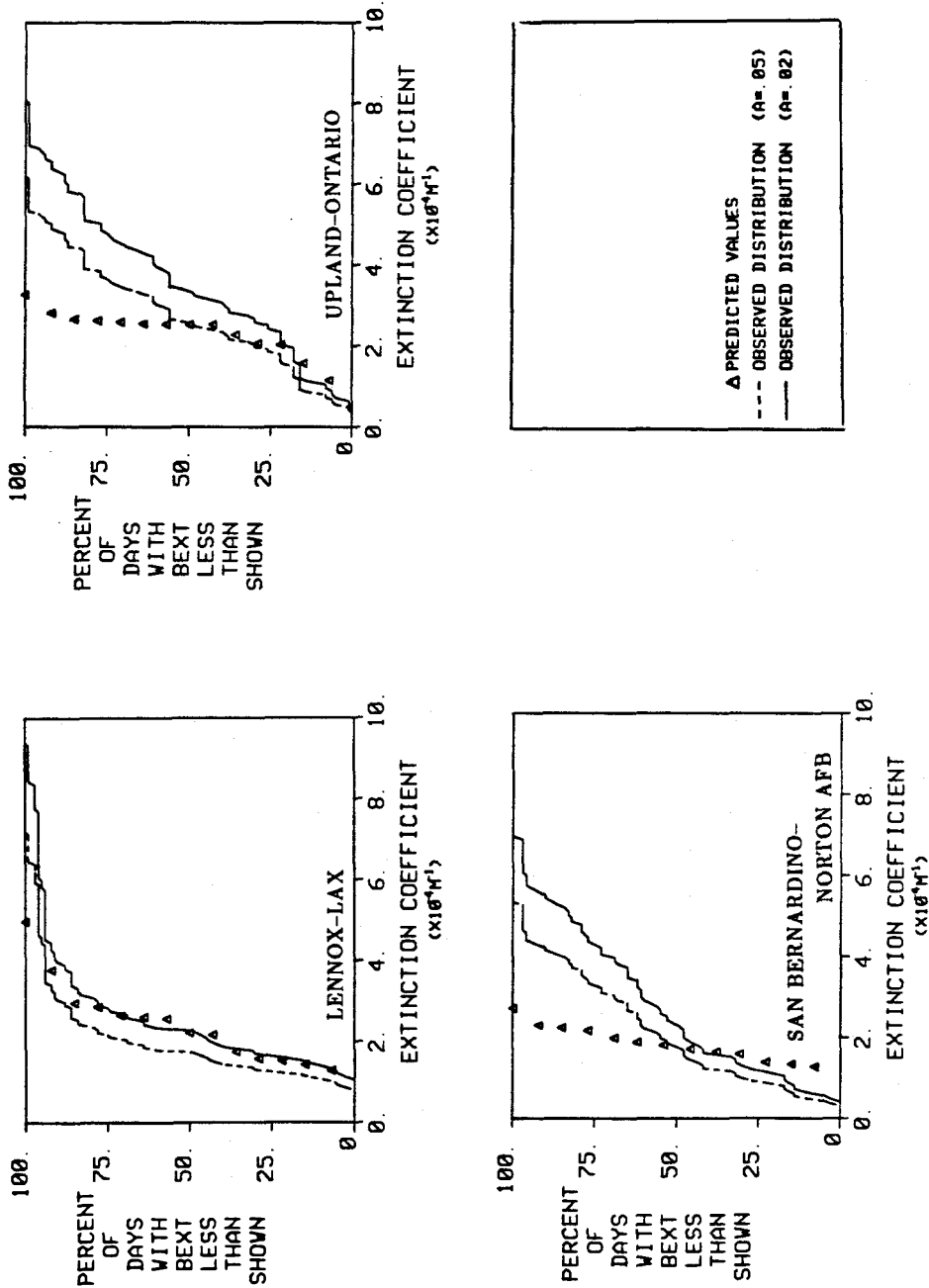
FIGURE 2.9. Measured versus modeled (wavelength=550 nm) extinction coefficient frequency diagram for each airport site.

Upland-Ontario site and for the San Bernardino-Norton Air Force Base location. At these sites, the higher extinction events are not reproduced well. The scaled Pasadena aerosol size distribution may not accurately reflect the actual particle size distribution at these two locations, perhaps due to aerosol aging and growth or because those sites are downwind of a different set of pollutant emission sources.

2.5 Conclusions

Summer midday (1000-1400 hours average) extinction coefficient values in the Los Angeles area range from less than 0.5×10^{-4} m^{-1} (corresponding to a visual range of more than 78 km) to more than 9×10^{-4} m^{-1} (corresponding to a visual range of less than 4.3 km). By sampling at five sites at six day intervals over the summer of 1984, it has been possible to identify the pollutants that are responsible for this distribution of midday visual range values. Light extinction calculations show that most of the light attenuation is due to fine particle scattering. Fine particle scattering and absorption make up 83% of the total light extinction averaged over the five sites studied. Examination of the chemical composition of the summer midday fine aerosol shows that carbonaceous aerosols and sulfates together account for 49% of the fine aerosol averaged over the sites studied. Emission control strategies aimed at midday visibility improvement in the Los Angeles area must be focused on the abatement of aerosol carbon and sulfates.

The frequency distribution of summer midday extinction coefficient values at Pasadena, California, can be modeled with reasonable accuracy by a procedure which combines on-site aerosol size distribution and chemical composition measurements with a calculation procedure based on theories of light scattering and absorption. Since that procedure is based on fundamental aerosol and gaseous pollutant properties, the new distribution of visual ranges could be computed that would prevail if specific changes were made in the composition or size of the Pasadena aerosol as the result of emission controls.

2.6 Acknowledgements

2.7 References

Ahlquist, N.C. and Charlson, R.J., 1967. A new instrument for measuring the visual quality of air. *Journal of the Air Pollution Control Association* **17**, 467-469.

Ahlquist, N.C. and Charlson, R.J., 1968. Measurement of the vertical and horizontal profile of aerosol concentration in urban air with the integrating nephelometer. *Environmental Science and Technology* **2**, 363-366.

Cass, G.R., 1979. On the relationship between sulfate air quality and visibility with examples in Los Angeles. *Atmospheric Environment* **13**, 1069-1084.

Charlson, R.J., Horvath, H., Pueschel, R.F., 1967. The direct measurement of atmospheric light scattering coefficient for studies of visibility and pollution. *Atmospheric Environment* **1**, 469-478.

Conklin, M.H., Cass, G.R., Chu, L.C., Macias, E.S., 1981. Wintertime carbonaceous aerosols in Los Angeles. An exploration of the role of elemental carbon, in *Atmospheric aerosols: Source/air quality relationships,* ed. E.S. Macias and P.K. Hopke, Washington, D.C., American Chemical Society.

DeMarrais, G.A., Holzworth, G.C., Hosler, C.R., 1965. Meteorological summaries pertinent to atmospheric transport and dispersion over Southern California. Washington, D.C., U.S. Weather Bureau Technical Paper No. 54.

Dixon, J.K., 1940. The absorption coefficient of nitrogen dioxide in the visible spectrum. *Journal of Chemical Physics* **8**, 157-160.

Dzubay, T.G., and Clubb, K.W., 1981. Comparison of telephotometer measurements of extinction coefficients with scattering and absorption coefficients. *Atmospheric Environment* **15**, 2617-2624.

Gray, H.A., 1986. Control of Atmospheric Fine Primary Carbon Particle Concentrations. Ph.D. thesis, California Institute of Technology, Pasadena, California.

Gray, H.A., Cass, G.R., Huntzicker, J.J., Heyerdahl, E.K., Rau, J.A., 1986. Characteristics of atmospheric organic and elemental carbon particle concentrations in Los Angeles. *Environmental Science and Technology* **20**, 580.

Groblicki, P.J., Wolff, G.T., and Countess, R.J., 1981. Visibility-reducing species in the Denver "Brown Cloud"– I. Relationships between extinction and chemical composition. *Atmospheric Environment* **15**, 2473-2484.

Harrison, A.W., 1979. Nephelometer estimates of visual range. *Atmospheric Environment* **13**, 645-652.

Harrison, A.W., and Mathai, C.V., 1981. Comparison of telephotometer and nephelometer measurements of atmospheric attenuation and its relationship to aerosol size distribution. *Atmospheric Environment* **15**, 2625-2630.

Heintzenberg, J., and Quenzel, H., 1973. Calculations on the determination of the scattering coefficient of turbid air with integrating nephelometers. *Atmospheric Environment* **7**, 509-519.

Hidy, G.M., et al., 1974. *Characterization of aerosols in California (ACHEX)*. Science Center, Rockwell International. Prepared under California Air Resources Board contract no. 358.

Hodkinson, J.R., 1966. Calculations of colour and visibility in urban atmospheres polluted by gaseous NO_2. *International Journal of Air and Water Pollution* **10**, 137-144.

Hoffmann, H.E., and Kuehnemann, W., 1979. Comparison of the results of two measuring methods determining the horizontal standard visibility with the visual visibility range. *Atmospheric Environment* **13**, 1629-1634.

John, W. and Reischl, G., 1980. A cyclone for size-selective sampling of ambient air. *Journal of Air Pollution Control Association* **30**, 872-876.

Johnson, R.L., Shah, J.J., Cary, R.A., and Huntzicker, J.J., 1981. An automated thermo-optical method for the analysis of carbonaceous aerosols in *Atmospheric Aerosols: Source (air quality relationships)*, ed. E.S. Macias and P.K. Hopke. Washington, D.C., American Chemical Society.

Johnson, R.W., 1981. Daytime visibility and nephelometer measurements related to its determination. *Atmospheric Environment* **15**, 1835-1845.

Larson, S.M., Cass, G.R., Hussey, K.J., Luce, F., 1987. Verification of Image Processing-Based Visibility Models. *Environmental Science and Technology, submitted for publication.*

Malm, W., Pitchford, A., Tree, R., Walther, E., Pearson, M., Archer, S., 1981. The visual air quality predicted by conventional and scanning teleradiometers and an integrating nephelometer. *Atmospheric Environment* **15**, 2547-2554.

McCartney, E.J., 1976. *Optics of the atmosphere-scattering by molecules and particles.* New York: Wiley.

Middleton, W.E.K., 1968. *Vision through the Atmosphere.* University of Toronto Press.

Ouimette, J.R., 1980. Chemical species contributions to the extinction coefficient. Ph.D. thesis, California Institute of Technology: Pasadena, California.

Penndorf, R., 1957. Tables of the refractive index for standard air and the Rayleigh scattering coefficient for the spectral region between 0.2 and 20.0 μm and their application to atmospheric optics. *Journal of the Optical Society of America* **47**, 176-182.

Sloane, C.S., 1983. Optical properties of aerosols - Comparison of measurements with model calculations. *Atmospheric Environment* **2**, 409-416.

Sloane, C., 1984. Optical properties of aerosols of mixed composition. *Atmospheric Environment* **18**, 871-878.

Stelson, A.W., and Seinfeld, J.H., 1981. Chemical mass accounting of urban aerosol. *Environmental Science and Technology* **15**, 671-79.

Trijonis, J., 1979. Visibility in the Southwest - an exploration of the historical data base. *Atmospheric Environment* **13**, 833-843.

Trijonis, J., 1980. *Visibility in California*. Report to the California Air Resources Board. NTIS Accession No. PB 80 216765.

Waggoner, A.P., Weiss, R.E., Ahlquist, N.C., Covert, D.S., Will, S., Charlson, R.J., 1981. Optical characteristics of atmospheric aerosols. *Atmospheric Environment* **10/11**, 1819-1909.

White, W.H., and Roberts, P.T., 1977. On the nature and origins of visibility-reducing aerosols in the Los Angeles air basin. *Atmospheric Environment* **11**, 803-812.

Wickramasinghe, N.C., 1973. *Light scattering functions for small particles with applications in astronomy*. New York: Wiley.

Williamson, S.J., 1973. *Fundamentals of Air Pollution*. Addison Wesley, Reading, Mass.

CHAPTER 3

VERIFICATION OF IMAGE
PROCESSING-BASED VISIBILITY MODELS

3.1 Abstract

Methods are presented for testing visibility models that use simulated photographs to display results of model calculations. An experimental protocol is developed and used to obtain input data including standard photographs of chosen scenes on a clear day and during a smog event at Pasadena, CA. Using the clear day photograph as a substrate, pollutant properties measured on the smoggy day are introduced into the visibility model, and results of the model calculations are displayed as a synthetic photograph of the expected appearance of the smog event. Quantitative comparisons are made between the predicted and actual appearance of the smog event.

Diagnostic techniques developed are illustrated using the visibility modeling procedure proposed by Malm et al. (1983). That model is shown to reproduce the contrast reduction characteristic of urban air pollution, but produces synthetic photographs with sky elements that differ substantially from a real photograph of the actual smog event.

3.2 Introduction

The reduction of visibility is one of the most easily perceived features of a polluted atmosphere. Particulate matter and gaseous pollutants can act to decrease visual range, lower contrast, and even alter the observed color of objects. Since the amendment of the Clean Air Act in 1977 to encourage the prevention and control of visibility impairment in national parks and wilderness areas, visibility reduction in relatively pristine locations has received considerable attention (Hering et al., 1981, Macias et al., 1981, Trijonis, 1979). Visual range values reported in some sparsely populated portions of the western United States average greater than 180 km (Malm and Molenar, 1984), but other regions with many pollution sources and unfavorable meteorology have been shown to exhibit severe visibility problems. Husar et al. (1981) discuss trends in haziness in the eastern United States using data accumulated between 1910 and the present. They find the highest turbidities in major metropolitan areas. Denver is noted for its "brown cloud" (Sloane and Groblicki, 1981; Groblicki, et al., 1981), and the smog problem in the Los Angeles area has been studied extensively (Hidy et al., 1974; White and Roberts, 1977; Cass, 1979).

The atmospheric extinction coefficient, a measure of the amount of light scattered and absorbed in the atmosphere, can be measured or be calculated from the size distribution and chemical composition of atmospheric particulate matter and the concentration of gaseous pollutants. Often the extinction coefficient, b_{ext}, is used to predict the visual range (distance to extinction) using Koschmieder's formula:

$$V_R = \frac{-ln0.02}{b_{ext}} \tag{3.1}$$

where V_R is the predicted distance at which an average observer can just barely

distinguish a black object silhouetted against the horizon sky (McCartney, 1976). A visibility model based on Koschmieder's formula does not convey any information about the degraded appearance of objects in the mid-field or the near-field of view, and does not describe the discoloration, if any, of the scene.

Recently, visibility models have been proposed that utilize simulated photographs as a means to display the results of visibility calculations (Malm et al., 1983, Williams et al., 1980). Such models show promise as a tool for communicating a great deal of information on how air pollutants can affect the perceived visual quality of a scene, and could be employed to evaluate the visual consequences of proposed air pollution abatement programs. Existing models of this type, though, have not been tested extensively to confirm their ability to represent the appearance of heavy urban photochemical smog conditions.

The objective of the present study is to examine methods for verifying the accuracy of synthetic photograph-based visibility models. Procedures developed will be applied to assess the image processing-based visibility model proposed by Malm et al. (1983) and its ability to account for regional haze conditions. Examples will be illustrated using air pollutant measurements and photographs taken in Pasadena, California, under clear day and under heavy smog conditions.

A description of the design for this study is shown in Figure 3.1. Measurements of the aerosol size distribution and pollutant chemical composition made under heavy smog conditions are used to compute the extinction coefficient. The value of the extinction coefficient is introduced into the visibility model along with a digital representation of a "base photograph" of the scene of interest that was taken on a very clear day. Using the visibility model, the brightness and color balance of the picture elements in the digitized base photograph are recomputed. A new synthetic digital image of the scene is created with the brightness and

contrast expected for the conditions measured on the heavily polluted day. The accuracy of the visibility model can be tested by comparing the synthetic smog event image to a digitized actual photograph taken on the heavy smog day being modeled. Color photographic prints of the synthetic smog event image also can be created.

DESIGN FOR VISIBILITY MODELING STUDY
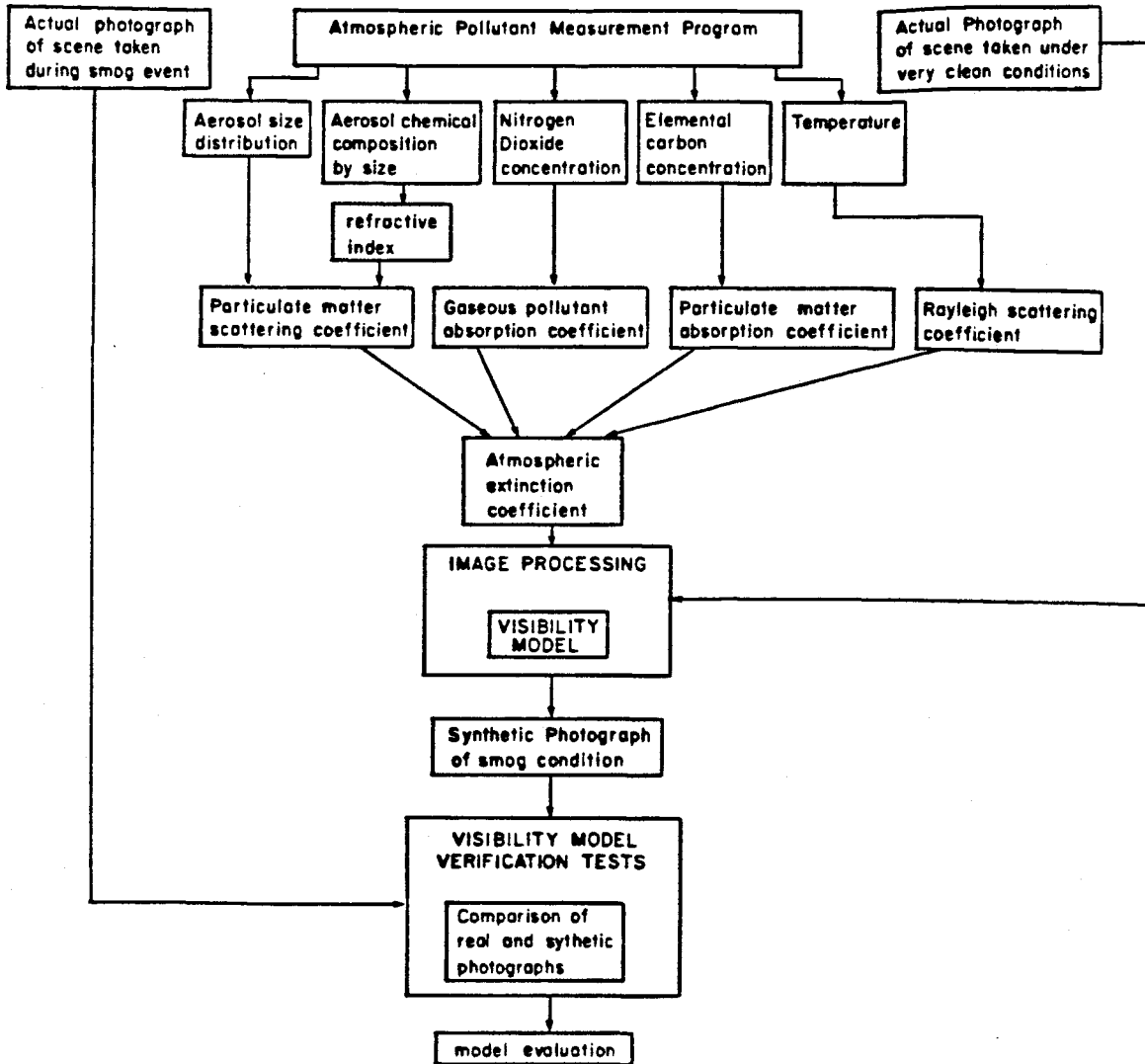
FIGURE 3.1. Visibility model verification procedure.

3.3 Experimental Program

On fifteen days during the period October 1982-August 1983, an experimental program was conducted to acquire observations on the size distribution and chemical composition of airborne particulate matter as well as on gaseous pollutant concentrations in the Los Angeles area. Photographs of chosen vistas were taken simultaneously with the pollutant measurements in order to document the appearance of the air basin under different pollutant loading conditions. The campus of the California Institute of Technology in Pasadena was chosen as the sampling site. Pasadena frequently suffers severe smog episodes during which visibility is reduced to a few kilometers.

Photographs were taken from the roof of the 44-meter-tall Millikan Library on the Caltech campus which afforded unobstructed views of five standard scenes. Photographs of each scene were taken at 1000, 1200, and 1400 hours Pacific Standard Time (PST) on each day of the experiment utilizing camera mounts and a tripod to ensure reproducibility of the field of view. Each time a scene was photographed, a series of three pictures was taken using a Canon TLb, 35 mm, single-lens-reflex camera equipped with an ultraviolet light cutoff filter. Two of these pictures were taken at different f-stops to ensure proper exposure, and the third photograph incorporated a Kodak color chart for use in confirming accurate color reproduction during photographic processing. Kodachrome ASA 25 film was used for all the field photographs.

From 1000 hours to 1400 hours PST on the day of each photographic session, an air pollutant sampling program was conducted on the roof of Caltech's Keck Laboratory building. Atmospheric aerosol size distribution measurements were

made over the fine particle size range from 0.0075 μm to 1.0 μm using a Thermal Systems Incorporated electrical aerosol analyzer (EAA), and over the coarse particle size range from 0.5 μm to 50 μm using a Particle Measurement Systems model CSASP-100-HV optical particle counter (OPC).

Information on the chemical composition of the atmospheric particulate matter was obtained from analysis of filter samples. Fine particle samples ($d_p < 2.1$ μm) were collected for the four hour duration of each experiment using three parallel filter holders located downstream of an AIHL-design cyclone separator (John and Reischl, 1980). Each of these filter assemblies contained a filter substrate that was compatible with a particular chemical or physical analysis. Aerosol samples collected at a flow rate of 10 lpm on a 47 mm diameter Teflon filter (Membrana) were used to determine dry fine aerosol mass concentration by repeated weighing at low relative humidity before and after use. The concentrations of 34 trace elements ranging in atomic weight from aluminum to lead were determined from the Teflon filter samples by X-ray fluorescence analysis (XRF). Fine aerosol samples for the determination of the light absorption coefficient and for ion chromatography were collected at a flow rate of 5 lpm on 47 mm diameter Nuclepore filters (0.4 μm diameter pore size). The aerosol light absorption coefficient, b_{absp}, was measured on these filter samples by the opal glass integrating plate technique (Lin et al., 1973, as modified by Ouimette, 1980). Ion chromatography provided information on the water soluble ions Na^+, NH_4^+, K^+, F^-, Cl^-, S(IV), NO_3^-, and SO_4^{-2} extracted from the Nuclepore filters. Quartz fiber filters (Pallflex 2500 QAO) operated at a flow rate of 10 lpm were used to collect samples for determination of organic and elemental carbon concentration. These filters were prefired to 600°C for 2 hours prior to use in order to reduce their carbon blank. The carbon analysis was carried out by the method of Johnson et al. (1981).

A comparable set of open-faced filters was used to collect total suspended particulate matter samples. The total aerosol Teflon, Nuclepore, and quartz fiber filters were analyzed in the same manner as the fine aerosol filters. Information on the atmospheric coarse particle fraction then was determined as the difference between the total and fine particle concentration data.

From these experiments, two days were chosen for further analysis. A very clear day event occurred on April 7, 1983, when winds from the desert prevailed in the Los Angeles basin, resulting in a visual range of approximately 82 km. The measured extinction coefficient averaged approximately 0.48×10^{-4} m^{-1} over the sampling period on that day. The Rayleigh limit for light scattering by air molecules in the absence of any air pollution is approximately 0.11×10^{-4} m^{-1} at a wavelength of 550 nm, indicating that the April 7, 1983, samples are an appropriate representation of a very clean day for the Pasadena area.

Samples collected on August 25, 1983, also were chosen for further analysis. The average extinction coefficient measured was approximately 5.5×10^{-4} m^{-1}. The visual range was about 7.1 km. The April 7th and the August 25th days are almost symmetrically spaced on either side of the summer solstice, and thus the shadow patterns in the photographs taken on these two days are nearly identical.

Photographs of two vistas taken at 1200 hrs PST on each of these two days were chosen for testing the image processing-based visibility model. The April 7 clear day digitized image of these two scenes is shown in Figures 3.2ab, and the photographs taken during the actual August 25, 1983, smog event are reproduced in Figures 3.3ab. Figures 3.2b and 3.3b will be referred to as the downtown Pasadena scene. The view in this direction is to the northwest overlooking downtown Pasadena. The dome of Pasadena City Hall is in the center of the picture at a distance of 2 km. The San Rafael hills at a distance of 5 km are along the

horizon. Office buildings form much of the center of the field of view. The fore-
ground consists of a tree-shaded parking lot. The vista shown in Figure 3.2a and
3.3a will be referred to as the San Gabriel Mountains scene. That view is to the
north. The San Gabriel Mountains at a distance of 9 km make up the background
for this scene. The midground is primarily residential. The Beckman Auditorium
of the Caltech campus is in the foreground.

3.4 Data Analysis

The volume distributions of the atmospheric aerosol on the clear day (April 7,
1983) and on the heavy smog day (August 25, 1983) are shown in Figure 3.4. The
usual bimodal nature of the volume distribution is evident. Particles in the fine
mode ($d_p < 2.1$ μm) are much more efficient light scatterers than are the coarse
particles, and the appreciable difference in the fine modes on the two days is the
main cause for the large difference in the extinction coefficient, and therefore in
the visual range, on the two days shown.

To construct a material balance on the chemical composition of the aerosol,
trace metals measured were converted to their common oxides (Stelson and Sein-
feld, 1981). The mass of organic carbonaceous material was taken to be 1.2 times
the organic carbon mass measured (Countess et al., 1980). The ionic material was
assumed to be distributed as follows:

Na^+ was associated with Cl^-.

NH_4^+ was associated with SO_4^{-2}.

NH_4^+ remaining, if any, was associated with NO_3^-.

Na^+ remaining, if any, was associated with remaining NO_3^-, if any.

Na^+ remaining, if any, was associated with remaining SO_4^{-2}, if any.

It is assumed that the unidentified aerosol mass is due to unmeasured chemical
species. Following the nomenclature proposed by Sloane (1984), the mass of dry
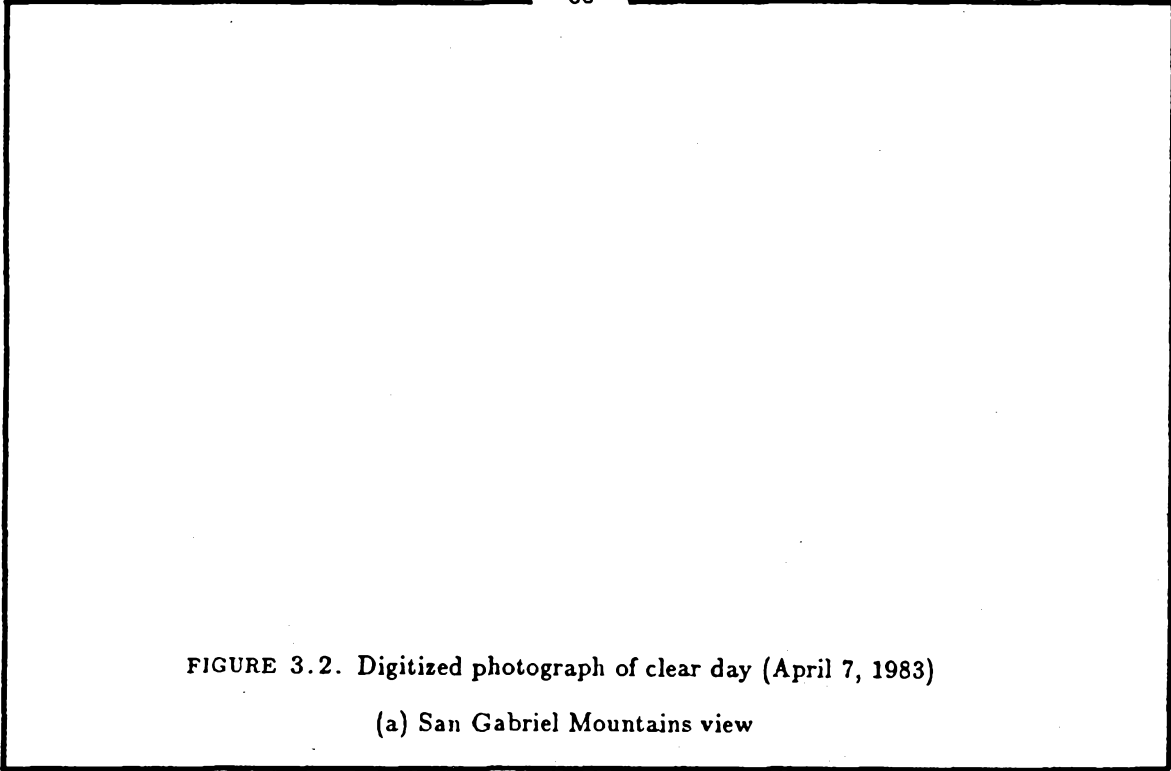
FIGURE 3.2. Digitized photograph of clear day (April 7, 1983)

(a) San Gabriel Mountains view
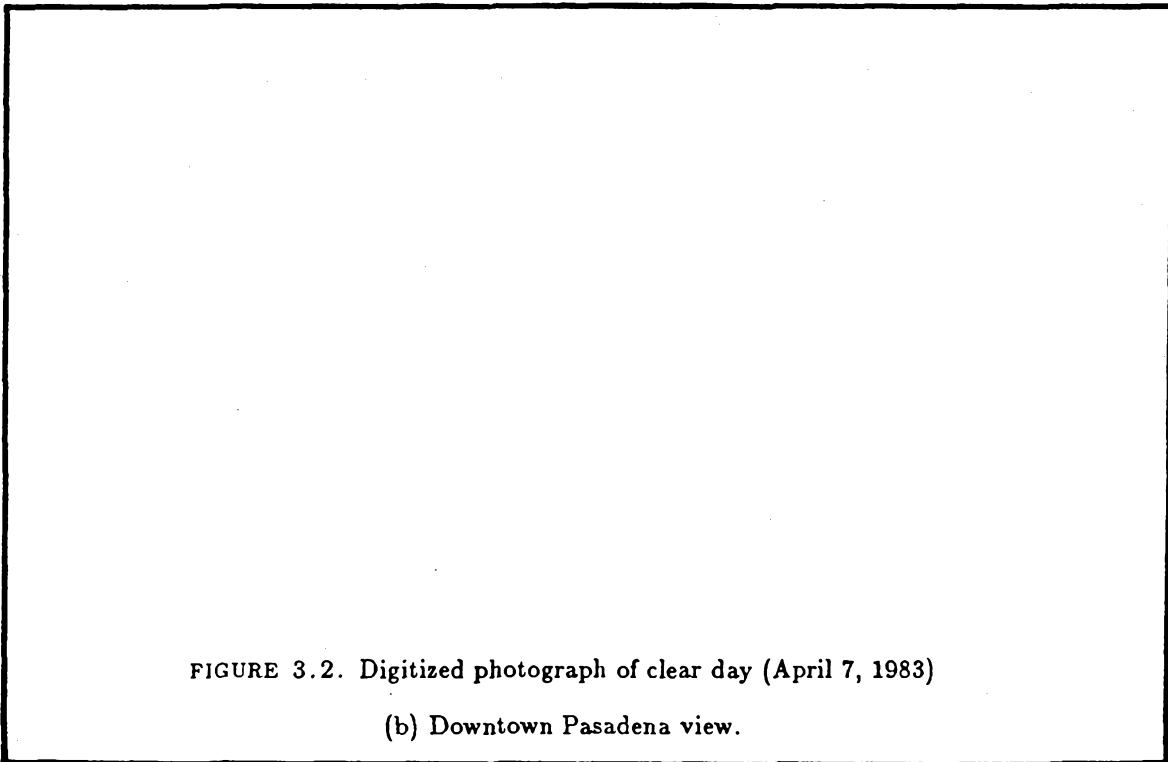
FIGURE 3.2. Digitized photograph of clear day (April 7, 1983)

(b) Downtown Pasadena view.
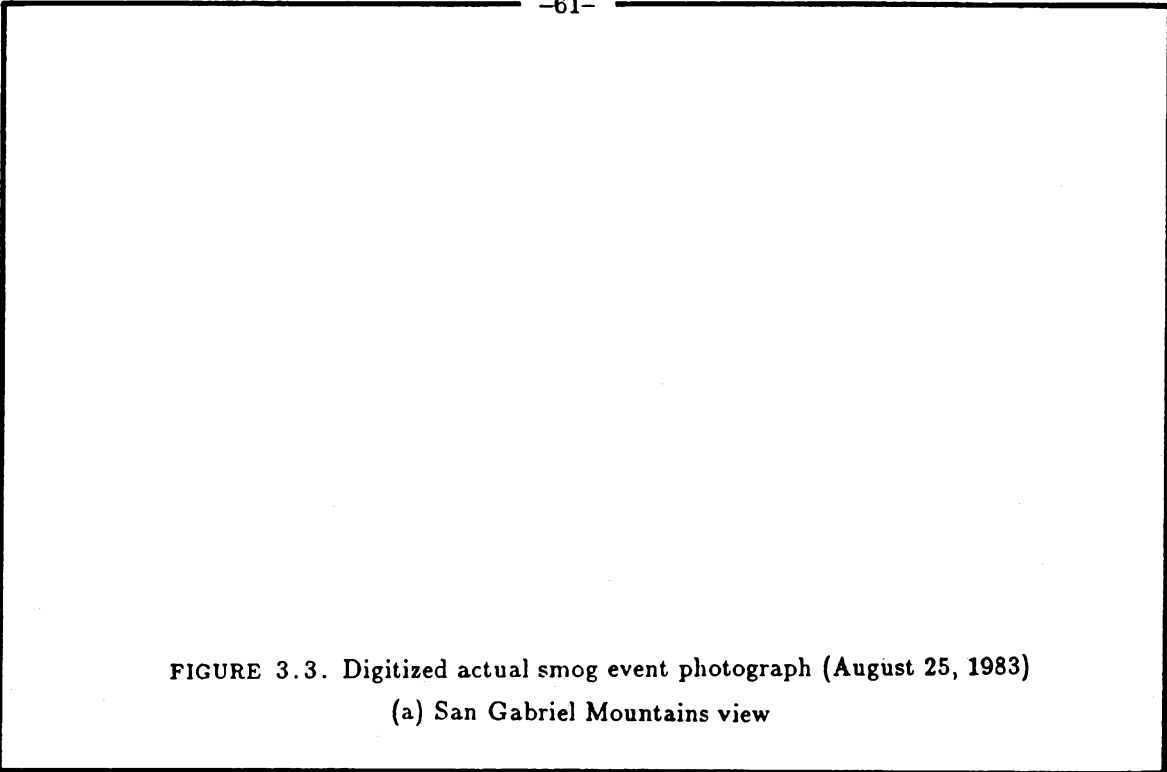
FIGURE 3.3. Digitized actual smog event photograph (August 25, 1983)

(a) San Gabriel Mountains view
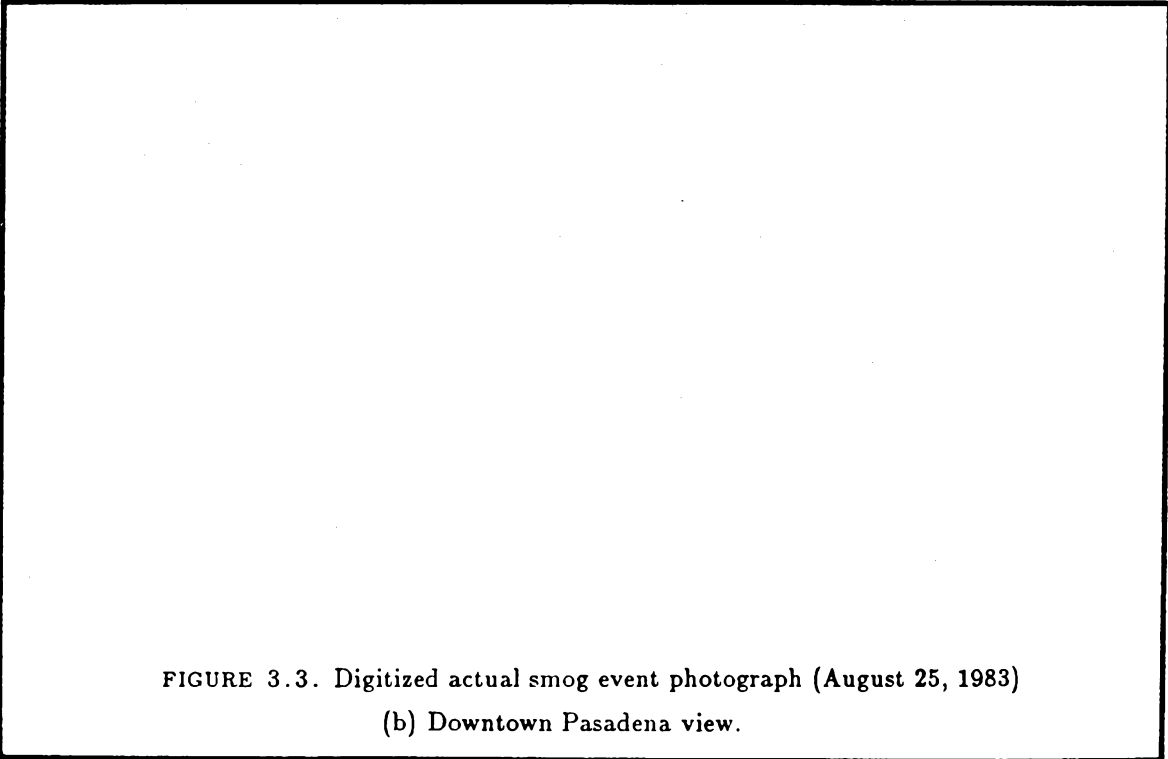
FIGURE 3.3. Digitized actual smog event photograph (August 25, 1983)

(b) Downtown Pasadena view.

AEROSOL VOLUME DISTRIBUTION OBSERVED AT
PASADENA, CA. ON APRIL 7 AND ON AUGUST 25,1983
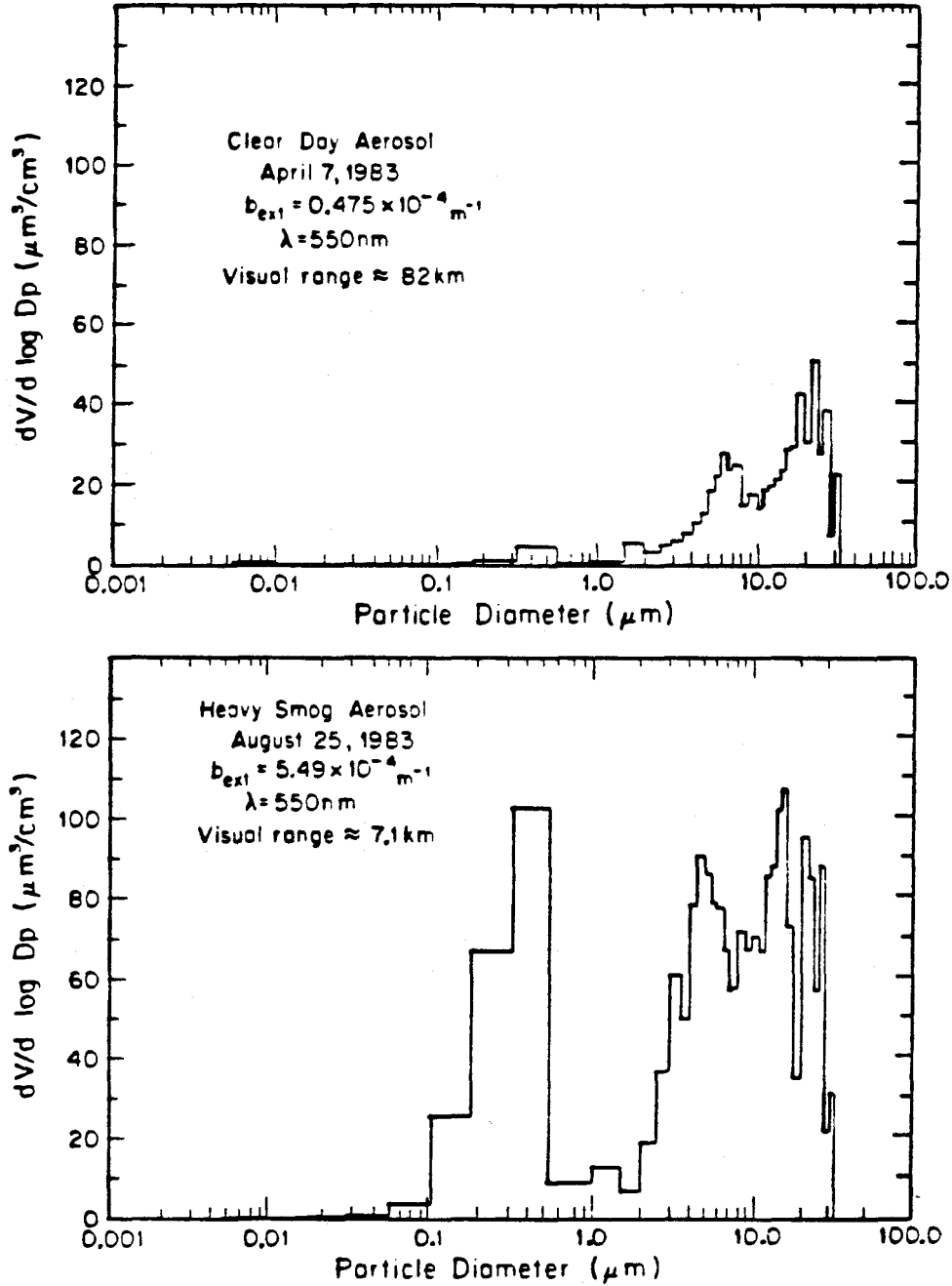
FIGURE 3.4. Aerosol volume distribution observed at
Pasadena, CA, on April 7 and on August 25, 1983.

material that is measured gravimetrically but not accounted for in the chemical analysis will be referred to as the "residue".

A balance on the chemical species contribution to fine and coarse aerosol volume is shown in Table 3.1. Densities for individual chemical species are assigned as shown in Table 3.2 (Handbook of Chemistry and Physics, 1975; Sloane, 1983). The residue is assigned a density of 2.3 g/cm^3 (Sloane, 1984). Using the individual densities and the measured masses of individual chemical constituents, a dry volume is calculated. The sum of volumes for each species gives the total volume that the aerosol would occupy if no water were present in the aerosol. When this dry aerosol volume is subtracted from the total aerosol volume computed from the size distribution measurements of the EAA and OPC, one estimate of the volume of water present in the aerosol is obtained. For comparison, the semi-empirical procedure for estimating aerosol water content formulated by Sloane (1984) was applied to the Pasadena fine aerosol measurements. In this approach, data on ambient relative humidity and the aerosol solubility are used to estimate the amount of water present in the fine aerosol. Sloane's method predicts that 0.26 μg/m^3 water is present in the fine suspended particulate matter for the April 7 day, and that 11.86 μg/m^3 water is present in the fine particles on August 25. This compares to 0.0 μg/m^3 and 9.53 μg/m^3 water predicted by the volume difference method for April 7 and August 25, respectively. These two approaches to estimating the amount of water present provide similar answers for the fine aerosol fractions. The semiempirical calculation is not well suited to estimate the water content of coarse particle material, and it is also possible that the OPC measurements overestimate coarse particle volume. The uncertainties associated with determining the coarse particle volume are unimportant to subsequent visibility calculations: coarse particles by virtue of their size contribute only a small fraction to total aerosol light scattering.

TABLE 3.1. Chemical Species Contribution to the Aerosol Volume Concentration.

Date	April 7, 1983		August 25, 1983	
Particle Fraction	Fine	Coarse	Fine	Coarse
Species	volume conc. $\frac{\mu m^3}{cm^3}$	volume conc. $\frac{\mu m^3}{cm^3}$	volume conc. $\frac{\mu m^3}{cm^3}$	volume conc. $\frac{\mu m^3}{cm^3}$
elemental carbon	0.295	0.200	3.985	0
organic carbon	3.993	0.850	20.10	3.286
$(NH_4)_2SO_4$	1.853	0.147	6.734	1.672
$NaNO_3$	—	—	1.434	4.230
NH_4NO_3	0.419	0.297	—	1.041
Na_2SO_4	—	—	1.164	—
other ions	0.095	1.087	0.965	0.552
Al_2O_3	0.131	0.580	0.444	1.914
SiO_2	0.296	1.674	0.843	5.913
K_2O	0.027	0.128	0.194	0.431
CaO	0.023	0.115	0.071	0.492
Fe_2O_3	0.027	0.147	0.134	0.740
PbO	0.007	2.5×10^{-4}	0.078	0.013
other metals	0.113	—	0.396	0.230
Total Dry Volume of Identified Chemical Species	7.279	5.220	36.54	20.515
Volume of Residue	0.00	0.130	10.45	6.76
(2) Total Dry Volume	7.279	5.350	46.99	27.28
(1) Volume From Size Distribution	2.333	23.534	56.52	82.43
Volume H_2O [by (1)-(2)]	0.00	18.18	9.53	55.15

TABLE 3.2. Density and Refractive Index Values for Selected Chemical Species.

species	density (g/cm³)	refractive index	reference
elemental carbon	2.0	1.90-0.6i	2
organic carbon	1.40	1.55	2
$(NH_4)_2SO_4$	1.77	1.52	1
$NaNO_3$	2.26	1.59	1
NH_4NO_3	1.72	1.55	1,2
Na_2SO_4	2.68	1.48	1
other ions	2.30	1.53-0.005i	2
Al_2O_3	3.96	1.76	1
SiO_2	2.30	1.48	1
K_2O	2.32	1.50	1
CaO	3.25	1.84	1
Fe_2O_3	5.24	3.01	1
PbO	8.00	2.61	1
other materials	2.30	1.53-0.005i	2
water	1.00	1.33	1

1. *Handbook of Chemistry and Physics*, 1975.

2. Sloane, C.S., 1983.

Once the contributions to the aerosol volume from individual pollutants and from associated liquid water have been determined, it is possible to determine the volume average refractive index for the aerosol based on the refractive indices for each component as listed in Table 3.2. For the April 7 aerosol, the volume average refractive index is calculated to be 1.56-0.024i for the fine particle fraction and 1.39-0.005i for the coarse particle fraction. Refractive indices for the August 25 aerosol are 1.54-0.043i for the fine particle fraction and 1.42-0.004i for the coarse particle mode. Kerker (1969) discusses the validity of calculations based on the volume average refractive index. He finds the volume average index to be within approximately 20% of the exact refractive index for a typical internally mixed aerosol particle.

The extinction coefficient (b_{ext}), can be expressed as a sum of several components: light scattering by particles (b_{scatp}), light absorption by particles (b_{absp}), light absorption by gases (b_{absg}), and light scattering by air molecules $(b_{Rayleigh})$:

$$b_{ext} = b_{scatp} + b_{absp} + b_{absg} + b_{Rayleigh} \qquad (3.2)$$

Data from the sampling experiments were used to calculate each of these contributions to the extinction coefficient.

Using the aerosol size distribution and the volume average refractive indices for the coarse particle and fine particle modes, it is possible to compute the scattering coefficient for the aerosol, b_{scatp}. The computer algorithm used is a Mie scattering code as outlined by Wickramasinghe (1973). Mie's solution describes light scattered by a homogenous sphere in an infinite medium, determining the scattering efficiency factor, Q_{scat}. Q_{scat} depends on particle size, refractive index, and the wavelength of light. For a polydisperse aerosol, b_{scatp} can be expressed as

$$b_{scatp} = \int_0^\infty Q_{scatp} \frac{\pi}{4} d_p^2 n(d_p) d(d_p) \qquad (3.3)$$

where $n(d_p)d(d_p)$ is the number of particles per unit air volume with diameter between d_p and $d_p + d(d_p)$ (McCartney, 1976). For a measured aerosol size distribution, in histogram form, the integral is approximated by a sum:

$$b_{scatp} = \sum_{i=1}^{m} Q_{scatp}\frac{\pi}{4}d_{p_i}^2 N(d_{p_i}) \tag{3.4}$$

where the d_{p_i} represent the central points of successive diameter intervals, d_{p_1} is the smallest diameter interval, d_{p_m} is the largest diameter interval for which number concentration information is available, and $N(d_{p_i})$ is the number concentration of particles in the size interval surrounding size d_{p_i} (McCartney, 1976).

Equation 3.4 was applied to calculate the scattering coefficient of the aerosol observed on April 7 and on August 25, 1983. Separate refractive index values were used for coarse particle and for fine particle modes of the aerosol volume distribution. The refractive index is assumed constant over the visible spectrum (Nicholls, 1984).

Color photographic slides can be separated into three different color planes: red, green, and blue. The superposition of these planes creates a full color image. The Kodachrome ASA 25 film used to produce the slides taken in the field has a wavelength sensitivity profile that is given in Kodak publication E-77, "Kodak Color Film" (1980). The yellow-forming layer is blue-sensitive; the magenta-forming layer is green-sensitive; and the cyan-forming layer is red-sensitive. To incorporate the color sensitivity of the slide film into the visibility model, the scattering coefficient was calculated at each of 13 different wavelengths within the visible spectrum, and these values were weighted according to the film sensitivity curves. This results in three values of a weighted average scattering coefficient, one corresponding to each color plane of the film. The weighted green value should most closely match the scattering coefficient value measured by the nephelometer during the field experiments. The measured and computed scattering coefficient

values agree to within about 20% (Table 3.3).

Equation 3.2 shows that light absorption by aerosols and gases, plus light scattering by air molecules, must be added to the aerosol scattering coefficient in order to estimate the total atmospheric extinction coefficient. The particle absorption coefficient, b_{absp}, (due to elemental carbon) was measured using the opal glass integrating plate technique. The principal light absorbing gas in urban atmospheres is NO_2. The wavelength dependence of this absorption is discussed by Dixon (1940). The results of his study were put in a more practical form by R.J. Hodkinson (1966) (Groblicki et al., 1981). Using this dependence, the weighted average gaseous absorption coefficients b_{absg}, (for the red, blue, and green wavelength bands) were determined.

Light scattering by air molecules, Rayleigh scattering, has been studied extensively. Penndorf (1957) presents tables of the Rayleigh scattering coefficient for standard air over a wide band of wavelengths, including the visible. He points out that Rayleigh scattering is temperature-dependent and that this dependence cannot be ignored. These tables and Penndorf's temperature correction formula were used to determine the weighted averages for the Rayleigh scattering coefficients in the red, green, and blue.

The individual components of the extinction coefficient and their sum are shown for the two days of interest in Table 3.4.

For use in modeling calculations, the clear day and heavy smog day photographic slides were converted into a numerical representation of each picture. In this process of digitization, the 35 mm slides were gridded into a 1800 X 1200 sample pattern, for a total of 2.16×10^6 picture elements (pixels) per picture, each pixel being 25 μm on a side. The density of the film at the location of each pixel was scanned by a microdensitometer through three color separation filters (Wratten 92, 93, 94). This produces digital images in each of three color planes –

TABLE 3.3. Comparison of Measured Scattering Coefficient to Computed Scattering Coefficient at $\lambda \approx 550$ nm (units are 10^{-4} m^{-1}).

	Clear Day Aerosol (April 7, 1983)	Heavy Smog Aerosol (August 25, 1983)
b_{SCAT_p}-Calculated	0.259	4.08
$b_{Rayleigh}$-Calculated	0.111	0.107
b_{SCAT}-Calculated	0.369	4.19
b_{SCAT} Measured	0.29	5.1
percent difference	24%	20%

TABLE 3.4. Components of the Extinction Coefficient (units are 10^{-4} m^{-1}).

DATE	COLOR PLANE	b_{SCAT_p}	b_{ABS_p}	b_{ABS_g}	b_{RAY}	b_{ext}
April 7	blue	0.305	0.0930	0.0541	0.281	0.733
	green	0.259	0.0930	0.0118	0.111	0.475
	red	0.231	0.0930	0.00278	0.0659	0.393
Aug. 25	blue	5.56	0.787	0.136	0.273	6.76
	green	4.08	0.787	0.0299	0.107	5.00
	red	3.52	0.787	0.00694	0.0639	4.38

red, green, and blue, which when superimposed result in a full color image. The density of each pixel was recorded in each color plane in terms of a numerical density (DN) scale which ranged from zero (dark) to 255 (light). At the end of the digitization process, each pixel of each color plane has an assigned numerical density, for a total of 6.48×10^6 numerical values used to describe each color slide.

The correspondence between film density and exposure is given in the "D vs. E" characteristic curves provided by the film manufacturer. Given this relationship, and by relating exposure to radiance, the film can be used as a light-measuring device, and the color slide can be described by arrays (one array for each color plane) of radiance values, each value of an array representing one pixel in the corresponding color plane of the slide.

3.5 Visibility Model Description and Application

A relatively uncomplicated visibility model for use with synthetic image processing techniques has been proposed by Malm et al. (1983). In that model, the radiance, $N(s)$, of an object at a distance s from that object is represented by:

$$N(s) = N(0)e^{-b_{ext}s} + N_{sky}(1 - e^{-b_{ext}s}) \qquad (3.5)$$

where $N(0)$ is the "inherent radiance," the radiance of an object at the object. N_{sky} is the radiance of the sky in the direction viewed. The first term on the right side of Equation 3.5 accounts for light from the object that is attenuated by the intervening atmosphere. The second term, called the path radiance, is a representation of the light from all directions that is scattered into the line of sight.

To create a synthetic smog photograph according to the model tested, a number of separate images are needed:

[1] A distance image. In this study, highly resolved distance images were created to accompany the downtown Pasadena and San Gabriel Mountains scenes.

The downtown Pasadena scene in particular is quite complex. Using walking surveys, maps and aerial photographs, the distances from the camera mount to approximately 400 objects were measured for the downtown Pasadena scene. A less detailed distance map for the San Gabriel Mountains scene was created based on 250 surveyed points. The remainder of each distance map was created by interpolation between measured points. Since an object and its background could be separated by a great distance but still occupy neighboring pixels in a digitized picture, care must be taken during the distance interpolation process to outline individual buildings and geographic features using the distances assigned to the edges of those objects.

[2] A sky radiance, N_{sky}, map for the red, green and blue. The horizon sky radiance, N_{sky}, according to Malm et al.'s procedure (1983), is obtained by evaluating the film densities at locations along the horizon on the clear day image. For objects below the horizon, the approximation of horizon viewing is still assumed to be valid, and N_{sky} values are determined using an extrapolation of sky brightness trends to below the horizon. In this study, the trends were extrapolated for approximately two degrees below the horizon and then held constant for objects lower than this.

[3] The inherent radiance, $N(0)$, map for each of the red, green, and blue planes. Malm, in his image processing procedure, back-calculates the inherent radiance of the objects at each point in the clear day picture by rearranging Equation 3.5, giving

$$N(0) = N(s)e^{b_{ext}s} + N_{sky}(1 - e^{b_{ext}s}) \qquad (3.6)$$

To apply this equation to the clear day photo, since the sky radiance and distance images are determined, the only unknown is an array of $N(s)$ values. To obtain an array of $N(s)$ values corresponding to each object in the field of view, Malm et

al.'s modeling procedure (1983) uses the clear day photographic slide of the scene of interest and calculates the $N(s)$ values from the measured densities of the clear day slide and the relationships between density, exposure and radiance. With the extinction coefficient value for the clear day, the distance image, the sky radiance image, and the array of $N(s)$ values from the clear day, the clear day inherent radiance values, $N(0)$, are obtained from Equation 3.6. According to Malm et al.'s model (1983), the assumption is made that the inherent radiance, $N(0)$, and the sky radiance values, N_{sky}, are independent of atmospheric pollutant loading. Therefore, $N(0)$ and N_{sky} for every object in any pollution condition are constant, and can be determined from the clear day photograph.

With the distance from object to observer determined, in order to simulate a smoggy day, one must only set b_{ext} in Equation 3.5 at the proper level and then determine a new radiance for each object. This produces an array of new $N(s)$ values that corresponds to the smog event to be simulated. That new array of $N(s)$ values is translated into a new array of numerical film density values which in turn are used to create a new image. The calculation is done for each picture element in each of the three color planes. Superimposing these planes results in a synthetic image that can be played back onto photographic film using a film-writing device. A color negative results, from which color prints can be made.

Using this procedure, synthetic images were produced which predict the appearance of the August 25 heavy smog event from the April 7 clear day image plus the extinction coefficient values computed for those days. The procedure was carried out for both the downtown Pasadena and the San Gabriel Mountains scenes. The playbacks of these synthetic images are shown in Figures 3.5ab.

Production of a synthetic image requires a large number of photographic steps. The original slide must be: [1] taken during the field experiments; [2] developed; [3]
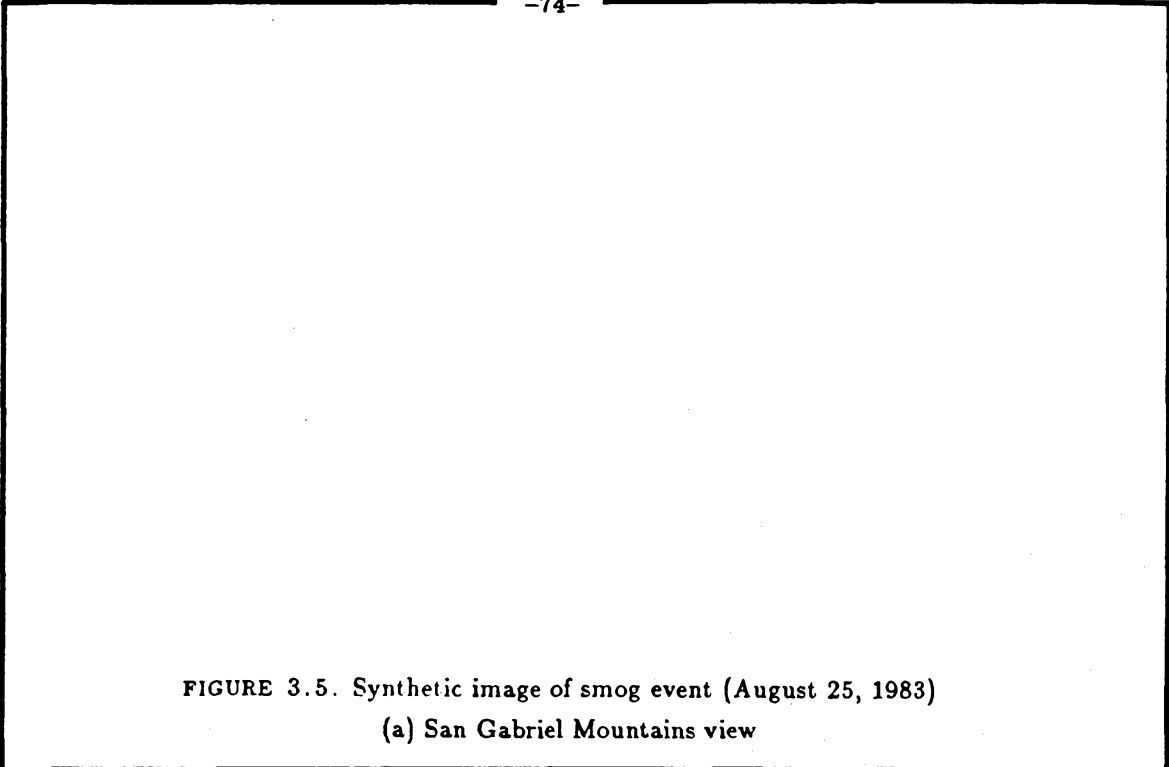
FIGURE 3.5. Synthetic image of smog event (August 25, 1983)

(a) San Gabriel Mountains view
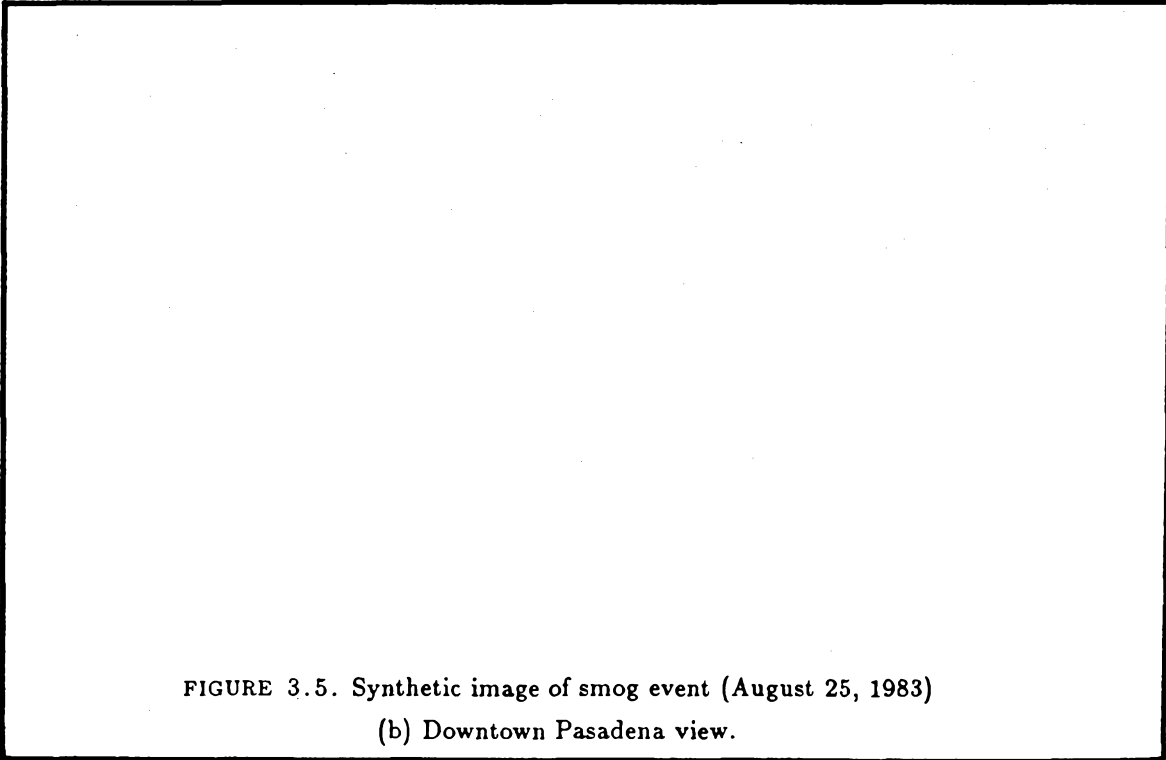
FIGURE 3.5. Synthetic image of smog event (August 25, 1983)

(b) Downtown Pasadena view.

digitized; [4] processed by computer to render a synthetic photograph; [5] played back onto negative film; and [6] printed onto color photographic paper. In this work, deliberate steps are taken to *prevent* any subjective enhancements of the actual photographs taken. When the slides used in this study were digitized, a standard Kodak #2 steptable gray wedge with 21 steps representing the range of gray levels also was digitized. To correct for any possible distortion of the digital image, the digitized gray wedge was examined, and the correction factors needed to exactly restore the Kodak gray scale were determined. This "gray wedge correction" is then applied to the entire digitized image. This standardizes and corrects the digital images for any distortion created while scanning the slides. These gray-wedge-corrected data are used in the production of the synthetic smog images. After processing, the gray-wedge-corrected data are played back along with a copy of the actual gray wedge which is embedded in the image. The photo lab then printed the photographs exactly to the gray wedge specification contained on each negative. This ensures color control of all images processed and ensures the validity of any comparison between photographs.

3.6 Comparison of Predicted and Observed Images

Synthetic images of the August 25, 1983 smog event produced by the visibility model, Figures 3.5ab, are compared to digitized photographs taken of the actual August 25, 1983 smog episode in Figures 3.3ab. The general impression is that the visual range and contrast in both synthetic images appear to be approximately correct. The synthetic smoggy day photographs, however, have a blue cast to them when compared to the actual photographs of the smog event, and in particular the upper reaches of the sky in the synthetic smog images are far too blue.

In order to quantitatively compare the synthetic and actual photographs, numerical density distributions are plotted for each color plane in the San Gabriel

Mountains scene in Figure 3.6. The numerical density scale ranges from 0 (least bright) to 255 (brightest) and Figure 3.6 shows the frequency of occurrence of picture elements with a given numerical density level. It is evident that the synthetic smog day photograph is fairly close to actual observations in the red plane but has higher numerical density values than the actual smog event in the blue. To the extent that the model result for the synthetic smoggy day is brighter than the actual smog event at all wavelengths, the combined effect would be to add white light to the picture, making it appear "washed out". The excess brightness shift, however, is most pronounced in the blue plane and is of greater magnitude in the downtown Pasadena view than in the San Gabriel Mountains scene. To the extent that more blue than red or green light is added, the synthetic photographs appear both brighter and too blue.

The numerical density distributions are a means of comparing the overall brightness levels of one photograph to the overall brightness levels of another photograph. A point-to-point comparison of the photographs can be made, provided that the photographs are registered, that is, if any point A in one digitized photograph has the pixel coordinates (x,y), then the same point A in another digitized photograph will be assigned the same (x,y) coordinates. Then specifying coordinates (x,y) allows a direct comparison of brightness levels for any single point A in the two images.

The synthetic and actual smoggy day photographs of downtown Pasadena were registered and a point-to-point comparison made. This comparison is illustrated in Figure 3.7, where the average absolute difference in brightness levels is presented as a function of distance. The highest differences are in the blue plane, and for shorter observer-object distances. For reference, recall that numerical density is represented on a scale from 0 to 255, so that a difference of 25 DN units is equal to only 10% of full scale.
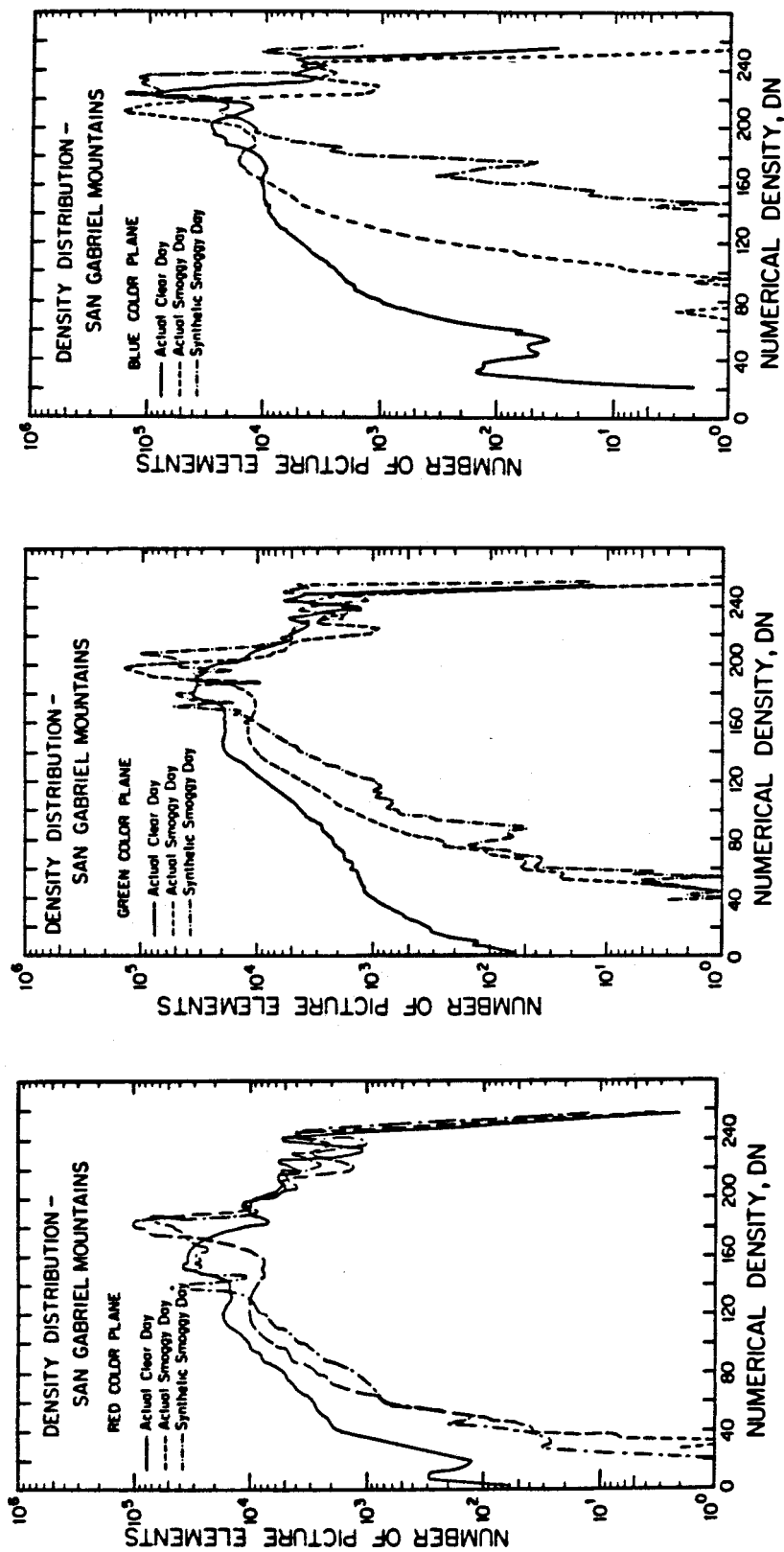
FIGURE 3.6. Numerical density distributions for the San Gabriel Mountains view.
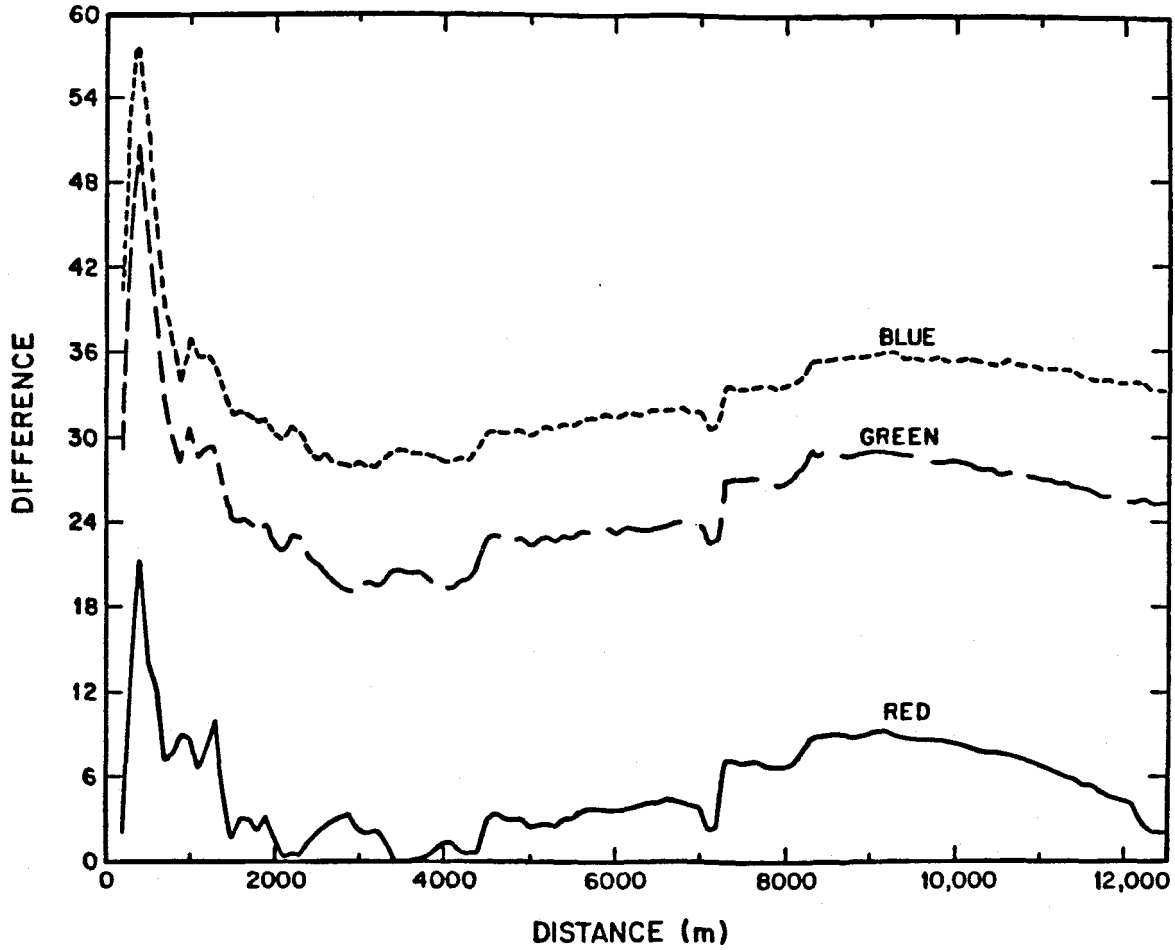
FIGURE 3.7. Average numerical density difference between actual smog event and synthetic image as a function of distance for the downtown Pasadena view.

The numerical density difference is the absolute value of the difference between the predicted and observed DN values. The distances are the distances from the camera position to the picture elements.

These absolute differences between all of the objects in the synthetic and actual smog event images also can be presented in contour drawings that overlay the scene photographed. Contour diagrams showing a point-to-point comparison of the difference in numerical density between the three different color planes are given for the downtown Pasadena scene in Figure 3.8. In the upper half of each contour diagram, which depicts the bulk of the cityscape, the mountains and the sky, large areas of the synthetic and actual smog photos differ in density by only a small, nearly constant value. Despite the enormous complexity of the scene and the sometimes great distances between particular buildings and the objects or mountains behind them, individual buildings and the mountains within the simulated photo blend into the haze just as smoothly as in the actual smog events (i.e., contrast reduction appears to be simulated fairly well for objects in the far field of view). Overall differences between observed and predicted images in the upper half of each contour diagram are in general fairly smooth functions of distance above or below the horizon. Isolated high difference areas in the foreground of the picture probably result from comparing photographs "taken" essentially on different days. The actual smog photograph was taken on August 25. The synthetic smog photograph is made from a clear day base photo taken on April 7. Differences in vegetation, cars in the foreground parking lot, and other similar factors cause these isolated high contours in the foreground of the picture. (Note, however, that these differences in foreground clutter are smaller than might otherwise be expected because shadow patterns in the two photographs are very similar. The sun position on those two days was in essentially the same place and little error is introduced from shadow pattern variation.)

Use of CIE chromaticity coordinates provides an alternative method to compare and to test color agreement between synthetic and actual smog event photographs. Billmeyer and Saltzman (1981) detail several methods of describing color
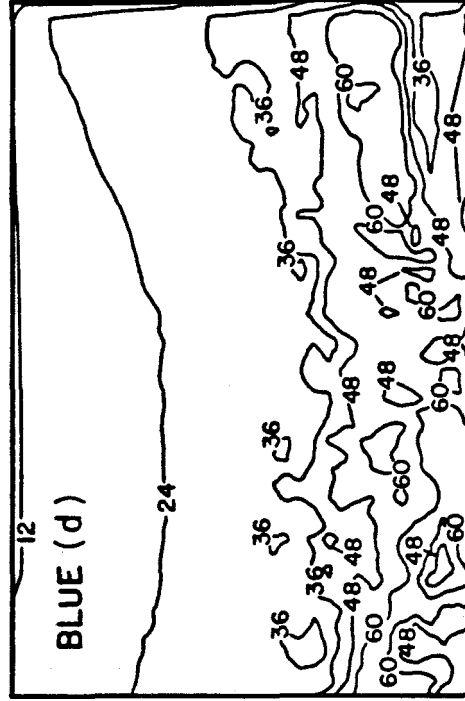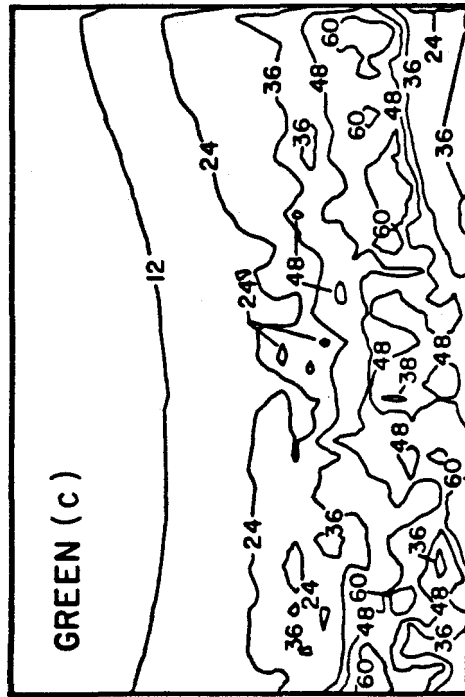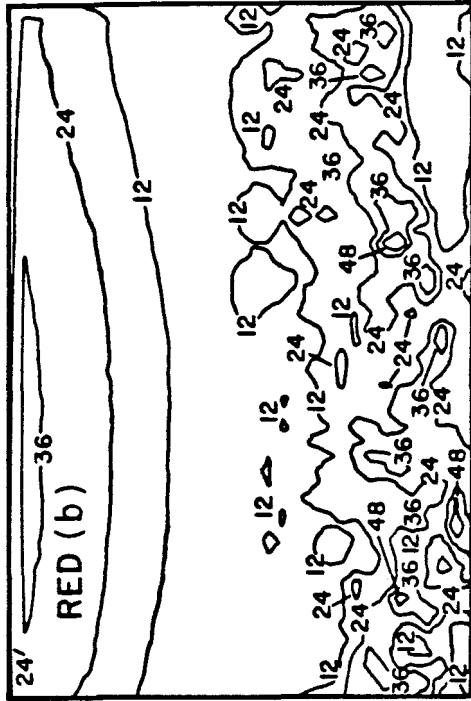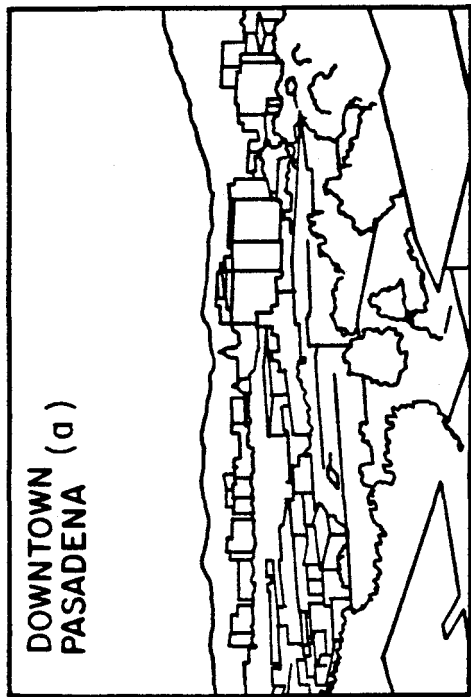
FIGURE 3.8. Contour diagram of numerical density difference between the actual
smoggy day photograph and the synthetic smog image of downtown Pasadena.
(a) Schematic of the view, (b) Red color plane, (c) Green color plane, (d) Blue color plane.

and color differences. The CIE System (Commission International de l'Eclairage or International Commission on Illumination) standardizes the source of illumination and the observer, and incorporates a procedure to numerically describe a color viewed under a standard light source by a standard observer. The color measurement procedure yields the chromaticity coordinates x and y and allows the calculation of a quantity, ΔE, which describes the color difference beween two colors. In order to determine chromaticity values, diffuse reflectance spectra were measured at a large number of paired locations on color photographic prints of the digitized clear day, the digitized actual smoggy day and the synthetic smoggy day using a Diano Matchscan II reflectance spectrophotometer. Chromaticity coordinates and color difference between paired points (ΔE, using the CIE 1976 $L^*a^*b^*$ formula), were computed for CIE Illuminant C from these reflectance spectra.

Interpretation of the results of these colorimetric measurements of model performance is illustrated in Figure 3.9. Figure 3.9a shows CIE color space, with a rectangular box that outlines the domain of the data taken from measurements made on the photographic prints. In Figure 3.9b, an expanded view of that rectangular area is depicted. Measurement point 19 referred to in Figure 3.9b represents a point on the front face of the San Gabriel Mountains. In the digitized clear day photograph, that location is greenish-blue in color, while on the digitized heavy smog photograph that point falls much closer to the location of Illuminant C (which would be essentially white). The visibility model calculation takes as input the digitized clear day mountain point 19 and from it produces a prediction of the appearance during the smog event which is fairly close to the actual digitized smog event photograph.

In Figure 3.10a this color comparison is made for a number of locations along the mountainsides and foothills shown in Figure 3.2a, 3.3a, 3.5a. The comparison is quite favorable; the points examined in the synthetic smog photo (Figure 3.10a)
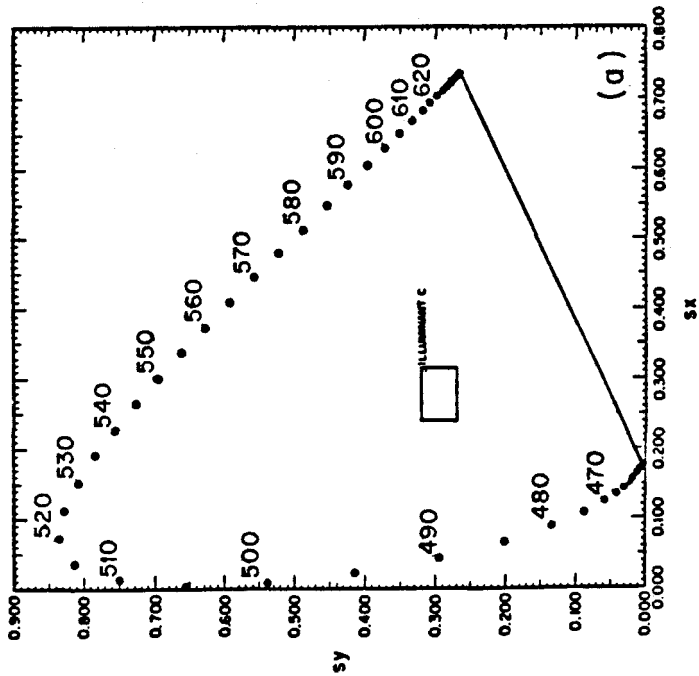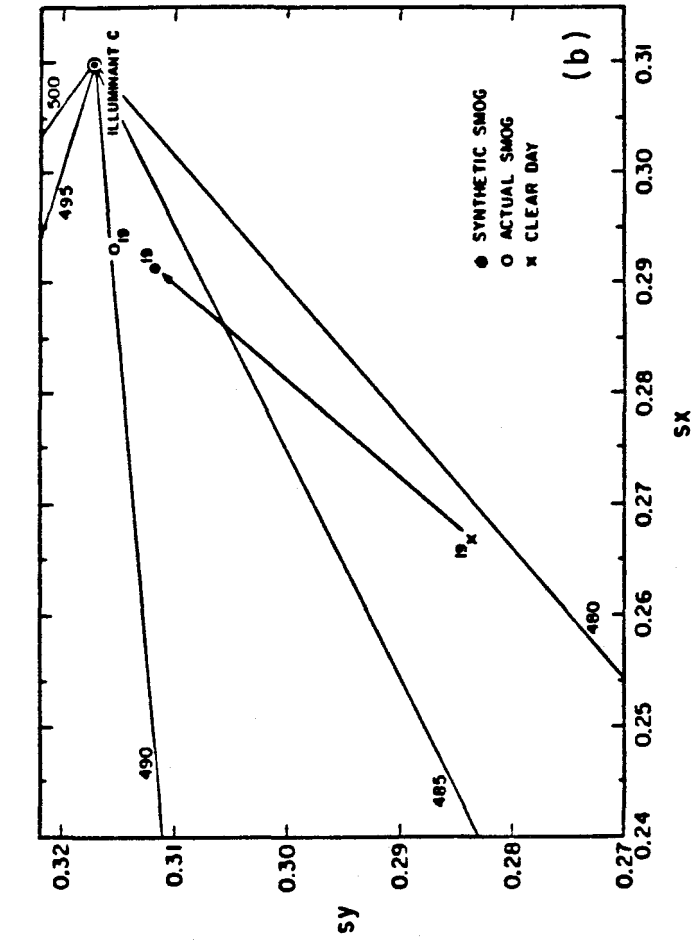
FIGURE 3.9. CIE chromaticity diagram

(a) CIE chromaticity diagram, (b) Illustration showing how a point on the digitized clear day photograph is moved through color space by the visibility model to create the synthetic smog photo. That theoretical prediction is compared to the same point on the digitized actual smog photograph. Dominant wavelength values in nanometers are noted along lines radiating from Illuminant C.

differ from corresponding points in the digitized actual smog photograph by an average of 7.8 ΔE units, while the digitized clear day base photograph differed from the digitized actual smog event photo by an average of 22.2 ΔE units over those points. In Figure 3.10b, it is seen that the visibility model fails dramatically in its treatment of the sky. The simulated smog event retains the appearance of the clear day blue sky while the digitized actual smog event sky is much closer to the Illuminant C location in color space (i.e., closer to being white).
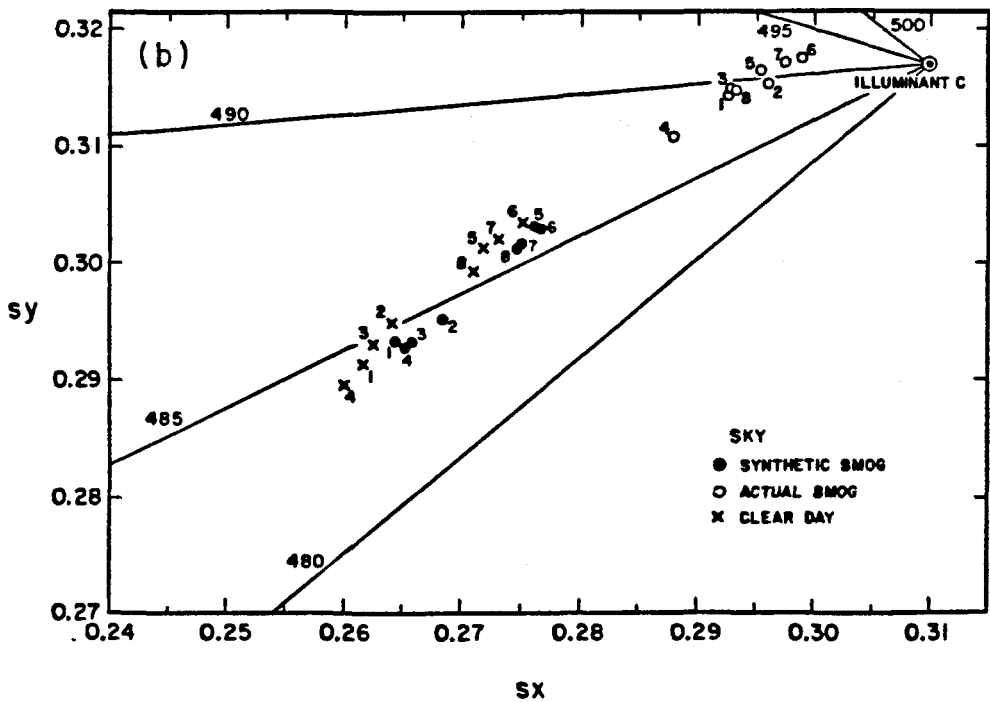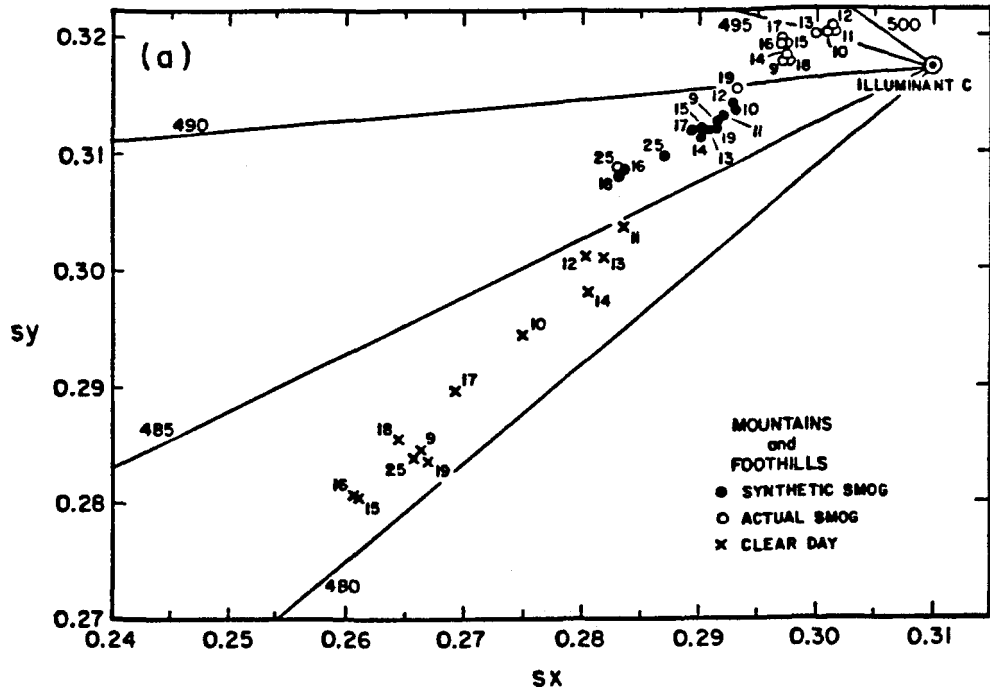
FIGURE 3.10. Corresponding points from photographs plotted on the CIE chromaticity diagram. Points are from prints of the San Gabriel Mountains view for the digitized clear day, synthetic smog event, and digitized actual smog event. (a) Mountains and foothills; (b) Sky. Dominant wavelength values in nanometers are noted along lines radiating from Illuminant C. Measurements made using the actual (not digitized) smog event photograph indicate that smoggy sky chromaticity values fall in the vicinity of (sx = 0.31, sy = 0.33).

3.7 Discussion

The comparison of the synthetic and actual photographs indicates that the model tested could be improved. Although contrast and visual range seem to be fairly well reproduced, excess blueness is introduced into the synthetic smog images. This is due to a feature inherent in the mathematical model used, which causes too much blue skylight to be added to the line of sight. In Equation 3.5, the path radiance term, $N_{sky}(1 - e^{-b_{ext}s})$, dominates the object radiance term, $N(0)e^{-b_{ext}s}$, at large distance, s. Picture elements located within the sky portion of the photographs are assigned a very large value of s, and as a result the blue clear day sky is reproduced in the synthetic smoggy day image even though the actual smog event sky is closer to being white. If the value of N_{sky} is sufficiently large, the path radiance term can cause a significant amount of light to be added to the appearance of objects located below the horizon only a relatively short distance from the camera. Analysis of the input data shows that for the red and green color planes the path radiance makes a signifiant contribution to the total radiance at large distances but that at short distances the inherent radiance of the objects viewed dominates. In the blue color plane, however, the path radiance term in Malm et al.'s model (1983) dominates even for short distances. The assumption that the clear day horizon sky radiance is the appropriate factor in the path radiance term of Equation 3.5 to use to model all points in the smoggy day is not valid. In addition, the model assumes horizon viewing for objects below the horizon and obtains N_{sky} for these points by extrapolating the sky brightness values below the horizon. This extrapolation means that N_{sky} is higher for points below the horizon, and this further increases the value of the path radiance term. Malm et al.'s procedure (1983) for extrapolation below the horizon should be abandoned in favor of a procedure that more accurately represents the path radiance term in

the model.

An improved visibility model would more accurately represent the object inherent radiance and the path radiance terms. Multiple scattering, the aerosol phase function, ground reflection, object reflectivity, and atmospheric variations should be considered. Image processing procedures could also be streamlined. The present procedure for handcrafting distance images is very labor intensive. An automated procedure for creating the distance image based on stereoscopic photography is feasible, and should be developed. The data base and methods developed in the present paper can then be used to verify the accuracy of these improvements.

3.8 Acknowledgements

3.9 References

Billmeyer, F.W., Jr., and Saltzman, M., 1981. *Principles of Color Technology* 2nd edition, New York: John Wiley & Sons.

Cass, G.R. 1979. On the relationship between sulfate air quality and visibility with examples in Los Angeles. *Atmospheric Environment 13:* 1069-84.

Countess, R.J., Wolff, G.T., and Cadle, S.H. 1980. The Denver winter aerosol: a comprehensive chemical characterization. *Journal of the Air Pollution Control Association 30:* 1194-1200.

Dixon, J.K. 1940. The absorption coefficient of nitrogen dioxide in the visible spectrum. *Journal of Chemical Physics 8:* 157-160.

Groblicki, P.J. Wolff, G.T., and Countess, R.J. 1981. Visibility-reducing species in the Denver "Brown Cloud" – I. Relationships between extinction and chemical composition. *Atmospheric Environment 15:* 2473-2484.

Handbook of Chemistry and Physics 1975. 56th edition, CRC Press, Cleveland, OH.

Hering, S.V., Bowen, J.L., Wengert, J.G., and Richards, L.W. 1981. Characterization of the regional haze in the southwestern United States. *Atmospheric Environment 15:* 1999-2009.

Hidy, G.M., et al. 1974. *Characterization of aerosols in California (ACHEX).* Science Center, Rockwell International. Prepared under California Air Resources Board contract no. 358.

Hodkinson, J.R. 1966. Calculations of colour and visibility in urban atmospheres polluted by gaseous NO_2. *International Journal of Air and Water Pollution 10:* 137-144.

Husar, R.B., Holloway, J.M., and Patterson, D.E. 1981. Spatial and temporal pattern of eastern U.S. haziness: a summary. *Atmospheric Environment 15:* 1919-1928.

John, W. and Reischl, G. 1980. A cyclone for size-selective sampling of ambient air. *Journal of Air Pollution Control Association 30:* 872-876.

Johnson, R.L., Shah, J.J., Cary, R.A., and Huntzicker, J.J. 1981. An automated thermo-optical method for the analysis of carbonaceous aerosols, in *Atmospheric Aerosols: Source /air quality relationships,* ed. E.S. Macias and P.K. Hopke. Washington, D.C., American Chemical Society.

Kerker, M. 1969. *The scattering of light and other electromagnetic radiation.* New York: Academic Press.

Kodak Color Films 1980. Kodak Publication Number E-77. Rochester, New York: Eastman Kodak Company.

Lin, C., Baker, M., and Charlson, R.J. 1973. Absorption coefficient of atmospheric aerosol: a method for measurement. *Applied Optics 12:* 1356-63.

Macias, E.S., Zwicker, J.O., Ouimette, J.R., Hering, S.V., Friedlander, S.K., Cahill, T.A., Kuhlmey, G.A., and Richards, L.W. 1981. Regional haze case studies in the southwestern U.S. - I. Aerosol Chemical Composition. *Atmospheric Environment 15:* 1971-1986.

Malm, W.C.; Molenar, J.V. 1984. Visibility measurements in national parks in the western United States. *Journal of the Air Pollution Control Association 34:* 899-904.

Malm, W., Molenar, J., and Chan, L.L. 1983. Photographic simulation techniques for visualizing the effect of uniform haze on a scenic resource. *Journal of the Air Pollution Control Association 33:* 126-129.

McCartney, E.J. 1976. *Optics of the atmosphere-scattering by molecules and particles.* New York: Wiley.

Nicholls, R.W. 1984. Wavelength-dependent spectral extinction of atmospheric aerosols. *Applied Optics 23:* 1142-1143.

Ouimette, J.R. 1980. Chemical species contributions to the extinction coefficient. Ph.D. thesis, California Institute of Technology: Pasadena, California.

Penndorf, R. 1957. Tables of the refractive index for standard air and the Rayleigh scattering coefficient for the spectral region between 0.2 and 20.0 μm and their application to atmospheric optics. *Journal of the Optical Society of America 47:* 176-182.

Sloane, C.S. 1983. *Optical properties of aerosols of mixed composition.* General Motors Research Laboratories, Warren, MI. GMR-4351 ENV #157.

Sloane, C. 1984. Optical properties of aerosols of mixed composition. *Atmospheric Environment 18:* 871-878.

Sloane, C.S., and Groblicki, P.J. 1981. Denver's visibility history. *Atmospheric Environment 15:* 2631-38.

Stelson, A.W., and Seinfeld, J.H. 1981. Chemical mass accounting of urban aerosol. *Environmental Science and Technology 15:* 671-79.

Trijonis, J. 1979. Visibility in the Southwest - an exploration of the historical data base. *Atmospheric Environment 13:* 833-843.

White, W.H., and Roberts, P.T. 1977. On the nature and origins of visibility-reducing aerosols in the Los Angeles air basin. *Atmospheric Environment 11:* 803-812.

Wickramasinghe, N.C. 1973. *Light scattering functions for small particles with applications in astronomy.* New York: Wiley.

Williams, M.D., Treiman, E., and Wecksung, M. 1980. Plume blight visibility modeling with a simulated photograph technique. *Journal of the Air Pollution Control Association 30:* 131-134.

CHAPTER 4

IMPROVEMENT OF IMAGE PROCESSING-BASED VISIBILITY MODELS

4.1 Abstract

A two-stream approximate solution to the radiative transfer equation is incorporated within a simple image processing-based visibility model. The two-stream solution gives fairly accurate results without the great computational effort required of more exact radiative transfer codes. The resulting synthetic photographs show a predicted sky color that is much closer to the color of the sky recorded in actual smoggy day photographs than has been the case for the simple visibility models proposed previously. Objects below the horizon in the synthetic photographs are brighter than actually observed, indicating a need to improve the model performance for objects below the horizon.

4.2 Introduction

Synthetic photographs are a powerful means of displaying the results of a visibility modeling calculation (Malm et al.,1983; Williams et al., 1980, 1981; Larson et al., 1987). Such synthetic photographs simulate the appearance of a scene under specified air pollution conditions, and can include a vast amount of information on how the apparent contrast and apparent color of each object in the field of view are altered within a polluted atmosphere.

Verification tests performed on a simple image processing-based visibility model (Larson et al., 1987) indicate that it may be possible to drastically improve the performance of the model that was tested in that study by including a more exact treatment of the appearance of the sky and by calculating the contribution of skylight to the perceived intensities of objects in the field of view more accurately. This work concentrates on improving the appearance of the sky in the synthetic photographs. To investigate the possibility for improvement in sky appearance, a light scattering code is employed to produce synthetic photographs such that the intensity of singly scattered skylight is computed exactly and a two-stream approximation is used to obtain the intensity of light that is multiply scattered.

The resulting synthetic photographs can be compared to actual photographs of the same scene taken under the conditions modeled. The degree of improvement in the model's representation of the sky then can be assessed.

4.3 Image Processing-Based Visibility Models

The light reaching an observer from an object consists of two components: the light from the object that is attenuated by the scattering and absorbing properties of particles and gases in the atmosphere, and the skylight which is scattered toward

the observer along the line of sight. This second contribution is called the path radiance. The apparent intensity, I, of an object as seen by an observer then can be written as:

$$I = I_0 e^{-b_{ext}x} + I_{sky}(1 - e^{-b_{ext}x})$$ (4.1)

for a horizontal line of sight (Duntley, 1948; Middleton, 1950; Duntley et al., 1957; Masaki, 1960; Middleton, 1968). I_0 is the inherent intensity of the object viewed. This is the intensity of light from an object received by an observer who is at the location of the object. The term, b_{ext}, is the atmospheric extinction coefficient, a quantity which describes the amount of light that is scattered or absorbed in the atmosphere. The distance between the observer and the object is x, and I_{sky} is the intensity of the horizon sky in the direction of the line of sight. Equation 4.1 is central to the image processing-based visibility model that was proposed by Malm et al. (1983) and was tested against field observations by Larson et al. (1987).

In the simplest image processing-based visibility model, a photographic slide of a scene taken under very clean conditions is used as a base photograph. The base photograph is employed to create a synthetic photograph of how the same scene would appear under specified air pollution conditions. For each of several million points in the base photograph, for each of the three color planes (red, green, and blue) that make up the slide, the film density is measured by a microdensitometer. Film density is then related to the light intensity value that exposed the film through the film characteristic curves given by the film manufacturer. These intensity values, I, are used to determine the values of I_0 for each point in the clear day picture in each color plane by rearranging Equation 4.1 to solve for I_0:

$$I_0 = I e^{b_{ext}x} + I_{sky}(1 - e^{b_{ext}x})$$ (4.2)

where the value of b_{ext} is the extinction coefficient from the clear day. By definition,

the value of b_{ext} for a clear day is very small, so inaccuracies in this procedure for obtaining I_0 are not particularly important when the model at hand is to be used to depict very heavily polluted urban areas. The resulting array of I_0 values are assumed to be independent of pollutant loading. In order to create a synthetic photograph of the same scene under heavily polluted conditions, a distance image, which is a matrix of values assigning a distance, x, to each point in the photograph, and a sky radiance image, which gives a value of I_{sky} to each point in the photograph, are needed along with the value of the extinction coefficient, b_{ext}, for the condition to be modeled. Using these values in Equation 4.1, a new array of intensity values, I, are produced. The new intensity array is converted back to an array of film density values. Then through a film writing device, a photograph is produced representing the film densities calculated for the heavy smog event.

In the procedure proposed by Malm et al. (1983), the sky radiance image (the array of I_{sky} values) was determined from the sky in the clear day photograph, and values of I_{sky} needed for calculating skylight addition to the appearance of objects located below the horizon were obtained by extrapolating trends in I_{sky} values to below the horizon. The field of inherent intensities, I_0, in Malm et al.'s model was also assumed to be independent of pollutant loading and thus was determined from the clear day photo, as described by Equation 4.2 above. In reality, both I_{sky} and I_0 are dependent on the extinction coefficient. Using the sky radiance image and the inherent intensity image derived from the clear day photograph to create a synthetic image produces a synthetic photograph that is too bright and too blue (Larson et al., 1987).

Using the clear day photograph to determine the sky radiance image results in the sky of every synthetic photograph being modeled as the clear day sky. This

occurs because if the distance to the target viewed is allowed to go to infinity in Equation 4.1 (as for the sky), the target intensity is equal to the intensity of the clear day blue sky, even though the actual smog event sky is closer to being white. In addition, the path radiance values for objects below the horizon would have a greater blue component than is realistic. The appearance of the synthetic photograph is fairly sensitive to the sky radiance image used in its production. At very small object to observer distances, the contribution of the path radiance term should be small, since at close range, most of an object's apparent radiance is due to light coming directly from the object. If the clear day sky radiance image is used in the production of a photograph which simulates a smoggy day, the value of I_{sky} can be large enough to make a significant contribution to an object's apparent radiance even at small object to observer distances. This effect is especially prominent for the blue color plane in those cases where the clear day sky is used to define the skylight intensities.

In an alternative image processing-based procedure, Williams et al. (1980, 1981) attempted to depict the appearance of regional haze and distinct power plant plumes as a function of object color, object distance from the observer, and the level of air pollution in the atmosphere. In that model, Williams et al. incorporated a radiative transfer code based on the numerical technique of Braslau and Dave (1972). To test the results of the model, the resulting plume images were compared to actual plume photographs, but, at best, only reasonable agreement was found. Williams et al. also tested the results of the radiative transfer code by comparing the implemented code (that used three Fourier coefficients in the expansion to determine radiance) to the results of the code when six coefficients were used. Results agreed to within 20% depending on sun and viewing angles. Radiative transfer simulations were also compared to measured radiance on a

moderately hazy day. These agreed to within an average of 24%. Williams et al. concluded that more validation work was needed to fully test the model.

4.4 Radiative Transfer

In order to predict the visual appearance of light within the earth's atmosphere, Dave (1980) states that descriptions of the following are necessary: the solar spectrum in the range of 365 nm to 784 nm, the scattering properties of air molecules and of suspended particulate matter in the atmosphere, the absorption properties of gases and of suspended particulate matter, the spectral and directional reflectances of surfaces, the atmospheric composition, and "a complete psychophysical specification of color." Fortunately, the last requirement is not necessary to solve the radiative transfer equation which describes how light is propagated through the atmosphere. In solving the radiative transfer equation, horizontal inhomogeneities in the atmosphere are very difficult to treat. Solutions to the equation generally assume that a plane parallel atmosphere is present which is homogenous in character in the horizontal direction and infinite in extent. Inhomogeneities can be incorporated in the vertical direction, which is finite in extent. Vertical gradients in aerosol properties, gas concentration, pressure and temperature can be included in the calculations. The light intensity calculated is a function of the wavelength of light considered, the elevation of the observer relative to the ground, the angle of the sun, the viewing direction, and the specification of the solar spectrum.

The equation of radiative transfer is given by Isaacs (1981):

$$\mu \frac{dI_\lambda(\tau, \mu, \phi)}{d\tau} = I_\lambda(\tau, \mu, \phi) - J_\lambda(\tau, \mu, \phi) \qquad (4.3)$$

with:

$$J_\lambda(\tau, \mu, \phi) = \frac{\omega_0}{4} F_\lambda P(\mu, \phi; \mu_0, \phi_0) exp\left(\frac{-\tau}{\mu_0}\right) +$$

$$\frac{\omega_0}{4\pi} \int\limits_0^{2\pi} \int\limits_{-1}^{+1} P(\mu, \phi; \mu', \phi') I_\lambda(\tau, \mu', \phi') d\mu' d\phi' \qquad (4.4)$$

where

λ is the wavelength of light considered.

I_λ is the wavelength dependent radiance.

J_λ is the source function.

πF_λ is the incident solar irradiance.

ω_0 is the single scattering albedo (the ratio of the scattering coefficient to the extinction coefficient).

τ is the optical depth, $\tau = \int_0^x b_{ext} dx'$.

μ is the cosine of the zenith angle of the observer's line of sight.

μ_0 is the cosine of the zenith angle of the sun.

ϕ is the azimuth angle of the observer's line of sight.

ϕ_0 is the azimuth angle of the sun.

$P(\mu, \phi; \mu', \phi')$ is the angular scattering function which describes the probability that light from the direction (μ', ϕ') will be scattered in the direction (μ, ϕ).

The first term on the right-hand side of Equation 4.3 describes the loss of intensity as light is scattered and absorbed as the light travels through the atmosphere. The second term on the right side of Equation 4.3 accounts for the gain of intensity as light is scattered into the line of sight. This term, called the source function, $J_\lambda(\tau, \mu, \phi)$, consists of singly scattered light (the first term on the

right-hand side of Equation 4.4) and of multiply scattered light (the second term on the right-hand side of Equation 4.4). Equations 4.3 and 4.4 are subject to boundary conditions both at the top and at the bottom of the atmosphere. There are several classes of approaches to solving a radiative transfer problem. Three of these are numerical, exact analytical, and approximate analytical solutions.

Many numerical techniques exist to solve this equation subject to its boundary conditions. (Hansen and Travis, 1974, have reviewed a number of these.) Numerical techniques have the advantage of being very exact, but require extensive computing time. Although some numerical solutions have been used to calculate predicted light intensities in clean and polluted atmospheres (Williams et al., 1979, 1980; Dave, 1975, 1978, 1981), for the application of radiative transfer calculations to visibility modeling, less exact, more computationally manageable approaches are preferred. The numerical methods serve as standards against which to compare approximate solutions. For a few cases exact analytical solutions exist, but the approximate analytical techniques can be applied to many more general situations.

In an approximate analytical solution, assumptions are made in order to simplify the radiative transfer equation. If the single scattering approximation is made, the second term on the right-hand side of Equation 4.4, which describes multiple scattering, is set to zero. This simplification is only valid in the limit of clean atmospheric conditions. When the solutions for the single scattering case are compared to numerical solutions that involve multiple scattering, errors of up to 15% even for clean atmospheric conditions for the single scattering approximation are reported (Isaacs, 1981). The error increases with pollutant loading. Dave (1964) reports that sky intensities are underestimated by 15% when higher orders of scattering are not included in a light scattering calculation, and that errors up to factors of two to four are possible if the single scattering approximation is used

to model polluted conditions. Single scattering results that were 20% to 50% lower than the results of multiple scattering calculations were found by Bergstrom et al. (1981), and Isaacs and Özkaynak (1980) calculated singly scattered intensities that were 30% to 40% lower than intensities calculated with more accurate techniques.

In order to account for multiple scattering while still maintaining computational efficiency, the multiple scattering term in Equation 4.4 can be approximated. In the diffuse field method, this approximation is accomplished by assuming that the skylight radiance field is isotropic (independent of angle) and that flux conservation holds (Latimer et al., 1978; Özkaynak et al., 1979). The errors associated with the diffuse field approximation can be large. It is possible to have up to a 30% difference when results from the diffuse field approximation are compared to results from a numerical calculation (Isaacs, 1981), and this error increases when more polluted conditions are modeled. Bergstrom et al. found that when the diffuse field approximation was used to calculate horizon sky intensities, the results were within 10% to 20% of values obtained from numerical solutions to the full radiative transfer equation.

Another class of approximate analytical solutions are the finite stream approximations. Analytical two-stream (Chu and Churchill, 1955; Coakley and Chylek, 1975) and four-stream (Liou, 1974) approximations exist. The two-stream formulations are useful since they are computationally efficient and are fairly accurate. In the two-stream approximation, the term representing multiple scattering is estimated by asuming that the intensity, $I(\tau, \mu, \phi)$, can be written as the sum of an upward and downward component, $I^+(\tau)$ and $I^-(\tau)$, where $I^+(\tau)$ is an averaged intensity over the upper hemisphere:

$$I^+(\tau) = \frac{\int\limits_0^{2\pi}\int\limits_0^1 I(\tau,\mu,\phi)\mu d\mu d\phi}{\int\limits_0^{2\pi}\int\limits_0^1 \mu d\mu d\phi} \tag{4.5}$$

and $I^-(\tau)$ is the averaged intensity over the lower hemisphere:

$$I^-(\tau) = \frac{\int\limits_0^{2\pi}\int\limits_{-1}^0 I(\tau,\mu,\phi)\mu d\mu d\phi}{\int\limits_0^{2\pi}\int\limits_{-1}^0 \mu d\mu d\phi} \tag{4.6}$$

This approximation reduces the equation of radiative transfer to a set of equations that can be solved analytically. It does not require the assumption of flux conservation, as in the diffuse field case, and results in a better treatment of multiple scattering and a more accurate description of the angular distribution of scattered light. In comparison of the results of two-stream approximations against the calculations done using numerical techniques, Isaacs (1981) reported agreement within 5% to 13%, and Coakley and Chylek (1975) reported agreement to within 12% for sky intensities.

Other methods exist to determine sky intensity. Monte Carlo simulations, employing techniques based on the theories of probability, have been applied to light scattering problems. Such simulations rely on the principle that if the probability of occurrence of each event in a series of events is known, it is possible to predict an estimate of the final outcome. As light travels through the atmosphere and encounters a particle, there is a chance that the light will be scattered or absorbed. If the light is scattered, the phase function of the particle gives the probability of the light being scattered at a certain angle. If the light reaches the ground, there is a chance that it will be absorbed or reflected. By simulating a number of interactions between light and particles and atmospheric boundaries using the methods

of probability, it is possible to compute the predicted light intensities reaching an observer. The Monte Carlo methods for simulating light scattering are generally applied to difficult cases, such as non-plane parallel atmospheres, or cloud problems, since other methods provide much more efficient means of modeling a plane parallel atmosphere with no horizontal variation.

When considering the appearance of the sky under clean conditions, it is possible that sky radiances may be determined by consulting measured data on the distribution of clear sky radiance (Steven, 1977). To determine the clear sky radiance distributions, many actinometer measurements are made of points in the sky. These individual radiance measurements are normalized by the total amount of horizontal diffuse irradiance. The normalized distributions are reported to be independent of turbidity, in the range of fairly clean conditions.

4.5 Calculation of Sky Intensities

The problem addressed in this study is to select and test a method for calculating skylight intensities within the context of a simple image processing-based visibility model. The method selected must meet two criteria: (1) skylight intensity predictions must be made that avoid the previously mentioned problems with calculations based solely on clear day sky photographs, and (2) the method must be computationally quick, as intensities at many points in the sky must be computed to define the sky shown in an arbitrarily chosen scene.

Because of its computational efficiency and accuracy, a two-stream approximation was chosen as a promising approach to the prediction of sky intensities for use in an image processing-based visibility model. A test of this approach then proceeds in two steps. First, a specific method for calculating skylight intensities was adopted. Then the skylight intensity results were merged with the remainder of the present image processing model.

The two-stream calculation of skylight intensities was based on the approach of Coakley and Chylek (1975) and on the analytical solution reported by Kaufman (1979). The light scattering computer code used to implement this scheme was written by Dr. Christine Sloane of General Motors Research Laboratories (Sloane, 1987). That code corrects for minor errors in Kaufmann's solution.

Input parameters to the skylight intensity model include the concentration of NO_2 (a light absorbing gas), information on the aerosol size distribution, data on the aerosol refractive index, the elevation of the observer relative to the ground, the sun angle, the viewing angles, the reflectivity of the ground, and the height of the atmospheric mixing layer below which the pollutants are trapped. The light source characteristics must also be specified. The code used allowed for six

different descriptions of the incoming solar radiation. The following results are based on the use of the standard daylight illuminant D65 as the source. The reflectivity of the ground was taken to be 0.15.

The first section of that program calculates the extinction coefficient given the concentration and properties of the gases and suspended particulate matter present. The gaseous absorption coefficient is calculated from the concentration of NO_2 and the relationship given by Hodkinson (1966). The Rayleigh scattering coefficient is taken to be 0.15×10^{-4} m^{-1} at a wavelength of 550 nm and to have an inverse fourth power dependence on the wavelength. The aerosol scattering and absorption coefficients are calculated from Mie theory. The radiative transfer equation is then solved with the two-stream approximation, and the resulting output gives values of the calculated intensities due to singly scattered light and intensities including both singly scattered and multiply scattered light for each viewing angle over a number of wavelengths. The visual range and chromaticity coordinates of the sky in the direction viewed also are given.

The chosen procedure for computing skylight intensities was inserted into the structure of the image processing-based visibility model previously proposed by Malm et al. (1983). This modification to Malm's model was accomplished by replacing Malm's sky radiance image that was based on the clear day photograph by a sky radiance image defined by the results of the two-stream radiative transfer calculation. The improved treatment of the sky then was tested by appliction to the clear day and smoggy day data sets collected at Pasadena, CA, by Larson et al. (1987). Of the two sets of digitized photographs present in that data base, the data for the view of downtown Pasadena were chosen for study.

To create the necessary sky radiance image for use with the downtown Pasadena data set, skylight intensity values were computed for the 27 viewing angles

leading to the sky points shown in Figure 4.1. Sky intensities were calculated for conditions present on both the clear day (April 7, 1983) and on the smoggy day (August 25, 1983). For this northwest facing scene of downtown Pasadena, intensities for viewing angles from 1° elevation above the horizon to 15° above the horizon in one degree increments were computed for a central vertical transect of the portion of the sky included in the photograph, as shown in Figure 4.1. Sky intensities for view angles of 1°, 6°, and 12° from the horizon were calculated for a vertical transect in the far left, far right, mid-left and mid-right sections of the photographs. For the area of the sky chosen, it was found that the computed intensities varied little in the horizontal direction. Therefore, the intensities calculated for the central postion of the sky were taken to apply for all sky positions at the same elevation. The remaining points in the sky image were filled in by interpolation in the vertical dimension between the elevations for which values were calculated.

The calculated skylight values are in the form of intensities, and the data needed for the production of the synthetic photographs must be in numerical density units, so a conversion is needed to relate the intensities to the densities. The clear day slide, which serves as the substrate upon which the visibility model calculations are performed, was used to construct a calibration curve that relates the calculated intensities to the densities at the corresponding points in the photograph of the sky. Densities in the red, green and blue planes of the slide were determined for each angle for which intensity calculations were performed. A linear regression analysis was carried out for each color plane to determine the relationship between the measured densities of those points studied in the sky and the logarithm of the corresponding intensities calculated for those points. The correlation coefficient in the red and green plane was 0.98. The correlation for
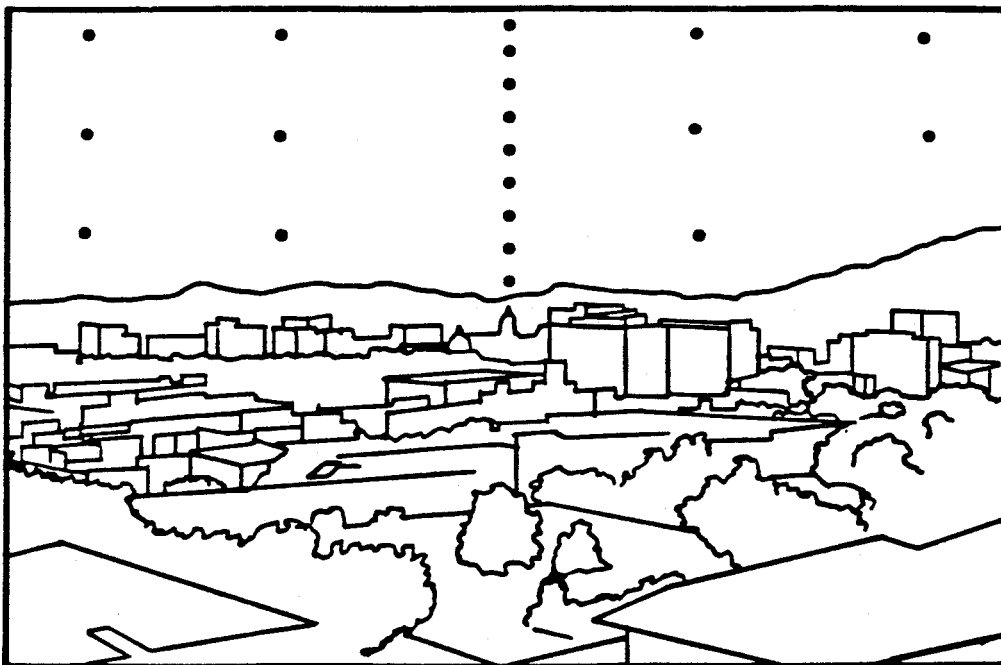
FIGURE 4.1. Dots illustrate points of the downtown
Pasadena photograph for which sky intensities were calculated.

the blue plane was lower, r=0.67. Using the calibration curves resulting from this regression analysis, the sky intensities calculated using the two-stream model for the smoggy day of August 25, 1983 were converted into densities and a new sky radiance image was formed. Intensities were held constant below the horizon. This sky radiance image was used in Equation 4.1 with the same procedure as described in Larson et al. (1987) to produce a synthetic photograph.

4.6 Results and Discussion

The synthetic photograph produced from the August 25, 1983 air pollution data and from the sky radiance image calculated for August 25, 1983 using a two-stream approximate solution to the radiative transfer equation is presented in Figure 4.2. The photograph is noticeably brighter than the synthetic photograph that resulted from application of a simple visibility model (Larson, et al., 1987), and the appearance of the sky is more accurately represented by the improved model than by the simple model. The sky in the new photograph is not predominately blue, as is the case with the synthetic photographs produced previously.

Graphs showing the average difference in numerical densities (DN) between a digitized version of an actual photograph of the August 25 smog event versus the synthetic photographs of that smog event as a function of observer to object distance are given in Figures 4.3 and 4.4. Both graphs are for the downtown Pasadena scene described by Larson et al. (1987). Figure 4.3 depicts the results for the old model, in which the clear day sky photograph provides the skylight intensity map, and Figure 4.4 illustrates the results of the new model in which sky color is determined from radiative transfer calculations. The differences in numerical densities can range from 0 to 255, so a difference of 30 DN units is a 12% difference relative to full scale, and a difference of 45 density units is only an 18% difference in full scale. Therefore in considering an observer's reaction to the

FIGURE 4.2. Synthetic image of smog event resulting
from new image processing-based visibility model.

The appearance of downtown Pasadena on August 25, 1983 is modeled in this synthetic photograph. The photograph results from a new image processing-based visibility model which incorporates a sky radiance image derived from radiative transfer calculations.

photographs produced, it is more important to look at the relative differences in the red, green, and blue color planes to evaluate color balance, than to consider the differences as an indication of absolute error. In the old model, differences between the actual and synthetic smog photographs for objects below the horizon, were larger in the blue color plane than in the green and especially in the red color plane. This meant than the synthetic photograph had a blue cast to it, relative to the actual smoggy day photograph. In the old model, average absolute differences in the sky for the red and blue were comparable, with lower differences in the green. This resulted in a sky color much closer to the clear day sky than to the color of the sky on a smoggy day. In the new model, the sky differences in the red, green and blue planes are similar, which points out that the sky is closer to the white color expected in a smoggy day photograph.

The new model predicts that the brightness levels of objects below the horizon are greater than the brightness levels which are observed in the actual smoggy day photograph for those objects. In the new model, the I_{sky} values are held constant below the horizon. However, since the sky intensities predicted for the new model are brighter than the sky intensities used in the old model (as is appropriate for the whitish sky of a smoggy day), when these values are held constant below the horizon, the contribution of the path radiance term to the apparent intensity of objects below the horizon is large. This contribution is large even for objects located at a short distance from the observer, in which case most of an object's apparent radiance comes from light coming directly from the object. A more accurate sky intensity array would have I_{sky} values dropping off below the horizon.

The sky portions of the photographs also can be compared by plotting points from the photographs in color space on the C.I.E. chromaticity diagram (Figure 4.5). In the old model, the synthetic smoggy day photographs had a sky that was

AVERAGE PIXEL DIFFERENCE BETWEEN

SYNTHETIC AND SMOGGY DAYS- PASADENA VIEW (OLD)
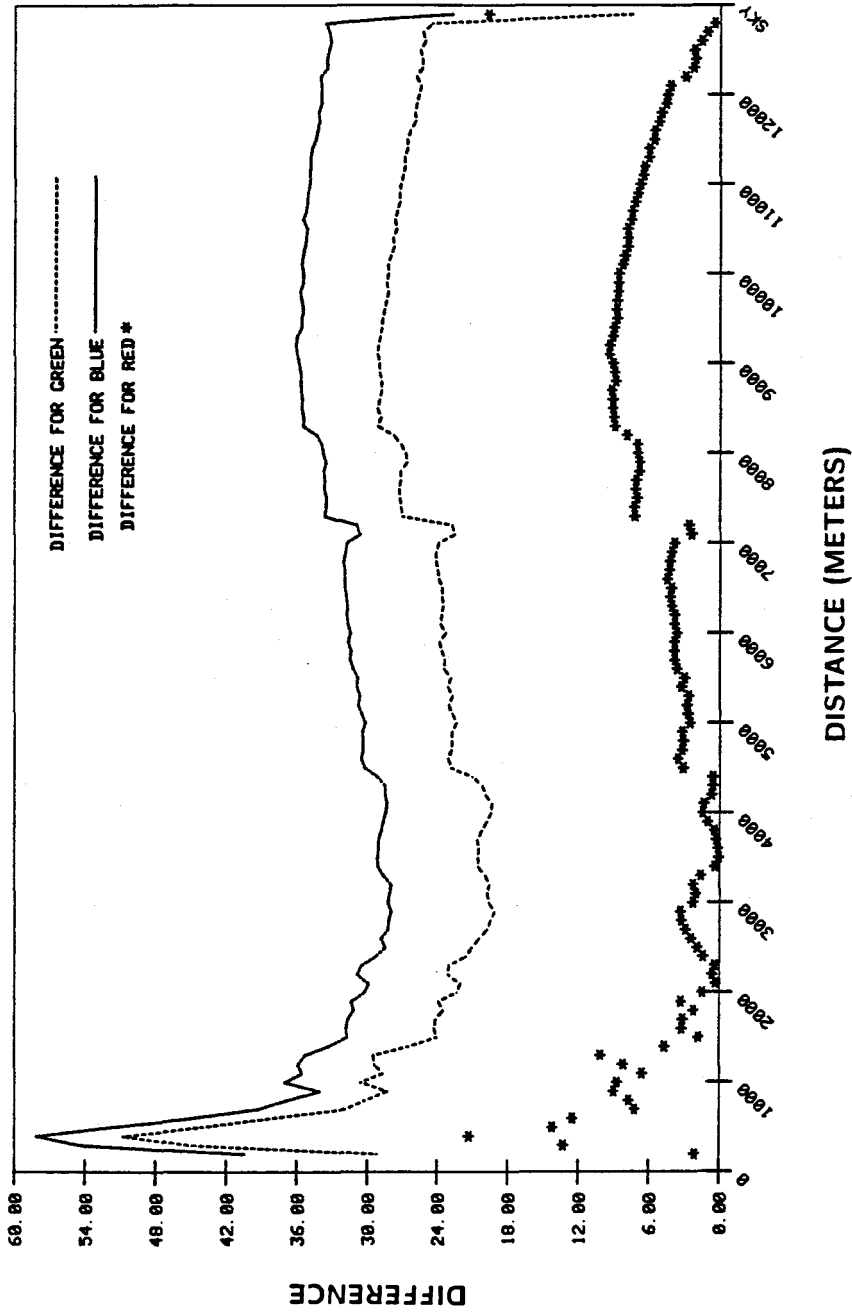
FIGURE 4.3. Average difference in photographic densities between the actual and synthetic photographs. (I)

Differences are presented as a function of the distance between object and observer for the downtown Pasadena scene. Synthetic photograph was produced by the old image processing-based visibility model.
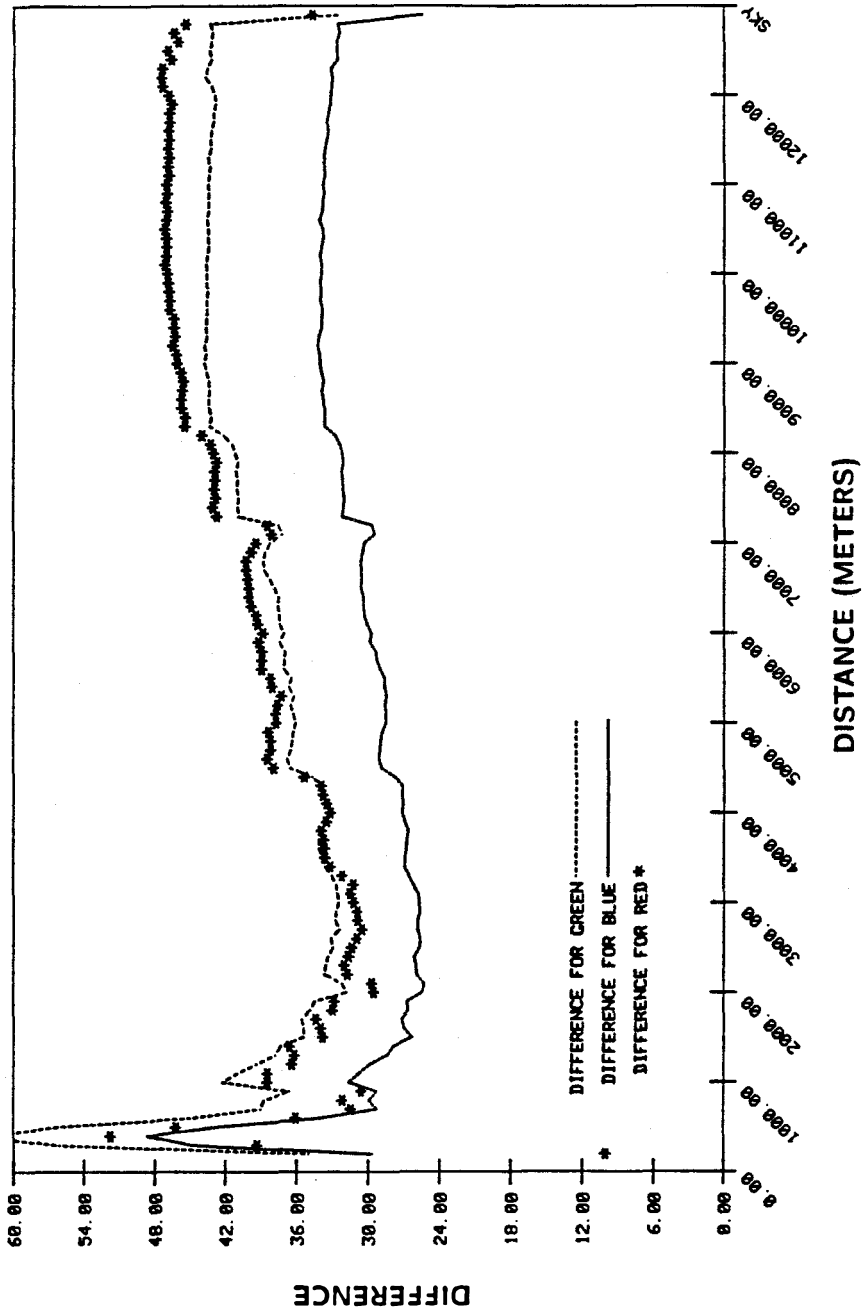
FIGURE 4.4. Average difference in photographic densities between the actual and synthetic photographs. (II)

Differences are presented as a function of the distance between object and observer for the down-town Pasadena scene. Synthetic photograph was produced by the new image processing-based visibility model.

not substantially different from the sky in the clear day photograph, as would be expected since the clear day sky image was used in the old model. Chromaticity coordinates calculated from the spectrum of clear day sky intensities resulting from the two-stream solution to the radiative transfer equation, fall close to the chromaticity coordinates for the clear day sky measured from the clear day photograph using a Diano Matchscan II reflectance spectrophotmeter. This indicates that calculated clear day intensities are a good representation of the intensities which originally exposed the photographic film. Points calculated from the radiative transfer code for the smoggy day sky, points measured from the synthetic smoggy day photograph resulting from the new model, and points measured from the undigitized actual smoggy day photographic print are virtually identical when plotted on the C.I.E. chromaticity diagram. This shows good agreement in modeling the smoggy day sky and good photographic control during image processing.
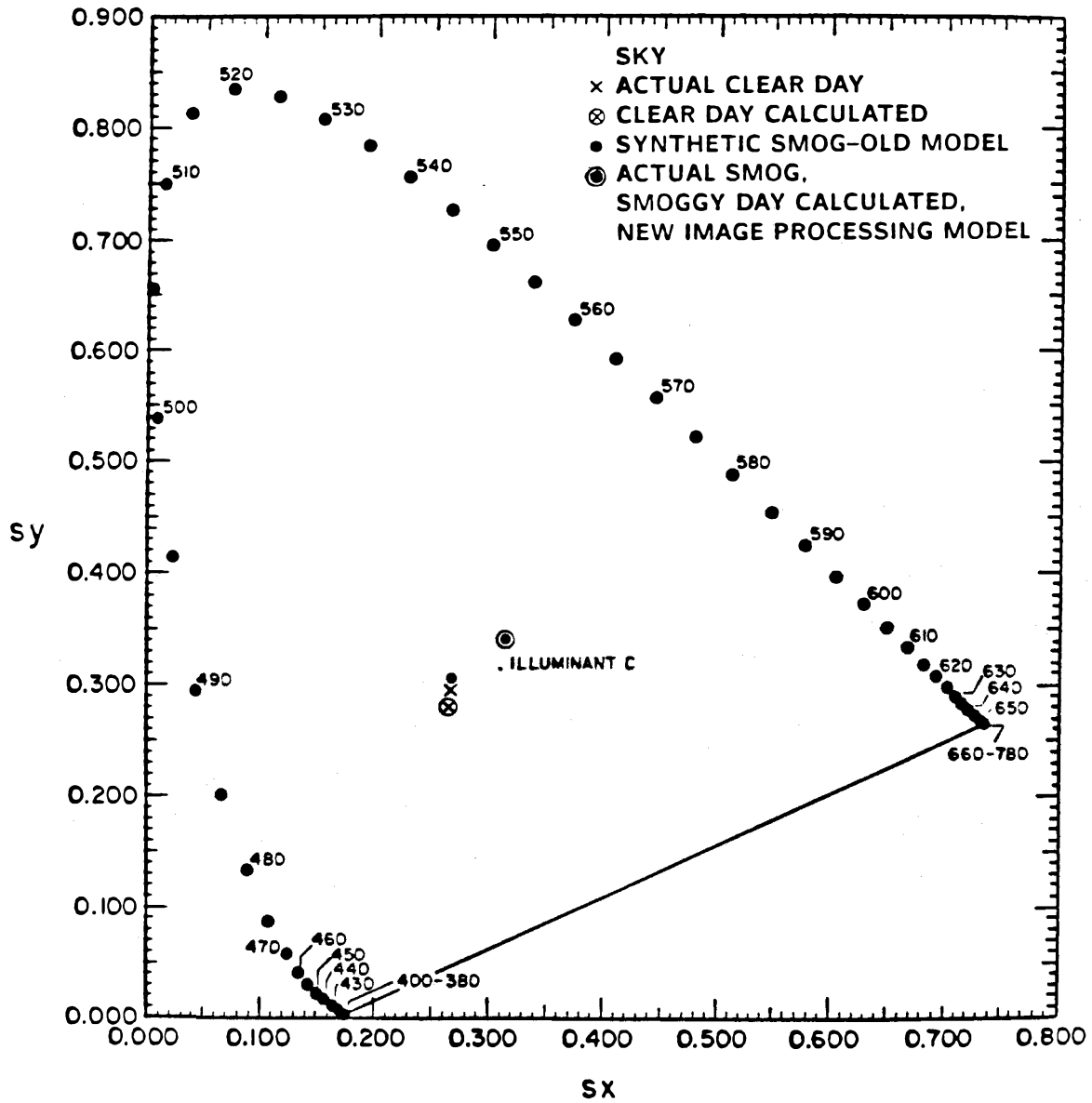
FIGURE 4.5. Comparison of sky color using the C.I.E. chromaticity diagram.

4.7 Conclusions

Synthetic photographs resulting from the visibility model proposed by Malm et al. (1983) can reproduce the contrast degradation present in polluted urban conditions, but do not closely reproduce the sky color observed on smoggy days. To improve the representation of sky color, a new sky radiance image was calculated using a two-stream approximate solution to the radiative transfer equation. The skylight intensity solutions from the two-stream approach are reported to agree with solutions calculated by more accurate numerical techniques to within 13%, while requiring much less computational effort than the numerical approaches (Isaacs, 1981). The synthetic photographs resulting from the improved model give a good representation of the actual smoggy day sky, but objects below the horizon in the new synthetic photographs are brighter than in the actual smoggy day photograph. This points out the need for improving the performance of the model in predicting intensities for objects below the horizon.

4.8 References

Bergstrom, R.W., Babson, B.L., Ackerman, T.P. 1981. Calculation of multiply-scattered radiation in clean atmospheres. *Atmospheric Environment* **15**, 1821-1826.

Braslau, N., Dave, J.V. 1972. Effect of aerosols on the transfer of solar energy through realistic model atmospheres. IBM Research Report RC4114, Palo Alto, CA.

Chu, C.M., Churchill, S.W. 1955. Numerical solution of problems in multiple scattering of electromagnetic radiation. *Journal of Physical Chemistry* **59**, 855-863.

Coakley, J.A., Chylek, P., 1975. The two-stream approximation in radiative transfer: including the angle of the incident radiation. *Journal of the Atmospheric Sciences* **32**, 409-418.

Dave, J.V. 1964. Importance of higher order scattering in a molecular atmosphere. *Journal of the Optical Society of America* **54**, 307-315.

Dave, J.V. 1975. A direct solution of the spherical harmonics approximation to the radiative transfer equation for an arbitrary solar elevation. Part I: Theory. *Journal of the Atmospheric Sciences* **32**, 790-798.

Dave, J.V. 1978. Extensive datasets of the diffuse radiation in realistic atmospheric models with aerosols and common absorbing gases. *Solar Energy* **21**, 361-369.

Dave, J.V. 1980. Simulation colorimetry of the earth–atmosphere system. *Remote Sensing of Environment 9*, 301-324.

Dave, J.V. 1981. Transfer of visible radiation in the atmosphere. *Atmospheric Environment* **15**, 1805-1820.

Duntley, S.Q. 1948. The reduction of apparent contrast by the atmosphere. *Journal of the Optical Society of America* **38,** 179-191.

Duntley, S.Q., Boileau, A.R., Preisendorfer, R.W. 1957. Image transmission by the troposphere I. *Journal of the Optical Society of America* **47,** 499-506.

Hansen, J.E., Travis, L.D. 1974. Light scattering in planetary atmospheres. *Space Science Review* **16,** 527-610.

Hodkinson, J.R. 1966. Calculations of colour and visibility in urban atmospheres polluted by gaseous NO_2. *Air and Water Pollution International Journal* **10,** 137-144.

Isaacs, R.G. 1981. The role of radiative transfer theory in visibility modeling: Efficient approximate techniques. *Atmospheric Environment* **15,** 1827-1834.

Isaacs, R.G., Özkaynak, H. 1980. Uncertainties associated with the implementation of radiative transfer theory within visibility models. Second Joint Conference on Applications of Air Pollution Meteorology, New Orleans, LA, 24-27 March, 362-369. American Meteorology Society, Boston, MA.

Kaufman, Y.J. 1979. Effect of the earth's atmosphere on contrast for zenith observation. *Journal of Geophysical Research* **84,** 3165-3172.

Larson, S.M., Cass, G.R., Hussey, K.J., Luce, F. 1987. Verification of image processing-based visibility models. Submitted to *Environmental Science and Technology*.

Latimer, D.A., Bergstrom, R.W., Hayes, S.R., Liu, M.K., Seinfeld, J.H., Whitten, P.Z., Wojcik, M.A., Hillyer, J.J. 1978. The development of mathematical models for the prediction of anthropogenic visibility impairment. EPA-450/3-78-110a,b,c, Systems Applications, Inc., San Rafael, CA.

Liou, K.N. 1974. Analytic two-stream and four-stream solutions for radiative transfer. *Journal of Atmospheric Sciences* **31,** 1473-1475.

Malm, W., Molenar, J., Chan, L.L. 1983. Photographic simulation techniques for visualizing the effect of uniform haze on a scenic resource. *Journal of Air Pollution Control Association* **33**, 126-129.

Masaki, H. 1960. Apparent colors of natural objects (II). *Science of Light* **9**, 39-54.

Middleton, W.E.K. 1950. The colors of distant objects. *Journal of the Optical Society of America* **40**, 373-376.

Middleton, W.E.K. 1968. *Vision through the atmosphere*, University of Toronto Press.

Özkaynak, N., Isaacs, R.G., Murphy, B.L. 1979. Sensitivity analysis for models of local and regional visibility degradation. Proc. of the Fourth Symposium on Turbulence, Diffusion and Air Pollution, 15-18 January, Reno, NV, 257-268. American Meteorological Society, Boston, MA.

Steven, M.D. 1977. Standard distributions of clear sky radiance. *Quarterly Journal of the Meteorological Society* **103**, 457-465.

Sloane, C.S 1987. Personal communication.

Williams, M.D., Chan, L.Y., Lewis, R. 1981. Validation and sensitivity of a simulated photograph technique for visibility modeling. *Atmospheric Environment* **15**, 2151-2170.

Williams, M.D., Treiman, E., Wecksung, M. 1979. The simulated photograph technique as a tool for the study of visibility impairment. Los Alamos Scientific Laboratory Report LA-8105-MS.

Williams, M.D., Treiman, E., Wecksung, M. 1980. Plume blight visibility modeling with a simulated photograph technique. *Journal of the Air Pollution Control Association* **30**, 131-134.

CHAPTER 5

CONTROL OF ATMOSPHERIC PRIMARY
CARBON PARTICLE CONCENTRATIONS
AND EFFECTS ON VISIBILITY
IN THE LOS ANGELES AREA

5.1 Abstract

The control of atmospheric primary carbonaceous particles is central to protecting visibility. In the Los Angeles area, fine particulate carbon accounts for 40% of fine particulate mass concentration on an annual average basis and 33% of the fine aerosol mass during summer midday periods. Visibility modeling shows that aerosol carbon contributes up to 39% of the total scattering coefficient and up to 44% of the extinction coefficient in the Los Angeles area during summer midday periods. Fine primary aerosol carbon is estimated to contribute 24% of the extinction coefficient, and 14% of the scattering coefficient during summer midday periods in Pasadena. Using the results of the primary aerosol carbon emission control strategy study by Gray (1986), which determined the least costly set of controls necessary to achieve reduced levels of primary carbonaceous aerosol in the Los Angeles area atmosphere, it is estimated that an 8% to a 14% decrease in the average 1984 summer midday extinction coefficient could be achieved at Pasadena if primary aerosol carbon emission controls costing 80.4×10^6 year^{-1} (1982 dollars) had been in place at that time. An 11% to a 19% decrease in the extinction coefficient is estimated to result from controls costing 423.5×10^6 year^{-1} (1982 dollars).

5.2 Introduction

Light scattering and absorption by airborne particles leads to visibility reduction. In cities like Los Angeles, visual range often is reduced to less than 5 km (Larson and Cass, 1987). In more remote areas, including national parks, even small amounts of pollutant-induced light extinction may obscure the vistas for which those parks are famous (Macias, et al., 1981; Malm and Molenar, 1984).

Governmental regulations set air quality goals for particulate air pollutants and protect visibility in national parks and wilderness areas. In order to meet these standards, emission controls, sometimes costly, must be implemented. It is therefore important that methods be developed for identifying the least expensive air pollution control strategy needed to reach a desired level of air quality. While considerable attention has been paid to the design of cost-effective strategies for meeting ambient pollutant concentration standards (Cass and McRae, 1981), little research has been pursued into identifying the least expensive way to improve regional visibility.

This work will consider the connection between cost-optimized emission control strategies and their resulting effects on visibility. Methods developed will be illustrated for the example of primary aerosol carbon particle control in the Los Angeles area. First an overview of the character of the aerosol carbon air pollution problem in the South Coast Air Basin that surrounds Los Angeles is given. Then the least-cost strategies for aerosol carbon control in that area developed by Gray (1986) are summarized. The estimated effect of these controls on visibility will be simulated through application of a visibility model, and the predicted changes in visibility will be discussed.

The fine airborne particulate matter in the South Coast Air Basin has been

found to consist mainly of sulfates, nitrates, and carbonaceous material (Hidy et al., 1974). Gray et al. (1986) reported that in 24-hour average samples of suspended particulate matter in the Los Angeles area, 40% of the fine particle mass is aerosol carbon. As the most abundant fine aerosol species in the Los Angeles atmosphere in recent years, aerosol carbon control will clearly be an important feature of any program designed to make a major improvement in local visual range.

Carbonaceous material in the aerosol that has been emitted directly to the atmosphere originates from combustion, industrial processes, and fugitive sources (Wagner, 1978; Siegla and Smith, 1981; Muhlbaier and Williams, 1982; Cass et al., 1982) and consists of elemental carbon (EC) and organic carbon (OC). Elemental carbon is a black soot-like material with a chemical structure similar to impure graphite (Rosen et al., 1978). Elemental carbon is a primary aerosol component, i.e., it is emitted from sources as elemental carbon and is not formed in the atmosphere by any physical or chemical process. Elemental carbon particles both scatter and absorb light (Waggoner and Charlson, 1977; Pierson and Russel, 1979; Conklin et al., 1981; Groblicki et al., 1981; Rosen et al., 1982; Wolff et al., 1982) and thus contribute to the reduction of visibility. Organic carbon aerosol may be due to either primary emissions from sources or to secondary formation in the atmosphere. In the latter case, organic aerosol is formed in the atmosphere by condensation of the low vapor pressure products of gas phase reactions involving hydrocarbon vapors (Grosjean and Friedlander, 1975; Schuetzle et al., 1975; Cronn et al., 1977; Grosjean, 1977; Appel et al., 1979). Methods implemented to control primary aerosol carbon emissions would affect elemental carbon concentrations and that fraction of the organic carbon concentrations that is due to primary aerosol emissions. The present analysis is limited to control of primary

aerosol carbon sources only. To the extent that some control measures evaluated may also reduce hydrocarbon vapors or other pollutant species, the improvements in visibility would be greater than shown here. In that sense the present analysis is a conservative one. Visual range improvement will be greater than or equal to the amounts shown.

5.3 Aerosol Carbon Concentrations in the Los Angeles Area

In 1982, a year long study of fine aerosol carbon levels in the South Coast Air Basin was undertaken (Gray et al., 1986). An air monitoring network was operated at six day intervals to obtain 24-hour average samples of fine $(d_p < 2.1 \ \mu m)$ particulate matter at 10 sites in the air basin. The monitoring sites used during the 1982 study are shown in Figure 5.1. The Lennox, Pasadena, Upland and Azusa sites also were included in a 1984 study of summer midday fine particle and coarse particle pollutant concentrations along with a new sampling site at San Bernardino (Larson and Cass, 1987). The samples from both studies were analyzed for elemental and organic carbon (by the method of Johnson et al., 1981), trace metals (by X-ray fluorescence), SO_4^{-2}, NO_3^{-1} (by ion chromatography) and NH_4^{+1} (by the phenolhypochlorite method, described by Solórzano, 1969). These experiments provided data which describe an annual cycle of fine particulate carbon air quality in the Los Angeles air basin during 1982, as well as the details of the pollutant loadings during summer midday periods when visibility reduction is most apparent to the general public.

The results from the year long study of 24-hour average samples can be compared to summer midday concentrations observed during 1984 (Larson and Cass, 1987). The 1982 study found that annual average dry fine suspended particulate matter concentrations varied from 23 μg/m^3 to 42 μg/m^3 over the sites in the Los Angeles area. Summer midday average fine dry mass concentrations ranged
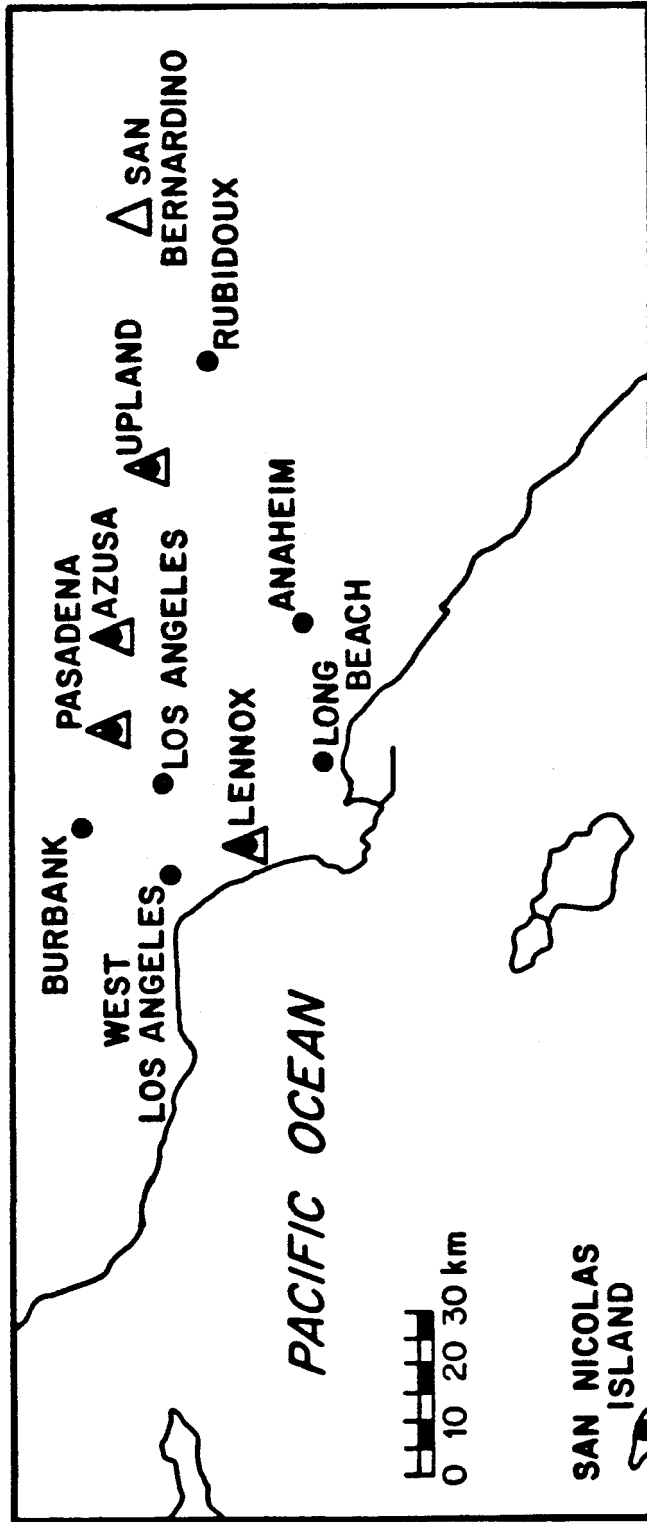
FIGURE 5.1. Sites used in the 1982 and 1984 air monitoring experiments.

Sites used in the fine particle air monitoring network used by Gray (1986) are indicated by solid circles (•). Sites used in the 1984 summer midday visibility study are denoted by triangles (△).

from 32 μg/m^3 to 72 μg/m^3 over the sites studied in 1984 confirming the human observer's impression that light scattering and fine aerosol levels are higher than average during summer midday periods. Average fine dry mass concentrations in the 1982 study were between 32% and 39% of the annual average total suspended particulate matter concentrations, which varied from a low of 63.6 μg/m^3 at West Los Angeles to a high of 126.7 μg/m^3 at Rubidoux. The percentage of the total dry suspended particulate mass that was fine dry mass ranged from 28% (at San Bernardino) to 64% (at Pasadena) for summer midday samples. Average summer midday total suspended particulate matter concentrations ranged from a low of 77.8 μg/m^3 at Pasadena to a high of 146.2 μg/m^3 at Azusa. Carbonaceous aerosol accounted for 40% of fine mass loading in the 1982 study averaged over the 10 sites, and for 33% of the fine mass concentrations in the 1984 summer study averaged over the five sampling sites.

The highest annual average concentration of fine total carbon (TC = OC + EC) was found in the most heavily trafficked areas of the city in the 1982 study, such as at central Los Angeles (12.2 μg/m^3) and Burbank (13.7 μg/m^3). This is due to stagnant atmospheric transport conditions in the winter that lead to very high aerosol carbon levels in the winter at those sites. In the summer, aerosol carbon emitted from traffic in central Los Angeles is blown inland by winds that are stronger than in the winter (Gray, 1986). Azusa, which is often directly downwind of Los Angeles in the summer showed the highest summer 1984 midday average fine total carbon levels (17.6 μg/m^3). A comparison of aerosol carbon data taken during these two studies is given in Table 5.1.

The ratio of total carbon to elemental carbon concentrations measured at a site can be used as an indication of the amount of secondary organic aerosol formation that has occurred since the air mass has moved from the emission sources to the

TABLE 5.1. Fine aerosol carbon concentrations at sites included in both the 1982 and 1984 Los Angeles area experiments.

	1982 24-hour samples annual mean $(\mu g/m^3)$		1984 4-hour samples summer midday mean $(\mu g/m^3)$	
	EC	TC	EC	TC
Lennox	4.51	10.69	1.70	7.97
Pasadena	3.95	10.73	2.50	14.64
Azusa	3.30	9.03	4.11	17.63
Upland	3.14	8.51	2.76	13.52

sampling location (Cass, Boone, and Macias, 1982; Gray et al., 1986). A total carbon to elemental carbon ratio of 3.39 : 1 is estimated for fine primary aerosol emissions in the Los Angeles area in 1982 (Gray, 1986). A ratio higher than this suggests that some secondary organic aerosol is present. The 1982 study showed little increase above the source ratio of total to elemental carbon as measured in the ambient air at the sites in the study on an annual average basis (the annual average being dominated by high primary aerosol concentrations that occur during morning and evening traffic peaks). There was little seasonal dependence in the TC to EC ratio, although the TC to EC ratio did increase as one moves from near coastal sites like Lennox to inland sites like Azusa. It was concluded that for 1982, secondary formation of organic carbon aerosol constituted no more than 16% of total aerosol carbon on an annual average basis at an inland site like Azusa. It could be expected that more secondary organic aerosol enrichment would be seen in summer during midday conditions favorable for photochemical reactions, with secondary organics formation increasing with distance inland as the air mass has had more time for secondary aerosol formation to occur. The 1984 summer midday study showed some evidence of enrichment with distance inland. Average fine particle total carbon to elemental carbon ratios ranged from 5.08 ± 1.59 : 1 at the Lennox coastal site to 8.35 ± 3.47 : 1 at the farthest inland site at San Bernardino.

For the purposes of modeling the effect of emission controls on the concentrations of carbonaceous particles in the atmosphere, it is important to be able to estimate the amounts of primary and secondary carbon in the ambient aerosol, since controls aimed at reducing the direct emissions of carbon particles from sources can only be guaranteed to affect primary carbon concentrations. The breakdown between primary and secondary organic carbon in the ambient aerosol can be estimated by comparing the TC:EC ratio for the ambient aerosol to the TC:EC

ratio expected for a primary aerosol. Table 5.2 shows the average contributions of primary, secondary and background elemental and organic carbon estimated for fine aerosol carbon measured at three sites used during the 1984 study for two different sets of primary TC:EC ratios. In the first data set, non-background organic carbon present above a TC:EC rato of 3.39 : 1 is assumed to be secondary in origin. That TC:EC ratio for primary aerosol of 3.39 : 1 is derived from the emissions inventory constructed by Gray, 1986. The second set of estimates of primary and secondary contributions results from predictions of the summer 1982 average ambient TC and EC concentrations for each site as computed by Gray's (1986) transport model. Since this model only tracks the transport from the primary aerosol carbon sources in the Los Angeles area, the model predictions can be used to determine a TC:EC ratio appropriate for the primary aerosol at each site. Subdivision of each daily summer 1984 fine elemental carbon and organic aerosol sample into background, primary and secondary fractions was accomplished by a method analogous to that shown in Table 5.2. Coarse particle aerosol carbon was assumed to be primary in origin.

5.4 Aerosol Carbon Contributions to Visibility

Investigations to estimate the contribution of aerosol carbon to the reduction of visibility have been carried out by a number of researchers. Regression analysis by White and Roberts (1977) estimated that organic components made a 9.4% contribution to the light scattering coefficient in the Los Angeles air basin. Conklin et al. (1981) determined that light absorption by elemental carbon could be responsible for up to 17% of the total extinction coefficient observed at downtown Los Angeles. Groblicki et al. (1981) report that for Denver, 31% of light extinction is due to fine particle absorption by elemental carbon. Since elemental carbon also scatters light, the total contribution to light extinction in Denver by

TABLE 5.2. Estimated origin of fine aerosol carbon concentrations – summer 1984 $(\mu g/m^3)$.

SITE	BEC [1]	BOC [2]	EC [3]	POC[4]	SOC[5]	Primary TC:EC
Lennox	0.16	1.40	1.58	3.78	1.58	3.39:1 [6]
Pasadena	0.16	1.40	2.34	5.59	5.15	3.39:1 [6]
Azusa	0.16	1.40	3.95	9.45	2.81	3.39:1 [6]
Lennox	0.16	1.40	1.58	2.44	2.57	2.54:1 [7]
Pasadena	0.16	1.40	2.34	5.50	5.24	3.35:1 [7]
Azusa	0.16	1.40	3.95	9.41	2.84	3.38:1 [7]

(1) Background elemental carbon determined from the average summer fine particle elemental carbon concentration as measured at San Nicholas Island in 1982 (Gray et al., 1986).

(2) Background organic carbon determined from the average summer fine particle organic carbon concentration as measured at San Nicholas Island in 1982 (Gray et al., 1986).

(3) Measured EC minus background EC.

(4) Primary organic carbon estimated from (primary TC:EC enrichment ratio minus 1) times non-background ambient EC concentration.

(5) Secondary organic carbon estimated from total organic carbon less POC and less BOC.

(6) TC:EC ratio in primary emissions from sources estimated from emissions inventory (Gray et al., 1986).

(7) TC:EC ratio in primary aerosol estimated from model predictions of primary TC and EC summer average concentrations at each site (Gray et al., 1986).

elemental carbon was higher, 38%. Fine particle organic carbon contributed 13% to the fine particle scattering coefficient in Denver.

The major light absorbing species in the Los Angeles aerosol is elemental carbon (Rosen et al., 1979). The amount of light extinction due to absorption by elemental carbon can be determined by direct measurement, using, for example, the opal glass technique (Lin et al., 1973) or can be estimated by utilizing a relationship between elemental carbon mass concentration, and the light absorption efficiency for elemental carbon, (Conklin et al., 1981). The contribution of elemental and organic carbon to the scattering coefficient may be more difficult to ascertain. The contribution can be estimated using regression analysis, or be calculated by Mie theory. In the case of Mie theory calculations, one must know whether the aerosol is an external mixture (each particle consists of only one substance, and a multi- component aerosol is achieved by suspending particles of different composition in the same air volume) or is an internal mixture (each particle contains a blend of all species found in particles of a certain size (Ouimette and Flagan, 1982)). If the aerosol exists as an external mixture, the scattering coefficient could be calculated for each chemical component separately. The sum of the individual scattering coefficients for each aerosol type would be the scattering coefficient for the entire aerosol suspension containing many different types of organic and inorganic particles. Comparing the contributions of elemental and organic carbon particles to the total scattering coefficient would allow the determination of the percent of the light scattering level that is due to carbon particles. If an internal mixture is hypothesized, the value of the scattering coefficient could be computed both with and without the carbonaceous aerosols in the internal mixture, and by difference the contribution of aerosol carbon to the total aerosol scattering coefficient could be deduced.

Figure 5.2 presents a comparison of the scattering coefficients calculated by

Mie theory, assuming an internal and external mixture for the Pasadena aerosol observed during the 1984 summer midday study. For all sites, the values resulting from the two methods of calculation are within 5% to 10% of one another and are well correlated (correlation coefficient, r=0.985 to r= 0.998). Assuming that the 1984 samples consisted of an external mixture, calculations indicate an average estimated ratio of the scattering coefficient due to carbonaceous aerosol to the total scattering coefficient of 0.39 and a value of 0.44 for the ratio of the extinction coefficient due to aerosol carbon to the total extinction coefficient. The internal mixture calculation yields a contribution from carbonaceous aerosol to the the scattering coefficients of 31% and to the extinction coefficient of 39%. Using estimates of primary and secondary aerosol carbon levels for Pasadena, it is calculated that primary aerosol carbon contributes an average of 24% of the summer midday extinction coefficient and 14% of the summer midday scattering coefficient at Pasadena. These calculations indicate that if the concentration of carbonaceous particles in the atmosphere were significantly reduced by means of emission controls, then visibility would be noticeably improved.

5.5 Control of Fine Primary Carbon Particle Concentrations

Gray (1986) combined an emission inventory for fine particle carbon, a Lagrangian air quality model, emission control information and the method of linear programming to identify the least expensive control strategy that would reduce the loadings of primary carbon aerosol in the Los Angeles air basin. Air quality modeling methods used in that study were verified by comparison to data taken during the 1982 Los Angeles field experiments discussed previously.

The air quality model was based on a Lagrangian particle-in-cell technique and incorporated the hourly sequence of wind speed and direction during 1982 to track air parcel transport within the 80 X 80 km grid shown in Figure 5.3. That grid
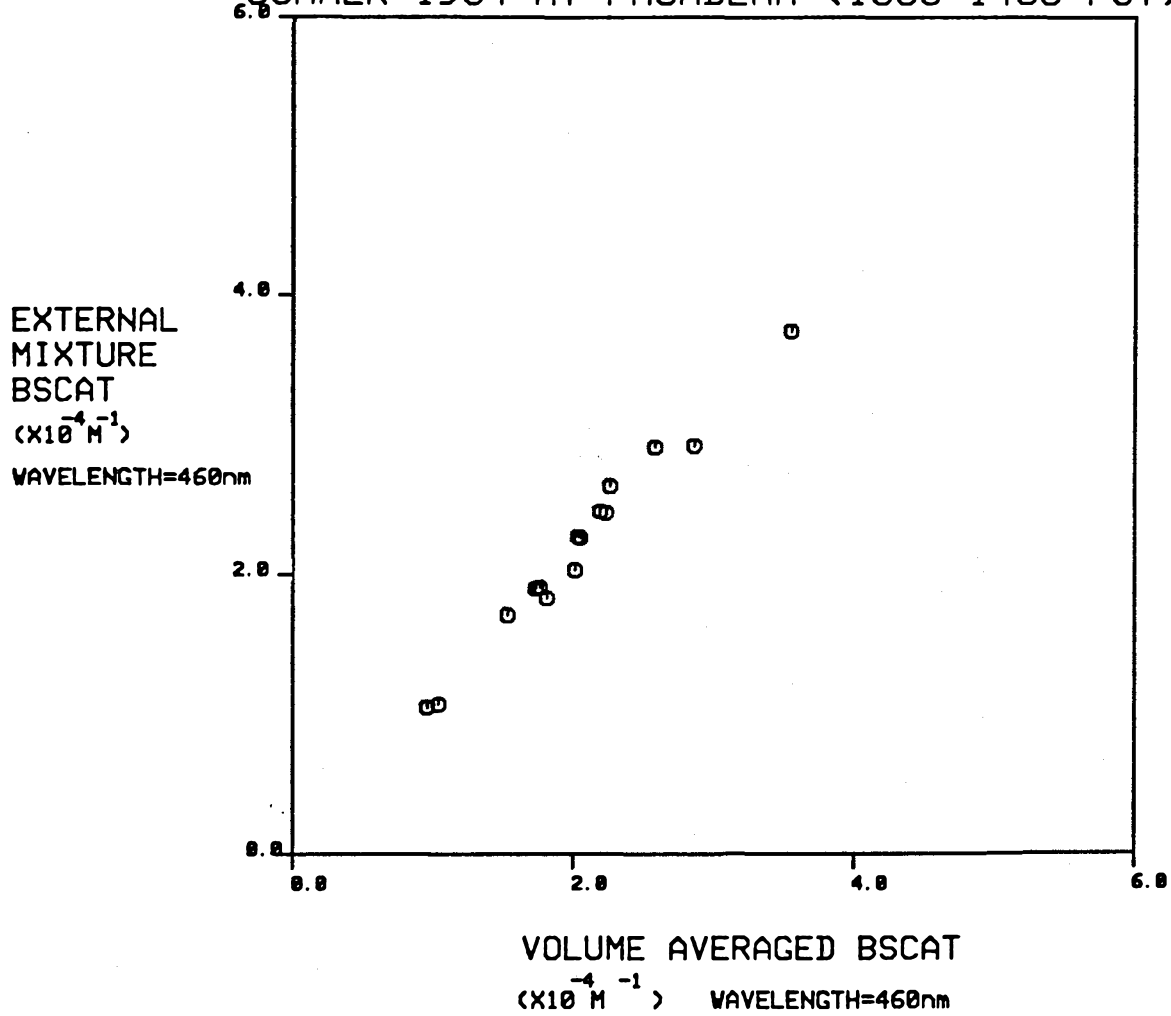
FIGURE 5.2. Comparison of the scattering coefficient calculated at
460 nm assuming an external mixture and assuming an internal mixture.

Scattering coefficients are calculated for summer midday periods in Pasadena, 1984.

system represents the western part of the South Coast Air Basin and is centered over downtown Los Angeles. Pollutant inputs from more than 70 types of mobile and stationary emission sources were included in those calculations. Seasonal and diurnal variation in source outputs were accounted for in the emissions inventory. Concentrations of pollutants were affected by the processes of advection, diffusion and dry deposition. The data required by the model included information on the emission sources, meteorological data, atmospheric dispersion parameters, deposition rates, background aerosol carbon levels, the definition of the receptor grid, the cell size, and time step for the calculations.

The model computed the contribution from each source to the ambient pollutant concentrations of elemental and primary particulate total carbon at each site of interest within the grid. All of the individual source contributions at a location were added to obtain the predicted air quality for that location. The model was used to predict the monthly average concentrations of fine primary carbonaceous aerosol for each month of 1982 for the seven monitoring sites located within the grid. The model was verified by comparing calculated monthly average concentration predictions to the monthly average concentrations observed at the seven sites by Gray et al. (1986). The model is shown to be a good predictor of annual and monthly average elemental and total carbon concentrations. Comparison of the predicted and observed monthly average total carbon and elemental carbon concentrations at the Pasadena site is shown in Figure 5.4. Figure 5.4 also illustrates the source class contributions to primary fine particle carbon concentrations at Pasadena.

The contribution to primary aerosol EC and OC concentrations at any location from any one source is predicted by the model. That contribution varies between monitoring sites because the spatial distributions of emissions differ be-
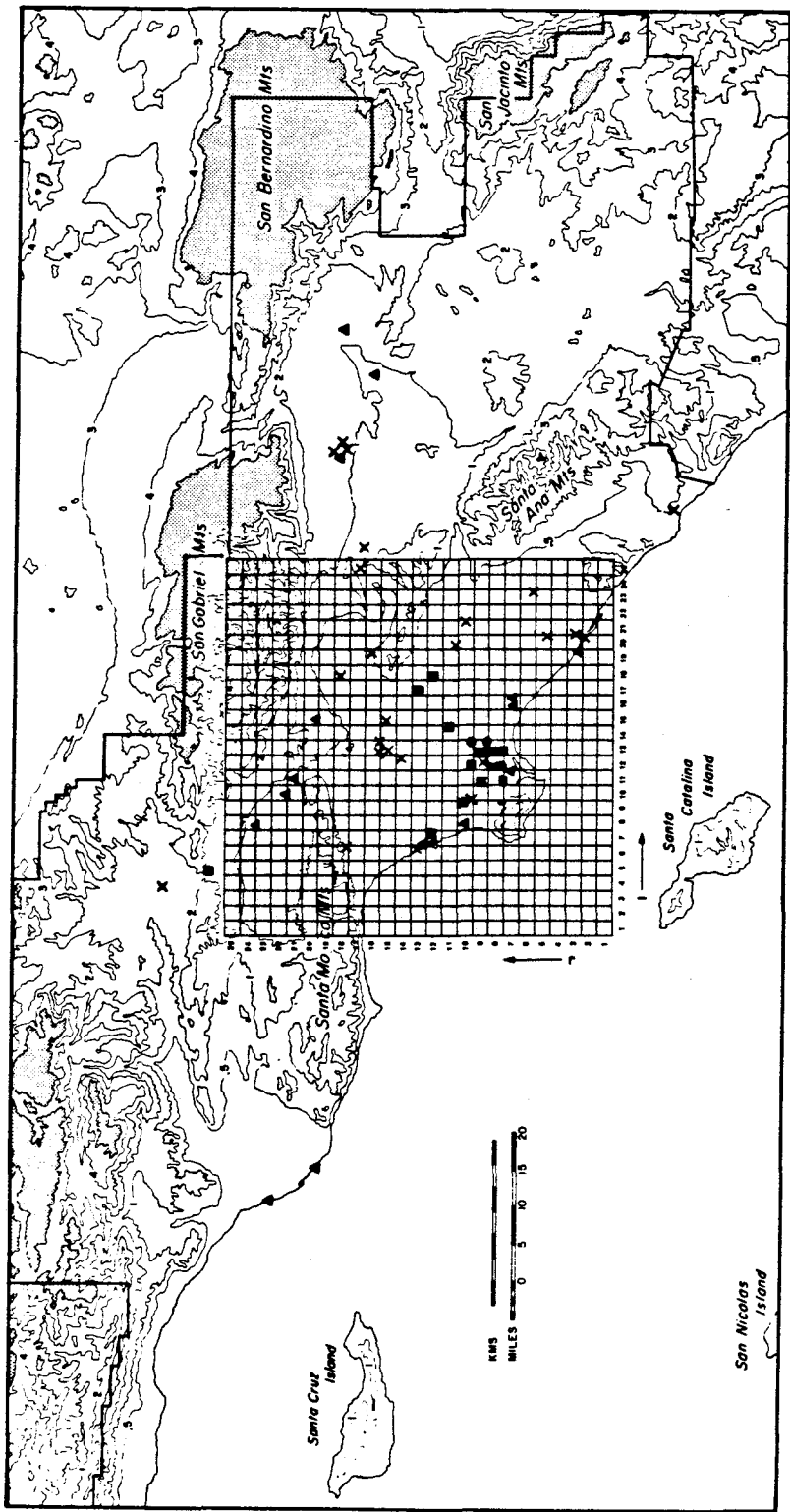
FIGURE 5.3. The central portion of the South Coast Air Basin showing the grid system used in the study by Gray (1986).

From Gray (1986).
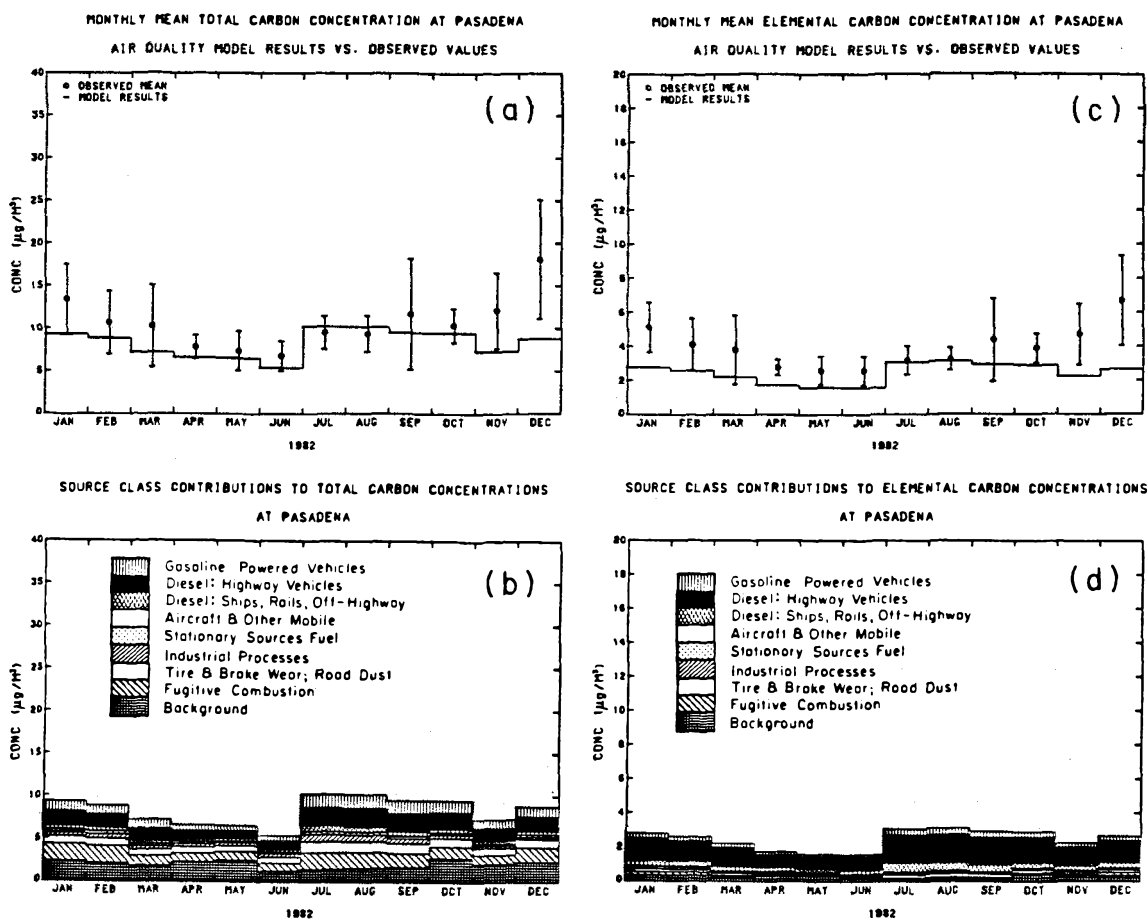
FIGURE 5.4. Observed versus predicted fine particle carbon concentrations and source class contributions to fine particle carbon concentrations. (a) Air quality model results versus observed values for the monthly mean fine particle total carbon concentration at Pasadena. (b) Source class contributions to fine particle total carbon concentrations at Pasadena. (c) Air quality model results versus observed values for the monthly mean fine particle elemental carbon concentration at Pasadena. (d) Source class contributions to fine particle elemental carbon concentrations at Pasadena. From Gray (1986).

tween source types. Variation is also caused by changes in such parameters as stack height and in diurnal emission patterns. For example, aircraft emissions are an important contributor to the aerosol carbon levels observed at Lennox (located near the Los Angeles International Airport), but not at other monitoring sites in the basin. Therefore, if controls were implemented on aircraft emissions, the largest change in ambient carbon levels would be at the Lennox site. At all the stations studied, the largest contributors to fine primary elemental carbon concentrations are diesel highway vechicles, which contributed 40% to 50% of fine elemental concentrations at most sites. Three classes of mobile sources: diesel highway vehicles, gasoline powered vehicles, and non-highway diesel sources were responsible for the majority of the elemental carbon concentrations observed at most sites. These mobile sources are also important contributors to total primary aerosol carbon concentrations. This implies that controls on these sources would be critical to controlling the levels of these pollutants.

The air quality model constructed by Gray has been linked with an analysis of available emission controls in order to evaluate alternative emission control strategies. Since the model is linear in emissions (i.e., a change in the atmospheric concentration due to any single source type is proportional to the incremental change in basin-wide emissions from that source type), a linear programming algorithm can be used to identify the least costly emission control strategy needed to gain a desired level of primary aerosol carbon air quality. A linear programming problem consists of an objective function to be optimized (here, to minimize the sum of control costs) and a set of constraints in the form of inequalities (here, that the pollutant concentration be below a certain limit at each site; that scarce resources such as natural gas not be used beyond their availability; that only compatible controls are implemented, and that a specific control not be applied to more than the number of sources present within the modeling region).

The linear programming problem for primary aerosol carbon control in the Los Angeles area was formulated for seven sites, 74 source types (summarized in Table 5.3) and 33 possible emission control measures (Table 5.4). The problem was solved by the simplex method (Gale, 1960; Franklin, 1980) using a modified version of a computer code provided by Sandia National Laboratories (1979). The program was solved repeatedly for progressively more stringent levels of aerosol carbon control, the results varying slightly depending on whether primary total or elemental carbon control was optimized. The results of the optimization calculations indicate that for a cost of $481 $\times 10^6$ year^{-1} (1982 dollars), a reduction of 24.86 tons/day of fine particle total carbon emissions (48% of 1982 daily total carbon emissions), could be obtained. At about the same cost, a reduction of fine elemental carbon concentrations by 9.83 tons/day (68% of 1982 daily elemental carbon emissions) could be achieved. For $102 $\times 10^6$ year^{-1} (1982 dollars) the maximum annual average concentration of fine primary total carbon could be reduced from greater that 14 μg/m^3 to 9.2 μg/m^3, and elemental carbon concentrations could be reduced from greater than 5 μg/m^3 to 2.4 μg/m^3 for $80 $\times 10^6$ year^{-1}. The optimal strategy and cost to achieve control over annual average and over monthly average primary aerosol carbon concentrations are approximately the same. Graphs of control measures needed to obtain a certain level of control versus the cost of that control strategy are presented in Figures 5.5 and 5.6. As the figures indicate, many of the controls involve the reduction of emissions by controlling the emissions from diesel fuel combustion.

5.6 Estimated Effect on Visibility

The study by Gray (1986) described above, provides information on the fraction reduction in total carbon and elemental carbon concentrations at each of seven sites in the Los Angeles area that could be expected if specific controls had

TABLE 5.3. 1982 annual average fine particulate
carbon emission summary within the 50×50-mile grid.

Major Source Category	Fine Total Carbon (kg/day)	Fine Elemental Carbon (kg/day)
Gasoline powered highway vehicles	5242.3	1261.1
Diesel: highway vehicles	7396.5	5665.7
Diesel: ships, rail, off-highway	2654.9	2033.7
Aircraft and other mobile	571.2	338.6
Highway fugitive (tire and brake wear; road dust)	8094.3	829.9
Other fugitive (fugitive combustion; livestock feedlots)	9247.9	537.9
Stationary source fuel combustion	1678.2	402.0
Industrial processes	4154.0	437.9
TOTAL	39039.3	11506.8

(From Gray, 1986)

TABLE 5.4. Cost and emissions reductions of control measures used in this study.

No.	Control Measure	Annual Cost (10⁶$/year)	Fine Carbon Emission Reductions (T/day) TC	EC	Source Types Affected [a]	Conflicts
D.2	Catalysts on non-catalyst autos and light trucks	236.352	3.7387	0.7053	non-cat light duty vehicles (3,4)	D.4, D.5
D.3	#1 diesel fuel use by light-duty diesel vehicles	4.317	0.2475	0.1896	light duty diesel vehicles (6,7)	D.3, D.5
D.4	Particle traps on light-duty diesel vehicles	8.148	0.9900	0.7583	light duty diesel vehicles (6,7)	D.3, D.4
D.5	Particle traps & #1 diesel fuel use for lt-duty diesel vehicles	12.456	1.0395	0.7962	light duty diesel vehicles (6,7)	
D.7	Catalysts on non-catalyst medium & heavy gas vehicles	66.453	1.1026	0.2080	non-cat medium/heavy vehicles (9,10)	
D.8	#1 diesel fuel use by heavy duty diesel vehicles	38.523	1.4808	1.1343	heavy diesel vehicles (11)	D.9, D.10
D.9	Particle traps on heavy-duty diesel vehicles	36.240	6.6637	5.1044	heavy diesel vehicles (11)	D.8, D.10
D.10	Particle traps & #1 diesel fuel for heavy-duty diesel vehicles	74.763	6.8118	5.2178	heavy diesel vehicles (11)	D.8, D.9
D.11	Air taxi modification (towing)	0.000	0.1354	0.1053	aircraft surface (11)	
D.12	0.5% S residual oil for shipping-berthing operations	2.253	0.0442	0.0088	shipping residual oil (16)	
D.13	#1 diesel fuel use by railroads	5.011	0.2858	0.2189	railroad diesel (18)	
D.14	#1 diesel fuel use in off-road diesel engines	8.725	0.4771	0.3654	off-road diesel (19)	D.15, D.16
D.15	Particle traps on off-road diesel engines	19.353	2.0827	1.5953	off-road diesel (19)	D.14, D.16
D.16	Particle traps & #1 diesel fuel for off-road diesel engines	28.260	2.1432	1.6417	off-road diesel (19)	D.14, D.15
D.18	Catalysts on off-road gasoline engines	15.615	0.0831	0.0157	off-road gasoline (20)	
D.19	Use of 0.1% S residual oil by utilites	30.442	0.1232	0.0247	utility residual oil (23)	D.34
D.20	Use of 0.1% S residual oil by refineries	1.367	0.0056	0.0011	refinery residual oil (28)	D.35
D.21	Use of 0.25% S residual oil in industrial boilers	0.445	0.0047	0.0009	industrial boiler residual oil (31)	D.22, D.36
D.22	Use of 0.10% S residual oil in industrial boilers	2.404	0.0100	0.0020	industrial boiler residual oil (31)	D.21, D.36
D.24	Catalysts on gasoline large industrial IC engines	0.113	0.0013	0.0001	industrial IC gasoline engine (35)	
D.25	#1 diesel fuel use in diesel industrial IC engines	1.566	0.0057	0.0057	industrial IC diesel engine (36)	D.26, D.27
D.26	Particle traps on diesel industrial IC engines	4.796	0.0257	0.0257	industrial IC diesel engine (36)	D.25, D.27
D.27	Particle traps & #1 fuel in diesel industrial IC engines	6.362	0.0263	0.0263	industrial IC diesel engine (36)	D.25, D.26
D.28	Use of 0.25% S residual oil by residential/commercial	3.094	0.0248	0.0049	residential/commercial residual oil (39)	D.37
D.29	Paved road flushing	430.689	—	—	paved road dust (61)	D.30
D.30	Paved road flushing and broom sweep	556.628	—	—	paved road dust (61)	D.29
D.31	Radial tire use on light-duty vehicles	0.0	0.1167	0.0385	tire attrition (62)	
D.32	Use of gas logs in fireplaces	23.897	4.2394	0.7199	fireplace (65)	
D.33	Charcoal broiler control	4.370	4.8541	0.0728	charcoal broilers (68)	
D.34	Substitute natural gas for residual oil in utility boilers	0.0	0.1971	0.0411	utility residual oil (23)	D.19
D.35	Substitute natural gas for residual oil in refineries	0.0	0.0063	0.0019	refinery residual oil (28)	D.20
D.36	Substitute natural gas for residual oil in industrial boilers	0.0	0.0098	0.0027	industrial boiler residual oil (31)	D.21, D.22
D.37	Substitute natural gas for residual oil in residential/commercial	0.0	0.0245	0.0016	residential/commercial residual oil (39)	D.28
	Fine particle emissions in the entire 4-county South Coast Air Basin		52.1055	14.5071		

(a) See Gray, 1986, Appendix D, Table D.38 for the numerical list of 74 source types.

From Gray, 1986.

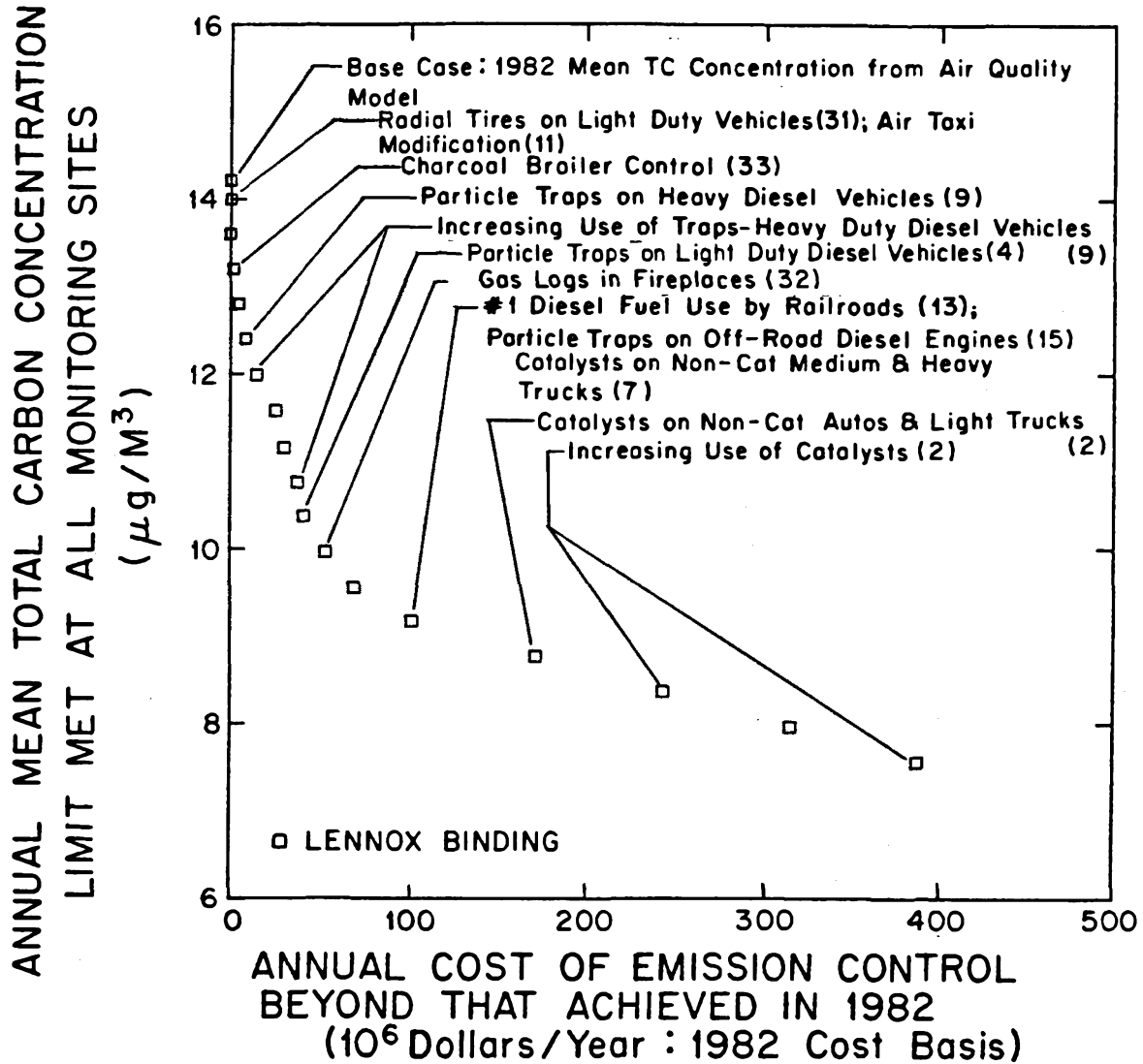# OPTIMAL STRATEGY FOR CONTROL OF FINE TOTAL CARBON CONCENTRATIONS

FIGURE 5.5. Annual mean of fine total carbon concentrations versus the annual cost of emission controls for the optimal strategy to control fine total carbon emissions.

From Gray (1986).

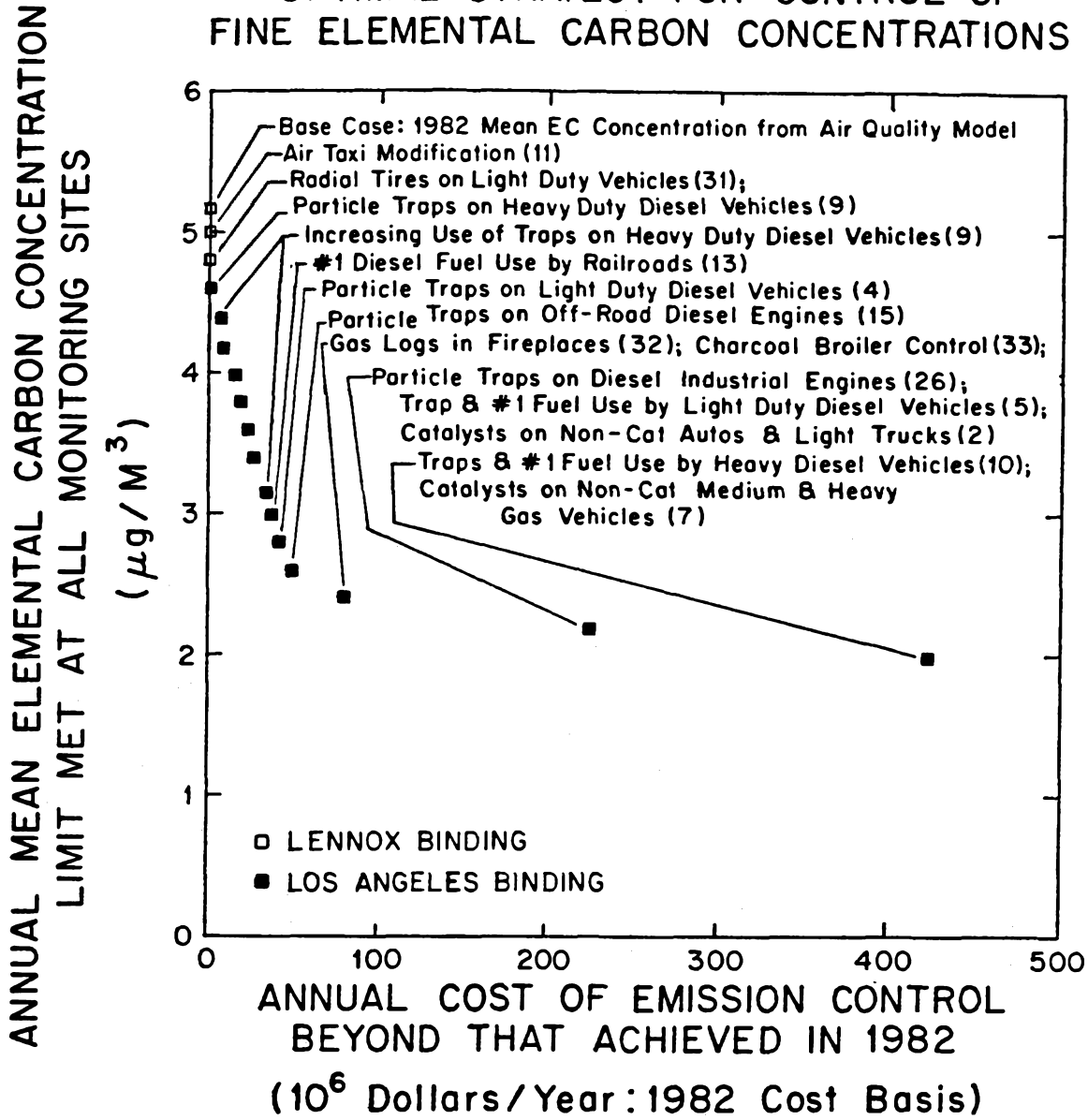## OPTIMAL STRATEGY FOR CONTROL OF FINE ELEMENTAL CARBON CONCENTRATIONS

FIGURE 5.6. Annual mean of fine elemental carbon concentrations versus cost of emission controls for the optimal strategy to control fine elemental carbon emissions. From Gray (1986).

been placed on primary aerosol carbon emission sources in 1982. To estimate the improvement in visibility that could occur in the presence of such controls, the visibility model of Larson et al. (1987) was applied to the 1984 summer mid-day air quality data set (Larson and Cass, 1987) before and after a reduction in primary aerosol organic and elemental carbon concentrations by the percentages predicted by the carbon particle control study (Gray, 1986). Three air monitoring sites were studied both in the 1982 control study and in the 1984 ambient sampling study: Azusa, Lennox and Pasadena. The estimation procedure employed when coordinating the data from these two studies assumes that the fractional reduction in ambient EC and primary OC concentrations predicted to result from a set of control measures as determined from the 1982 study, when 24-hour average samples were taken over a year's time, holds for 1984, when summer midday samples were obtained. The validity of the estimation procedure also depends on similar emission and weather patterns for 1982 and 1984 and on Gray's (1986) observation that control strategies that are optimal for the annual mean primary EC and OC air quality are also very close to the optimal strategy for a single month. Although the air pollution controls considered, which are aimed at reducing the concentration of fine primary carbonaceous aerosol, could also decrease the concentrations of other primary particulate matter species, it is worth noting that the major sources controlled (e.g., diesel engines) emit aerosol that is principally carbonaceous. But because some sulfate aerosol, for example, would also be controlled by these measures, the estimate of the visibility improvement obtained due to carbon particle reduction alone is a lower bound on the improvement in visibility that could be achieved with carefully planned emissions controls.

In order to simulate the controlled conditions, the aerosol was assumed to be an internal mixture. Figure 5.2 shows that similar results would have been obtained had an external mixture been assumed. Four cases were considered: a high cost

control strategy that was optimized for a high level of elemental carbon control, an intermediate cost control plan optimized for efficient elemental carbon control, plus high and intermediate cost control strategies that were for optimized for total primary aerosol carbon control. Three cases of the breakdown between primary and secondary carbonaceous material were considered: no secondary organic carbon formation (all of the measured aerosol carbon is primary), a split between primary and secondary organic carbon as predicted from the emissions inventory prepared by Gray (1986), and amounts of primary and secondary organic carbon estimated from TC:EC ratios predicted for each site using Gray's (1986) transport model. (See Table 5.2.) Primary organic carbon concentrations were multiplied by a factor of 1.4 to convert them to an estimate of primary organic compound concentrations before the visibility analysis was conducted. Background levels of TC and EC were obtained from the summer average concentrations of TC and EC measured during the 1982 study at San Nicholas Island, a remote offshore site. The emission controls considered and the cost of the controls for each case are presented in Table 5.5.

Visibility modeling calculations show that if all aerosol carbon were primary in origin, then a strategy selected to minimize the cost of elemental carbon control would produce an average 19% improvement in the mean summer midday 1984 extinction coefficient at Pasadena at a cost of $423.5 $\times 10^6$ year^{-1} (1982 dollars). For the same controls, an 11.3% and 11.4% decrease in the Pasadena average summer midday extinction coefficient was computed for the case where secondary organic carbon levels were estimated from the transport model predictions of TC:EC ratio for a primary aerosol and for the case where the emissions inventory was used to determine a primary aerosol TC:EC ratio, respectively. The intermediate cost control strategy optimized for elemental carbon control yielded an estimated decrease in the average Pasadena summer midday extinction coefficient of 14% at a

cost of \$80.4 $\times 10^6$ year^{-1} (1982 dollars), assuming no secondary organic aerosol formation, and approximately an 8% decrease if estimates of secondary organic formation are used. Results optimized for total primary aerosol carbon concentration control indicated a slightly lower percentage improvement in the extinction coefficient per dollar spent than in the case where elemental carbon control is optimized. Estimates of the mean summer midday extinction coefficient values that could be obtained at the Lennox, Pasadena, and Azusa sites, if the controls considered were in place in the summer of 1984 are given in Figure 5.7 as a function of the cost of those controls. The data presented in Figure 5.7 is for the case where the split between the primary and secondary organic carbon is estimated from a primary aerosol TC:EC ratio derived from transport model predictions.

Another means of illustrating the changes in visibility that could be achieved with varying levels of primary aerosol carbon control is to consider the shifts in the frequency of occurrence of high and low visibility events that would accompany such a control program. The frequency diagrams show the percentage of days with an extinction coefficient less than a specified amount. Such plots indicate how a range of different conditions, from lightly polluted to heavily polluted, would be affected by air pollution controls. Frequency diagrams showing how the distribution of midday summer events in 1984 might be altered had the specified control devices been in place are given in Figure 5.8 for the Pasadena, Lennox, and Azusa sites. Figure 5.8 presents results for the case of secondary organic carbon aerosol levels as predicted from the primary TC:EC ratio calculated from the transport model predictions for each site. Figure 5.9 presents the results for the case where all aerosol carbon is assumed to be primary. The controls affect the high extinction events more than the low extinction events and the median extinction events, especially at Pasadena. Controls on primary aerosol carbon sources only slightly alter the frequency distribution of visibility events at Lennox.

This indicates that species other than primary aerosol carbon are more important in reducing summer midday visibility at the Lennox site. Figure 5.8 shows that the 52nd percentile extinction coefficient $(\times 10^{-4} m^{-1})$ at Pasadena changes from 2.53 with no controls to 2.27 with an intermediate cost emission control plan to 2.15 with the implementation of a high cost emission control plan. If all the ambient aerosol carbon is assumed to be primary (Figure 5.9) the 52nd percentile extinction coefficient at Pasadena changes from 2.53 to 2.15 to 2.00, for no control, for intermediate cost controls and for high cost controls, respectively.

The results of the primary aerosol carbon control study and its effect on visibility can be illustrated through the use of synthetic photographs (Larson et al., 1987). Assuming no secondary aerosol formation, had the high cost levels of primary aerosol carbon control considered here been in place on August 25, 1983, the day is predicted to appear as shown in Figure 5.10. This figure can be compared to Figure 4.2 which simulates the appearance of the same day and scene had no primary aerosol carbon controls been in place. Although a considerable amount of air pollution is still apparent in the controlled case synthetic photograph, the effect of the carbon control strategy is to cause the San Rafael hills behind the city of Pasadena to reappear in the scene of interest. Graphs of the extinction coefficient on August 25, 1983 as a function of the cost of aerosol primary carbon control for the case of optimal elemental carbon control are shown in Figure 5.11.

TABLE 5.5. Strategies optimized for elemental and for total aerosol carbon control.

A STRATEGY OPTIMIZED FOR
ELEMENTAL CARBON CONTROL

Level of Control	Controls*	Cost $(\times 10^6 \text{ year}^{-1})$	Site	Fraction Reduction	
				Primary TC	Primary EC
Intermediate	4,9,11,13,	$80.45	Azusa	0.254	0.485
	15,31,32,33		Pasadena	0.298	0.514
			Lennox	0.319	0.541
High	2,5,7,9,10,	$423.50	Azusa	0.367	0.570
	11,13,15,26,		Pasadena	0.433	0.608
	31,32,33		Lennox	0.473	0.629

A STRATEGY OPTIMIZED FOR
TOTAL AEROSOL CARBON CONTROL

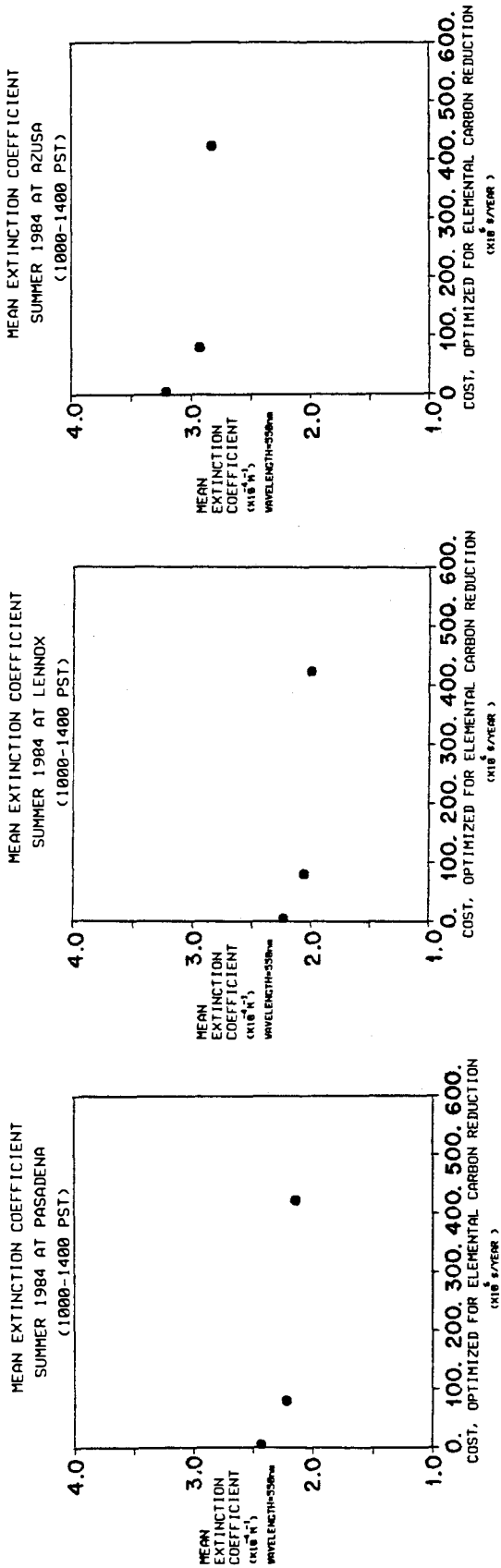| Level of Control	Controls*	Cost $(\times 10^6 \text{ year}^{-1})$	Site	Fraction Reduction	
				Primary TC	Primary EC
Intermediate	4,9,11,31,	$68.96	Azusa	0.240	0.422
	32,33		Pasadena	0.289	0.458
			Lennox	0.324	0.515
High	2,4,7,9,11,	$388.10	Azusa	0.361	0.561
	13,15,31,32,		Pasadena	0.426	0.597
	33		Lennox	0.465	0.619

* see Table 5.4.

FIGURE 5.7. Mean of summer midday extinction coefficients versus annual cost of emission controls.

Results are for the optimal strategy to control elemental carbon emissions for Pasadena, Lennox, and Azusa. Extinction coefficients predicted for each experiment day, assuming controls had been in place, are averaged to obtain the mean. Amounts of secondary organic carbon aerosol are estimated from the primary TC:EC ratio predicted for each site using a primary aerosol transport model (Gray, 1986).

SUMMER 1984 EXTINCTION COEFFICIENT AT PASADENA
FREQUENCY DISTRIBUTION (1000-1400 PST) (MODEL)
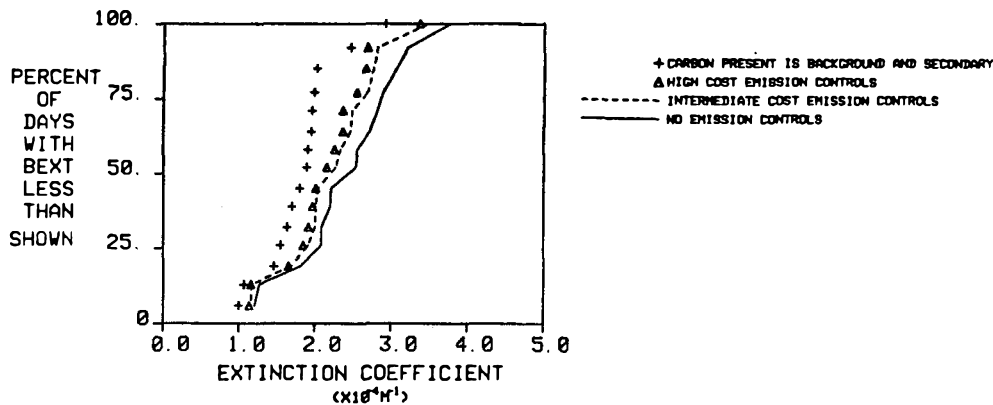
SUMMER 1984 EXTINCTION COEFFICIENT AT LENNOX
FREQUENCY DISTRIBUTION (1000-1400 PST) (MODEL)
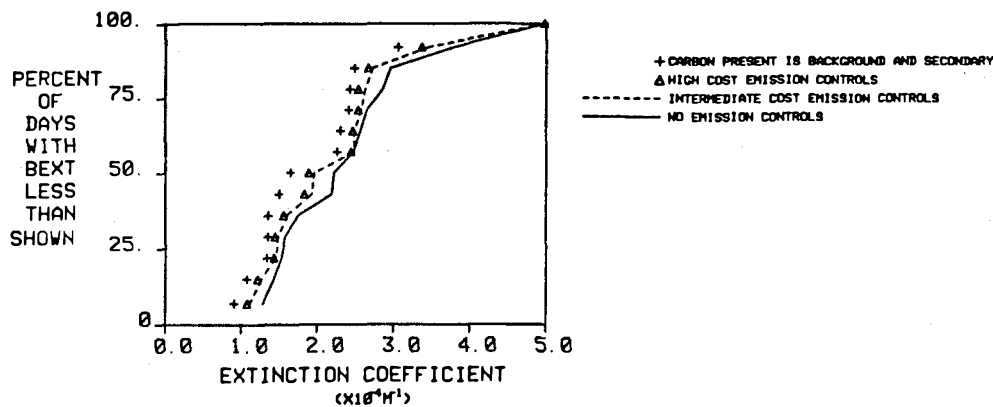
SUMMER 1984 EXTINCTION COEFFICIENT AT AZUSA
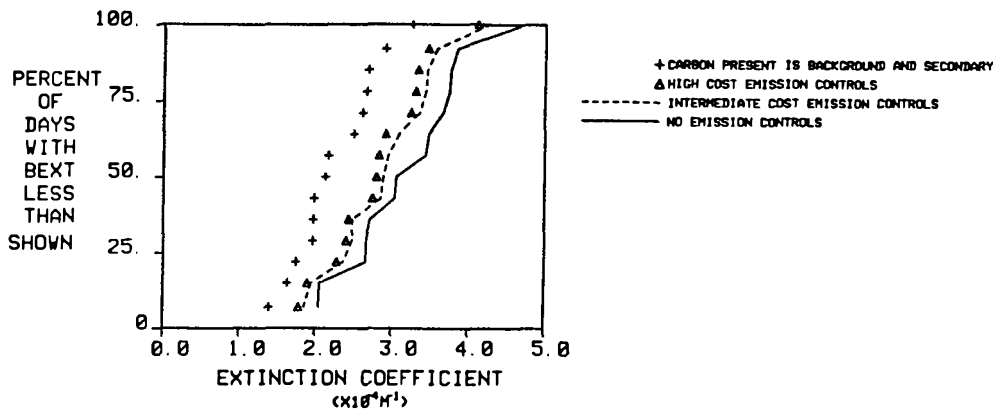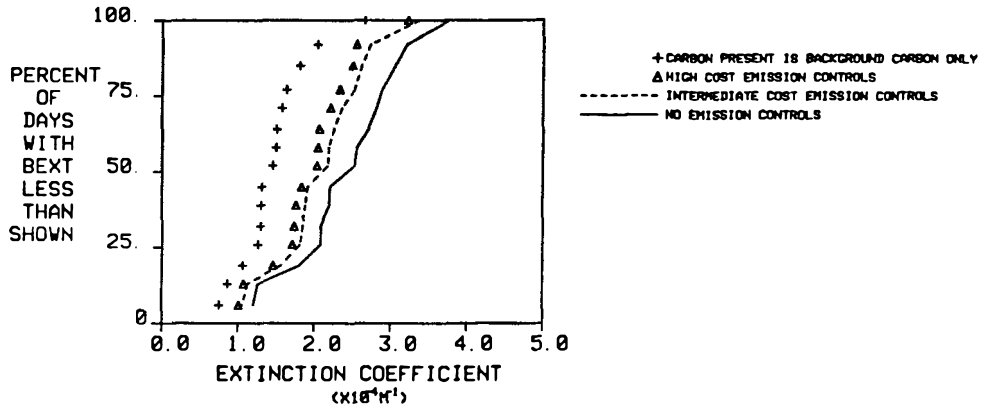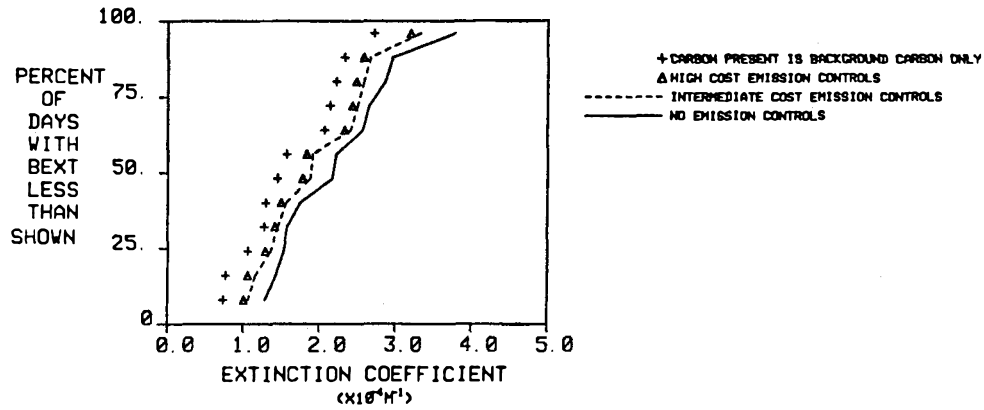FREQUENCY DISTRIBUTION (1000-1400 PST) (MODEL)

FIGURE 5.8. Frequency diagrams for no cost (uncontrolled), intermediate cost, and high cost control strategies to control elemental carbon emissions. (I)

Amounts of secondary organic carbon aerosol are estimated from the primary TC:EC ratio predicted for each site using a primary aerosol transport model (Gray, 1986).

SUMMER 1984 EXTINCTION COEFFICIENT AT PASADENA
FREQUENCY DISTRIBUTION (1000-1400 PST) (NOSEC)

SUMMER 1984 EXTINCTION COEFFICIENT AT LENNOX
FREQUENCY DISTRIBUTION (1000-1400 PST) (NOSEC)

SUMMER 1984 EXTINCTION COEFFICIENT AT AZUSA
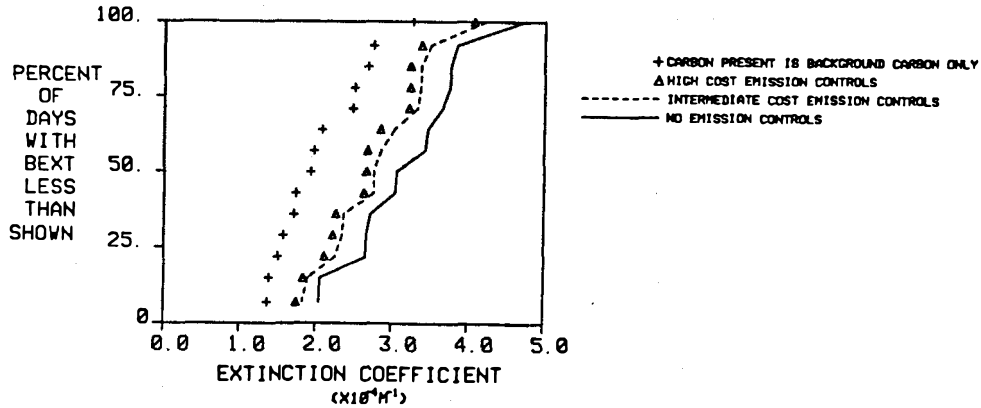FREQUENCY DISTRIBUTION (1000-1400 PST) (NOSEC)

FIGURE 5.9. Frequency diagrams for no cost (uncontrolled), intermediate cost, and high cost control strategies to control elemental carbon emissions. (II)

All aerosol carbon is assumed to be primary.

FIGURE 5.10. Synthetic photograph of downtown Pasadena
illustrating the effect of carbon reduction on visibility.

Photograph predicts the appearance of the scene on August 25, 1983 had high cost levels of primary aerosol carbon been in place. All aerosol carbon is assumed to be primary.

MODELED EXTINCTION COEFFICIENT
AUGUST 25, 1983 AT PASADENA
(1000-1400 PST)

MODELED
EXTINCTION
COEFFICIENT

$(X10^{-4}M^{-1})$

WAVELENGTH=550nm

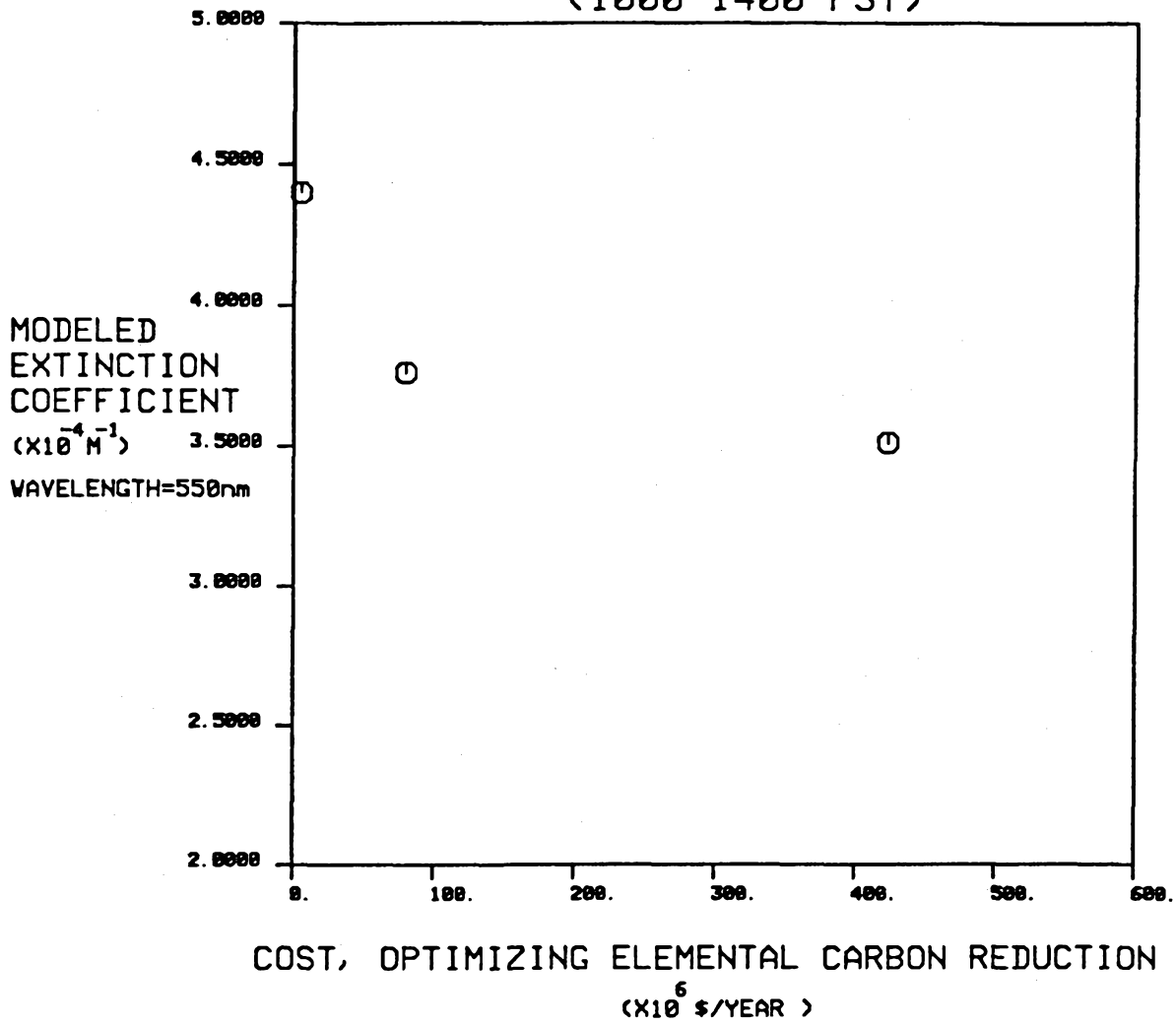COST, OPTIMIZING ELEMENTAL CARBON REDUCTION

$(X10^{6} \$/YEAR)$

FIGURE 5.11. Midday extinction coefficients versus annual cost of controls for the optimal strategy to control elemental carbon for Pasadena for August 25, 1983.

5.7 Conclusions

The control of carbonaceous aerosol is important from the standpont of improving visibility. Carbonaceous aerosol makes up 40% of fine particulate mass on a 24-hour average basis and 33% of the fine aerosol mass during summer midday periods in the Los Angeles area. Although little secondary organic aerosol enrichment is seen in annual average data, some secondary organic aerosol enrichment is evident in samples taken during summer midday periods. Aerosol carbon is calculated to account for as much as 39% of the total aerosol scattering coefficient and for as much as 44% of the extinction coefficient in the Los Angeles air basin during summer midday periods.

A Lagrangian air quality model was used by Gray (1986) along with 1982 emissions data, air quality data, wind data, and control costs to construct linear programming solutions to the optimal primary carbonaceous aerosol control strategy problem in the Los Angeles area. The emission control analysis predicts that a 68% decrease in fine elemental carbon emissions could be achieved at a cost of near $500 $\times 10^6$ year^{-1} (1982 dollars) and that a 48% decrease in elemental carbon concentrations could be achieved at a cost of $80 $\times 10^6$ year^{-1} (1982 dollars). Using the percentage reduction in primary aerosol carbon obtained in the study by Gray (1986), the improvement in summer midday extinction coefficient values for three sites in the Los Angeles basin was estimated. Approximately an 8% to a 14% decrease in the average extinction coefficient is predicted to be achieved at Pasadena (depending on the level of secondary organic aerosol formation) at a cost of $80.4 $\times 10^6$ year^{-1} (1982 dollars). An 11% to a 19% decrease (depending on the level of secondary organic aerosol formation) in the extinction coefficient could be obtained at Pasadena at a cost of $423.5 $\times 10^6$ year^{-1} (1982 dollars). The predicted frequency distributions of summer midday extinction coefficient values

before and after implementation of this emission control program were presented for the three sites studied. The influence of primary carbonaceous aerosol controls on visibility was also modeled for August 25, 1983, and a synthetic photograph is presented of how that day is computed to appear had the controls studied here been in place and if the carbonaceous aerosol on that day had been primary in origin. Comparison of that photograph to a photograph of the pre-control condition illustrates the change in appearance that a 25% decrease in the extinction coefficient (obtained at a cost of $423.5 $\times 10^6$ year^{-1}; 1982 dollars) would have on a typical view.

5.8 Acknowledgements

5.9 References

Appel, B.R., Hoffner, E.M., Kothny, E.L., Wall, S.M., Haik, M., Knights, R.L. 1979. Analysis of carbonaceous material in southern California atmospheric aerosols 2. *Environmenal Science and Technology* **13**, 98-104.

Cass, G.R., Boone, P.M., Macias, E.S. 1982. Emissions and air quality relationships for atmospheric carbon particles in Los Angeles, in *Particulate carbon: Atmospheric life cycle,* eds. G.T. Wolff, and R.L. Klimisch, Plenum Press, New York, NY.

Cass, G.R., McRae, G. 1981. Minimizing the cost of air pollution control. *Environmental Science and Technology,* **15**, 748-759.

Conklin, M.H., Cass, G.R., Chu, L.C., Macias, E.S. 1981. Wintertime carbonaceous aerosols in Los Angeles: An exploration of the role of elemental carbon, in *Atmospheric aerosols: Source/air quality relationships,* eds. E.S. Macias and P.K. Hopke, American Chemical Society, Washington, D.C.

Cronn, D.R., Charlson, R.J., Knights, R.L., Crittenden, A.L., Appel, B.R. 1977. A survey of the molecular nature of primary and secondary components of particles in urban air by high-resolution mass spectrometry. *Atmospheric Environment* **11** , 929-937.

Franklin, J.N. 1980. *Methods of mathematical economics.* Springer-Verlag.

Gale, D. 1960. *The theory of linear economic models.* McGraw Hill, New York, NY.

Gray, H.A., 1986. Control of atmospheric fine primary carbon particle concentrations. Ph.D. thesis, California Institute of Technology, Pasadena, California.

Gray, H.A., Cass, G.R., Huntzicker, J.J., Heyerdahl, E.K., Rau, J.A., 1986. Characteristics of atmospheric organic and elemental carbon particle concentrations in

Los Angeles. *Environmental Science and Technology* **20**, 580-589.

Groblicki, P.J., Wolff, G.T., Countess, R.J. 1981. Visibility-reducing species in the Denver "brown cloud"–I. Relationships between extinction and chemical composition. *Atmospheric Environment* **15**, 2473-2484.

Grosjean, D. 1977. Aerosols, in *Ozone and other photochemical oxidants*. National Academy of Sciences, Washington, D.C.

Grosjean, D., Friedlander, S.K. 1975. Gas-particle distribution factors for organic and other pollutants in the Los Angeles atmosphere. *J. Air Pollut. Control Assoc.* **25**, 1038-1044.

Hidy, G.M. et al., 1974. *Characterization of aerosols in California (ACHEX)*. Rockwell International, Science Center. Prepared under California Air Resources Board contract no. 358 (issued September 1974, revised April 1975).

IARC Working Group 1980. An evaluation of chemicals and industrial processes associated with cancer in humans based on human and animal data. *Cancer Research* **40**, 1-12.

Johnson, R.L., Shah, J.J., Cary, R.A., Huntzicker, J.J. 1981. An automated thermal-optical method for the analysis of carbonaceous aerosol, in *Atmospheric aerosols: Source/air quality relationships*, eds. E.S. Macias, and P.K. Hopke, American Chemical Society, Washington, D.C.

Larson, S.M., Cass, G.R. 1987. Characteristics of summer midday low visibility events in the Los Angeles area. Submitted to *Environmental Science and Technology*.

Larson, S.M., Cass, G.R., Hussey, K., Luce, F.R. 1987. Verification of image processing-based visibility models. Submitted to *Environmental Science and Technology*.

Lin, C., Baker, M., Charlson, R.J. 1973. Absorption coefficient of atmospheric aerosol: A method for measurement. *Applied Optics* **12**, 1356-1363.

Macias, E.S., Zwicker, J.O., Ouimette, J.R., Hering, S.V., Friedlander, S.K., Cahill, T.A., Kuhlmey, G.A., Richards, L.W., 1981. Regional haze case studies in the southwestern US-I. Aerosol Chemical Composition *Atmospheric Environment* **15**: 1971-1986.

Malm, W.C., Molenar, J.V., 1984. Visibility measurements in national parks in the western United States. *Journal of the Air Pollution Control Association* **34**, 899-904.

Muhlbaier, J.L., Williams, R.L. 1982. Fireplaces, furnaces and vehicles as emission sources of particulate carbon, in *Particulate carbon: Atmospheric life cycle,* eds. G.T. Wolff and R.L. Klimisch, Plenum Press, New York, NY.

Ouimette, J.R., Flagan, R.C., 1982. The extinction coefficient of multicomponent aerosols. *Atmospheric Environment* **16**, 2405-2419.

Pierson, W.R., Russell, P.A. 1979. Aerosol carbon in the Denver area in November 1973. *Atmospheric Environment* **13**, 1623-1628.

Pierson, W.R., Gorse, R.A., Szkarlat, A.C., Brachaczek, W.W., Japar, S.M., Lee, F.S-C., Zweidinger, R.B., Claxton, L.D. 1983. Mutagenicity and chemical characteristics of carbonaceous particulate matter from vehicles on the road. *Environmental Science and Technology* **17**, 31-44.

Pitts, J.N. 1983. Formation and fate of gaseous and particulate mutagens and carcinogens in real and simulated atmospheres. *Environ. Health Perspect.* **47**, 115-140.

Rosen, H., Hansen, A.D.A., Gundel, L., Novakov, T. 1978. Identification of the optically absorbing component in urban aerosols. *Applied Optics* **17**, 3859-3861.

Rosen, H., Hansen, A.D.A., Gundel, L., Novakov, T. 1979. Identification of the graphitic carbon component of source and ambient particulates by Raman spectroscopy and an optical attenuation technique, in *Proceedings: Carbonaceous particles in the atmosphere*, Lawrence Berkeley Laboratory, University of California.

Rosen, H., Hansen, A.D.A., Gundel, L., Novakov, T. 1982. Graphitic carbon in urban environments and the Arctic, in *Particulate carbon: Atmospheric life cycle*, eds. G.T. Wolff and R.L. Klimisch, Plenum Press, New York, NY.

Schuetzle, F., Cronn, D., Crittenden, A.L., Charlson, R.J. 1975. Molecular composition of secondary aerosol and its possible origin. *Environmental Science and Technology* **9**, 838-845.

Siegla, D.C., Smith, G.W., eds. 1981. *Particulate carbon: Formation during combustion*, Plenum Press, New York, NY.

Solórzano, L. 1969. Determination of ammonia in natural waters by the phenol-hyphochlorite method. *Limnol. Oceanogr.* **14**, 799-801.

Waggoner, A.P., Charlson, R.J. 1977. Measurements of aerosol optical properties, in *Denver Air Pollution Study-1973, Proceedings of a Symposium*, ed. P.A. Russell, vol. 2, U.S. Environmental Protection Agency EPA-600/9-77-001.

Wagner, H.G.G. 1978. Soot formation in combustion, in *17th symposium (international) on combustion*, The Combustion Institute, Pittsburgh, PA.

White, W.H., Roberts, P.T. 1977. On the nature and origins of visibility-reducing aerosols in the Los Angeles air basin. *Atmospheric Environment* **11**, 803-812.

Wolff, G.T., Groblicki, P.J., Cadle, S.H., Countess, R.J. 1982. Particulate carbon at various locations in the United States, in *Particulate carbon: Atmospheric life cycle*, eds. G.T. Wolff and R.L. Klimisch, Plenum Press, New York, NY.

CHAPTER 6

CONCLUSION

6.1 Summary

The reduction of visibility can be a severe problem in the Los Angeles area, especially during summer midday periods. In order to engineer a deliberate solution to this problem of visibility reduction, the pollutants that cause the visibility problem must be fully characterized. Mathematical models describing the link between emission sources, ambient pollutant concentrations, and visibility then can be used to evaluate the effect of proposed emission control strategies on visibility improvement.

During the summer of 1984, an air monitoring network was operated at five sites in the Los Angeles area in order to identify the pollutants causing the observed midday visibility reduction. Midday extinction coefficient values observed that summer ranged from less than 0.5×10^{-4} m^{-1} (corresponding to a visual range of more than 78 km) to more than 9.0×10^{-4} m^{-1} (corresponding to a visual range of less than 4.3 km). Measurements of the atmospheric aerosol size distribution were combined with refractive index values estimated from measurements of aerosol chemical composition in order to calculate the light scattering coefficient present on each experiment day by means of Mie theory. Light absorption coefficient values were computed from measurements of the concentration of airborne elemental carbon particles and NO_2.

The frequency distribution of summer midday extinction coefficient values constructed from the predicted scattering and absorption coefficient estimates was

compared to extinction coefficient data inferred from airport visual range observations. It was found that the frequency distribution of summer midday extinction coefficient values at Pasadena, California, can be modeled with reasonable accuracy by this procedure. Calculations show that most of the light attenuation in the Los Angeles atmosphere is due to scattering by fine particles. Fine particle scattering and absorption account for 83% of the total light extinction averaged over the five sites studied. Carbonaceous aerosol and sulfates together account for 49% of the fine aerosol averaged over the five sites studied.

The extinction coefficient is an important parameter in any visibility model which predicts the visual range, the contrast between objects in a scene, or the apparent intensity of light from an object as it reaches an observer. One powerful way of showing the results of a visibility modeling calculation in a readily understood fashion is to generate synthetic photographs that indicate how a scene would appear under specified air pollution conditions. In this work, methods were developed to test the accuracy of image processing-based visibility models. The results of these tests indicate that simple image processing-based visibility models can reproduce the contrast degradation observed on smoggy days. Radiative transfer calculations can be incorporated into these models in order to produce an accurate representation of the appearance of the sky under heavy smog conditions.

Aerosol carbon is one of the most abundant pollutant species found in the Los Angeles atmosphere. Carbonaceous aerosol makes up 33% of the fine particulate mass in the Los Angeles atmosphere during summer midday periods. During these periods, as much as 39% of the total scattering coefficient and as much as 44% of the total extinction coefficient in the South Coast Air Basin is due to carbonaceous aerosol. Emission control technologies have been identified that would reduce the emission of carbon particles by controlling the sources of the particles, resulting
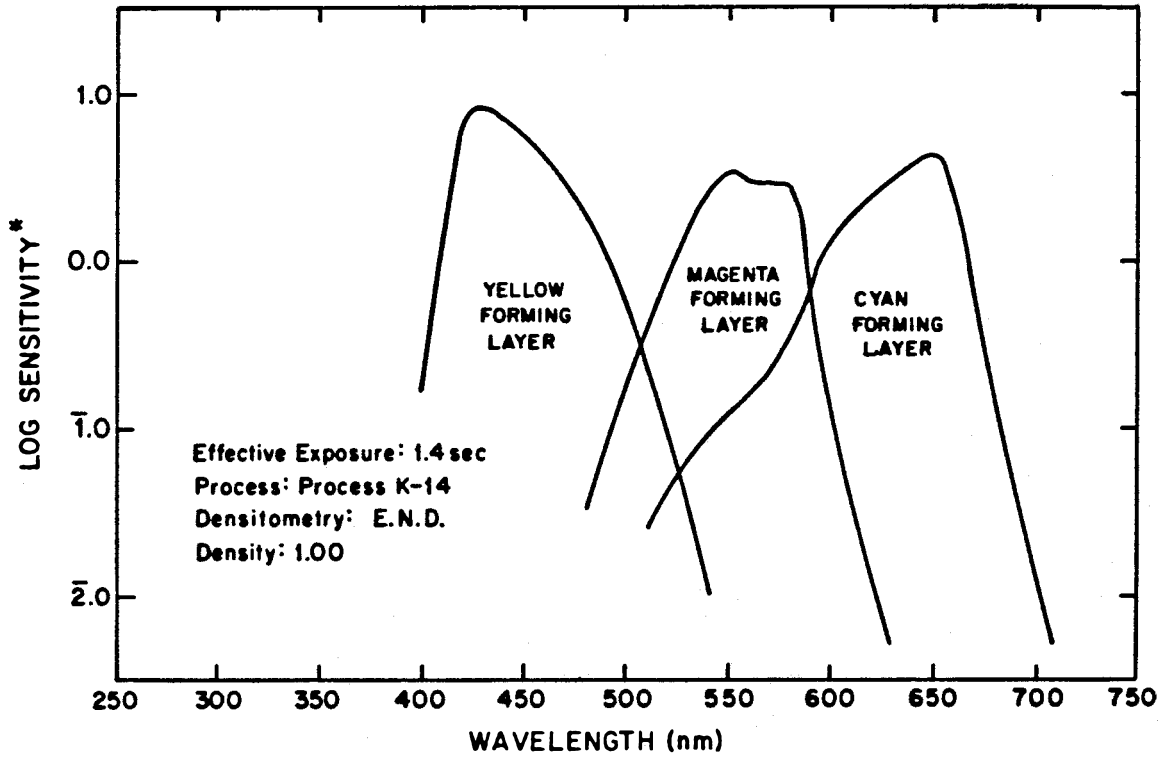
in an 8% to a 15% decrease in the average summer midday extinction coefficient at a cost of 80.4×10^6 year^{-1}. If controls on additional pollutant species were implemented, visibility in the Los Angeles area could be further improved.

APPENDIX
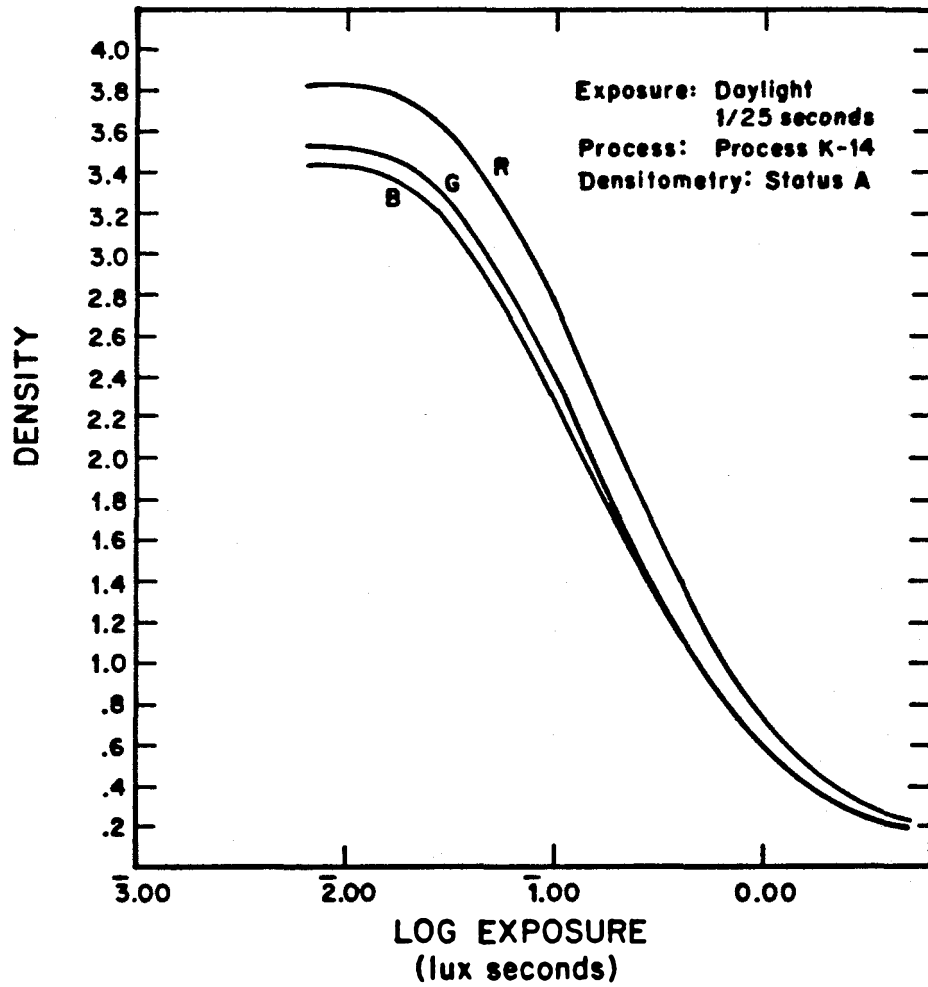
FIGURE A.1 Characteristic curves for Kodachrome 25 slide film.

FIGURE A.2 Spectral sensitivity curves for Kodachrome 25 slide film.